A Universal Mathematical Model for Porosity Prediction of Fluvial Sediments

Von der Fakultät für Bauingenieurwesen der Rheinisch-Westfälischen Technischen Hochschule Aachen zur Erlangung des akademischen Grades eines Doktors der Ingenieurwissenschaften genehmigte Dissertation

vorgelegt von

Rui Liang

Berichter: Univ.-Prof. Dr.-Ing. Holger Schüttrumpf
Univ.-Prof. Dr. Klaus Reicherter

Tag der mündlichen Prüfung: 20.05.2025

Contents

List of Figures

List of Tables

List of Abbreviations

Abbreviations	Full Terms
BUCPM	Binary-Unit Conceptual Packing Model
CPM	Compressible Packing Model
CT	Computed Tomography
DEM	Discrete Element Method
EPD	Equivalent Packing Diameter
GSD	Grain Size Distribution
IBUCPM	Integrated Binary-Unit Conceptual Packing Model
LMPM	Linear-Mixture Packing Model
LPM	Linear Packing Model
LS	Laser Scanning
MAE	Maximum Absolute Error
MAPE	Mean Absolute Percentage Error
NLP	Non-Linear Programming
NLPM	Non-Linear Packing Model
NSGD	Non-Smooth Granular Dynamics
RMSE	Root Mean Square Error
RSA	Random Sequential Addition
SD	Standard Deviation
SDP	Stochastic Digital Packing
SEM	Standard Error of Mean
WRM	Water Replacement Method

Zusammenfassung

Die Porosität eines Flussbetts ist eine zentrale strukturelle Eigenschaft, die sich aus der Packung von Flusssedimenten unterschiedlicher Größe und Form ergibt. Sie wird als das Verhältnis des Porenvolumens zum Gesamtvolumen definiert und ist für nahezu jede Untersuchung des Flussbetts von Bedeutung. Morphologisch bestimmt die Porosität die Sedimentkonzentration im Flussbett und somit die Geschwindigkeit von Änderungen des Sohlenprofils. Ökologisch beeinflusst sie den interstitiellen Raum der hyporheischen Zone, der für aquatische Lebensräume entscheidend ist. Geologisch dominiert die Bedeutung der Porosität die nutzbaren Reserven von Öl, Gas und Grundwasser, die in den Hohlräumen fluvialer Ablagerungen gespeichert sind.

Trotz ihrer wichtigen Rolle sind Informationen über die räumliche Variabilität der Porosität im Flussbett selten verfügbar. Stattdessen wird die Porosität oft als räumlich konstant angenommen, was zu systematischen Fehlern in morphologischen, ökologischen und geologischen Studien führen kann. Dies liegt teilweise an den hohen Kosten und dem Aufwand für In-situ-Messungen der Porosität. Als Alternative erweisen sich mathematische Porositätsprädiktoren als effektives Mittel, um die Porosität basierend auf beeinflussenden Faktoren wie Korngröße, Kornform und Packungszustand zu schätzen. Bisher konnte jedoch kein Modell zufriedenstellende Ergebnisse hinsichtlich Universalität, Genauigkeit und Effizienz liefern. Regressionsbasierte Modelle sind zwar einfach anzuwenden, aber oft unzureichend, wenn sie außerhalb des ursprünglichen Datensatzes verwendet werden. Bestehende analytische Modelle sind trotz ihrer allgemeinen Nützlichkeit komplex zu berechnen und unterschätzen systematisch die Porosität aufgrund ihrer grundlegenden Annahmen.

In dieser Arbeit wurde ein neuartiger mathematischer Porositätsprädiktor entwickelt, der allgemein, genau und einfach anzuwenden ist. Als erster Schritt wurde der Einfluss der Korngröße auf die Porosität untersucht, wobei die Sedimentform als sphärisch angenommen wurde. Im Gegensatz zu traditionellen analytischen Modellen, die typischerweise aus der Analyse binärer Mischungen von Kugeln abgeleitet und dann zu komplexen Modellen für beliebige Kugelpackungen erweitert werden, kehrt diese Studie diesen Prozess um, indem sie beliebige Kugelpackungen in eine binäre Kugelmischung konzeptualisiert. Dies wurde durch das neu vorgeschlagene Konzept der binären Einheit erreicht, das besagt, dass jede multi- oder kontinuierlich größenverteilte Kugelmischung durch identische Korngrößenstatistiken (Mittelwert, Standardabweichung und Schiefe) in eine äquivalente binäre Kugelmischung umgewandelt werden kann. Die erhaltene binäre Mischung stellt die elementarste Kugelpackungseinheit dar, die die Vielfalt der intrapartikulären Wechselwirkungen in den ursprünglichen Kugelmischungen d. h. die

Misch- und Entmischungseffekte äquivalent repräsentiert. Mit diesem Konzept kann das Modell, das als binäres Einheitspackungsmodell (BUC) bezeichnet wird, die Porosität komplexer Kugelpackungen allein durch die Nutzung von Modellen zur Vorhersage der Porosität binärer Kugelpackungen schätzen. Das Westman-Gleichungsmodell wird hierfür empfohlen. Die Validierung anhand von 85 digitalen Kugel-Flussbetten, die durch einen validierten nicht-glatten Granulardynamik-Algorithmus (NSGD) erzeugt wurden, zeigte, dass das BUC-Modell sehr genaue Porositätsvorhersagen mit einem mittleren quadratischen Fehler (RMSE) von 0,01 liefert.

Anschließend wurde der Einfluss nicht-sphärischer Kornformen in das BUC-Modell integriert, um die Porosität fluvialer Sedimente vollständig zu erfassen. Zunächst wurde eine ideale regelmäßige Form verwendet, um die komplexen Kornformen zu vereinfachen. 241 Sedimentpartikel wurden hochauflösend gescannt und mit vier Kandidaten regelmäßiger Formen verglichen: Quader, elliptische Scheibe, abgestumpftes Oktaeder und Ellipsoid. Es wurde festgestellt, dass das Ellipsoid die beste Formähnlichkeit zu fluviatilen Sedimenten aufweist und somit als angemessener Ersatz dient. Nach dem Konzept des äquivalenten Packungsdurchmessers kann eine nicht-sphärische (ellipsoide) Sedimentmischung in eine Kugelpackung mit einem äquivalenten Größeneffekt auf die Porosität umgewandelt werden. Diese kann gut vom BUC-Modell behandelt werden in Kombination mit einer Anfangsporosität, die den isolierten Effekt der nicht-sphärischen Form in einem bestimmten Packungsstadium erfasst. Die drei theoretischen Transformationen - von Sediment zu Ellipsoidpackung, von Ellipsoid zu Kugelpackung und von Kugel- zu binärer Kugelpackung - bilden die Grundlage des integrierten BUC (IBUC)-Modells.

Das IBUC-Modell erfordert nur zwei Eingaben: die Korngrößenverteilung (GSD) der transformierten Kugelpackung und die Anfangsporosität. Es wurde gezeigt, dass die GSD der Kugelpackung gut mit der gemessenen GSD der ursprünglichen Sedimentpackung approximiert werden kann. Für praktische Zwecke wurde die Verwendung einer gemessenen mittleren Anfangsporosität als allgemeine Repräsentation für einen untersuchten lokalen Standort vorgeschlagen. Trotz dieser Vereinfachung erreichte das IBUC-Modell immer noch genaue Porositätsvorhersagen mit einem RMSE von 0,03, validiert anhand von 138 Porositätsmessdaten aus vier verschiedenen Flussbetten: Rhein, Bès, Galabre und Kuqa.

Insgesamt positioniert sich das IBUC-Modell aufgrund seiner Allgemeingültigkeit, Einfachheit und Vorhersageleistung als ein hochmodernes Werkzeug zur Untersuchung der räumlichen Variabilität der Porosität im Flussbett. Darüber hinaus wird erwartet, dass das Konzept der binären Einheit, ein Schlüsselbestandteil des IBUC-Modells, über die Porositätsschätzung hinausgeht, da intrapartikuläre Wechselwirkungen eine Reihe anderer Faktoren beeinflussen. Potenzielle Anwendungen umfassen die Schätzung der Permeabilität in Sedimentmischungen, die Bestimmung der Grenzkorngröße für morphologische Veränderungen und sogar die Vorhersage des Beginns des Sedimenttransports.

Abstract

The porosity of riverbed is a key structural property arising from the packs of fluvial sediments in varied sizes and shapes, which is defined as the ratio of pore volume to total volume. It is significant to nearly every investigation related to riverbed. For instance, morphologically, porosity determines the sediment concentration in the river bed and hence the rate of bed level changes. Ecologically, porosity governs the interstitial space of the hyporheic zone for aquatic habitats. Geologically, porosity dominates the exploitable reserve of oil, gas, and groundwater stored in the voids of fluvial deposits.

Despite its important role, information regarding the spatial variations in porosity is rarely available in riverbed. Instead, porosity is often simply assumed to be spatially constant, which could cause a systematic error in morphological, ecological, and geological studies. The reason for this is partly due to the costly and arduous effort for in-situ measurements on porosity. As an alternative, mathematical porosity predictors turn out to be an effective way to estimate porosity based on porosity-controlling factors, such as grain size, grain shape and packing state. However, so far, no such a model can provide satisfactory results in terms of universality, accuracy, and efficiency. Regression-based models, while simple to use, is often insufficient when utilized in regions outside the original dataset. On the other hand, existing analytical models despite their general usefulness, are complex to compute and have been found to systematically underestimate porosity due to their intrinsic assumptions.

In this thesis, the objective was to develop a novel mathematical porosity predictor that is general, accurate, and simple to apply. As a first step, the grain size effect on porosity was explored by assuming sediment shape as spherical. Unlike traditional analytical models that are typically derived from the analysis of binary mixtures of spheres, and then extended into complex models for arbitrary spherical packings, this study reverses such process by conceptualizing arbitrary spherical packings into a binary spherical mixture. This was achieved based on a newly proposed binary-unit concept, which states that any multi-sized (or continuous) spherical mixture can be transformed into an equivalent binary-unit mixture of spheres through the link of identical grain size statistics of mean, standard deviation and skewness. The obtained binary mixture is actually the most elementary spherical packing unit that can equivalently represent the diversity of intraparticle interactions in the original spherical mixtures, i.e., the mixing and unmixing effects. With this concept, the model, namely the binary-unit conceptual (BUC) packing model, can be readily implemented to estimate the porosity of complex spherical packings solely by leveraging models capable of predicting the porosity of a

binary spherical packing. The Westman-equation model is recommended for this purpose. Validation against 85 digital riverbeds of spheres generated through a validated non-smooth granular dynamics (NSGD) algorithm suggested that the BUC packing model is able to provide very accurate porosity predictions, producing a root-mean-square error (RMSE) of 0.01.

Next, the non-spherical grain shape effect was integrated into the BUC packing model in order to fully resolve the porosity of fluvial sediments. Initially, an ideal regular shape was employed to simplify the complex grain shapes of fluvial sediments. 241 of sediment particles were scanned in high quality, and then compared to four candidate regular shapes: cuboid, elliptic disk, truncated octahedron, and ellipsoid. And it was found that the ellipsoid renders the best shape similarity to fluvial sediments, allowing it as a reasonable surrogate. Following the concept of equivalent packing diameter, a non-spherical (ellipsoid) sediment mixture can then be converted into a spherical packing with an equivalent size effect on porosity that can be well handled by the BUC model, alongside an initial porosity capturing the isolated non-spherical shape effect at a specific packing stage. The three theoretical transformations, i.e., from sediment to ellipsoid packing, from ellipsoid to spherical packing, and from spherical to binary-unit spherical packing, form the foundation of the integrated BUC (IBUC) packing model.

As a result, the IBUC packing model requires only two inputs: the grain size distribution (GSD) of the transformed spherical packing, and the initial porosity. It demonstrated that the GSD of the spherical packing can be well approximated with the measured GSD of the original sediment packing. For practical purposes, the use of a measured mean initial porosity has been proposed as a general representation for a local site being investigated. Despite this simplification, the IBUC packing model still achieved accurate porosity predictions with RMSE of 0.03, when validated against 138 porosity measurement data across four diverse riverbeds: the Rhine, Bès, Galabre, and Kuqa.

Overall, the generality, simplicity, and prediction performance of the IBUC packing model positions itself as a state-of-the-art tool for investigating the spatial variability in riverbed porosity. In addition, as a key component of the IBUC model, the binary-unit concept is expected to go beyond porosity estimation, as intraparticle interactions impact a range of other factors. The potential applications involve estimation of permeability in sediment mixtures, determination of the cut-off grain size for morphological alterations, and even prediction of the incipience of sediment transport.

Acknowledgements

This dissertation marks the culmination of a long academic journey, one that would not have been possible without the support, guidance, and encouragement of many wonderful people.

First and foremost, I would like to sincerely thank Univ.-Prof. Dr.-Ing. Holger Schüttrumpf, Head of the Institute of Hydraulic Engineering and Water Resources Management at RWTH Aachen University, and Univ.-Prof. Dr. Klaus Reicherter, Head of the Institute for Neotectonics and Natural Hazards at RWTH Aachen University. As my first and second examiners, their expertise, insightful feedback, and time played a crucial role in shaping and completing this work.

I am also deeply grateful to my teammates in the Morphodynamics and Sediments Research Group at the Institute of Hydraulic Engineering and Water Resources Management, whose collaboration and camaraderie made this journey enjoyable and intellectually stimulating. Special thanks to Dr. Roy Frings, for his professional support and all the fun we had during work and coffee breaks.

Last but never least, I want to thank my family for their unwavering love, patience, and belief in me. Your encouragement has been the bedrock of my perseverance. A heartfelt thank you to Ruijie, whose support carried me through the most challenging phases of this journey.

1

Introduction

Somewhere, something incredible is waiting to be known.
- Carl Sagan

1.1 Backgrounds

Riverbed porosity, defined as the ratio of pore volume to total volume in fluvial sediments, is a fundamental structural property that emerges from the natural arrangement of sediments. It plays a critical role in various riverbed studies, serving as a key input for calculating sediment density, hydraulic conductivity, and thermal conductivity. Understanding porosity is also essential for assessing riverbed mobility, evaluating environmental hazards, and guiding economic resource development, such as in groundwater management and mining operations.

Despite its significance, knowledge about spatial variations in riverbed porosity is still limited. This gap largely stems from the difficulties of conducting direct in-situ measurements, as riverbeds are frequently submerged by flowing water, making the process labor-intensive, time-consuming, and expensive. Although alternative methods such as laboratory measurements and numerical simulations can provide direct porosity estimates for specific cases, these approaches are also impractical for large-scale assessments. Laboratory studies require extensive sediment sampling, while numerical simulations demand precise information about sediment properties, both of which are challenging to obtain on a broad scale.

Given these constraints, mathematical porosity predictors have emerged as an effective alternative. These models estimate porosity based on factors that influence sediment packing, such as grain size, grain shape, and depositional environment that can result in either loose or dense packing states. Current porosity predictors can be broadly categorized into regression-based models and analytical models.

Regression-based models are developed through statistical analysis, fitting mathematical formulas to specific datasets. These models are often straightforward, requiring minimal input data, which makes them easy to implement. However, their simplicity comes at a cost; they may not perform well when applied to regions or conditions outside the scope of the original dataset.

Analytical models, in contrast, are grounded in theoretical frameworks that conceptualize the sediment packing system as an ensemble of different particle classes. These models simulate the interactions between particles to estimate the overall porosity of the system. While analytical models offer greater generality and can be applied to a wider range of conditions, they are often computationally intensive. More importantly, due to the assumptions inherent in these models, they tend to underestimate porosity, especially in complex or heterogeneous sediment packings.

In this thesis, the IBUC packing model is developed, i.e., the **I**ntegrated **B**inary-**U**nit **C**onceptual packing model, to fully resolve the porosity of fluvial sediments in a manner that is general, simple, and accurate. The basic principle of this model is to compress an arbitrary sediment packing into a binary-unit spherical mixture that embodies the equivalent size effects between particles, together with an initial porosity capturing all

other porosity-influencing factors, such as the grain shape and packing state. This work provides a new perspective on estimating riverbed porosity variations across different spatial scales and may also help in understanding other sediment-related issues in fluvial systems and hyporheic zone.

1.2 Outline

The main contents of this thesis are structured into six chapters that partially build on top of each other (Fig. 1.1).

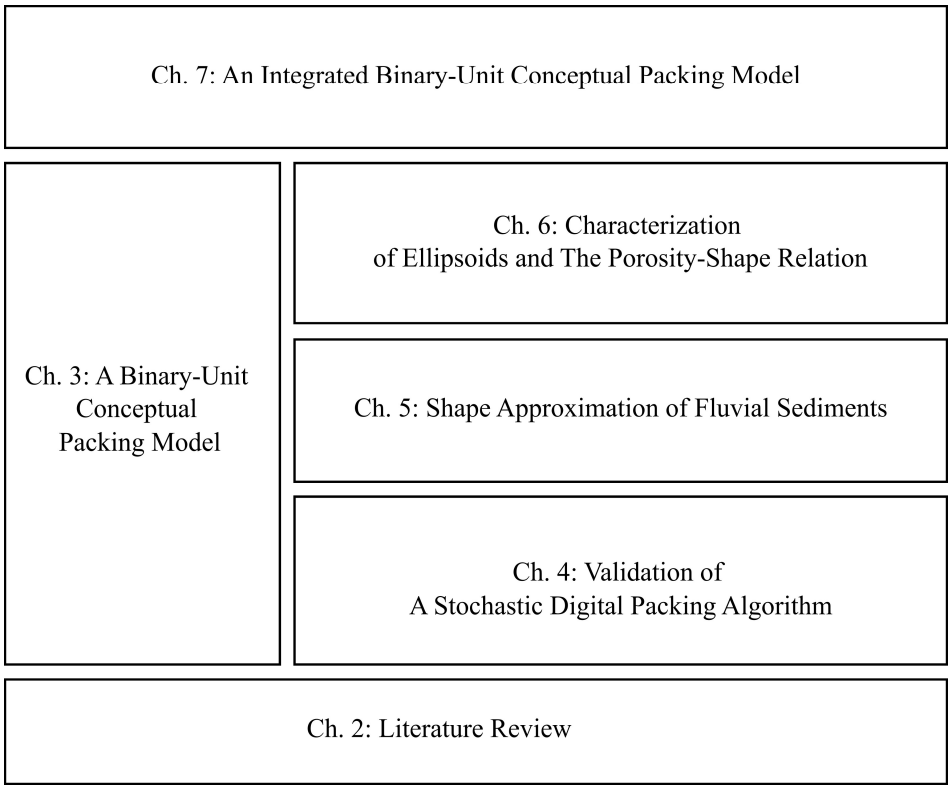

Figure 1.1. A visual representation of the thesis content, with each chapter stacked on top of the chapters they build upon. The size of each box is approximately proportional to the length of the corresponding chapter.

Chapter 2 reviews various methodologies in the estimation of packing porosity, including field and laboratory measurements, numerical simulations, as well as mathematical porosity predictors, and discusses their shortcomings.

Chapter 3 develops a novel porosity predictor for arbitrary spherical sediment packings, namely the binary-unit conceptual (BUC) packing model. The core of the BUC model is based on a newly proposed binary-unit concept, which enables to transform any multi-sized (or continuous) sphere mixture into an equivalent binary-unit mixture through the link of identical grain size statistics of mean, standard deviation and skewness. The obtained binary-unit mixture can be viewed as the most elementary packing unit that

embodies the equivalent interparticle interactions in the original mixture. With this concept, the porosity of spherical sediment packings, no matter how labyrinthine their grain size distributions are, can be readily computed through the utilization of models capable of predicting the porosity of a binary spherical packing.

Chapter 4 introduces a stochastic digital packing algorithm, which provides an innovative way to pack fluvial sediments of arbitrary shapes and sizes based on digitization of both particles and packing space. The purpose is two-fold: first, to test the applicability of this packing algorithm in predicting fluvial sediment porosity by comparing its predictions with outcomes obtained from laboratory measurements, and second, to demonstrate that apart from grain size, grain shape also has a clear impact on porosity.

Chapter 5 addresses the challenges associated with shape measurement, characterization, and control for the complex fluvial sediments, by employing an idealized regular shape that could approximate the overall form of fluvial sediments. Four potential candidate shapes are carefully selected: cuboid, elliptic disk, truncated octahedron, and ellipsoid. A comparison with high-resolution scans of sediment particles indicates that the ellipsoid shape can render the closest approximation of fluvial sediment shape in terms of surface area, volume, and sphericity. Further testing demonstrates that ellipsoids also exhibit similar packing behavior when utilized as surrogates for fluvial sediments.

Chapter 6 proposes a new ellipsoid diagram capable of describing the full range of ellipsoids using two well-defined parameters, Wadell's sphericity and Zingg's intercept ratio, which can be directly computed from semi-axis lengths. A non-linear programming algorithm (NLP) is presented to quantify the relationship between porosity and mono-sized ellipsoidal geometry, identifying three distinct porosity trends as functions of sphericity and intercept ratio. These trends have been formulated into a piecewise equation.

Chapter 7 establishes the fully integrated binary-unit conceptual (IBUC) packing model, an enhanced version of the original BUC model by integrating all other porosity-influencing factors, such as the effects of non-spherical grain shape and packing state. The IBUC packing model is formulized through three theoretical transformations, i.e., from sediment to ellipsoid packing, from ellipsoid to spherical packing, and from spherical to binary-unit spherical packing. The IBUC model's capacity to account for all porosity-controlling factors, along with its conversion into a binary packing unit, ensures both generality and ease of application. Validation against diverse porosity measurement data demonstrates that the model reliably estimates porosity in complex fluvial sediment mixtures.

Chapter 8 concludes all the work in this thesis and proposes some possible future research directions.

2

Literature Review

The chapter provides a short overview of various methodologies used for estimating packing porosity, including direct field measurements, controlled laboratory experiments, advanced numerical simulations, and mathematical porosity predictors, while also addressing their limitations.

2.1 Relevance

Riverbed porosity, defined as the ratio of pore volume to total volume, is a key structural property emergent from the natural packs of fluvial sediments. It plays a vital role in morphological, ecological, and geological applications.

Morphologically, porosity dictates the sediment concentration in a riverbed, thereby affecting the rate of bed level changes over time (Coleman & Nikora, 2009; Frings et al., 2008; Lokin et al., 2023; Núñez-González et al., 2016). The significant costs associated with using gravel to fill scour holes in waterways are also directly linked to the porosity of the gravel (Frings et al., 2014). Additionally, porosity impacts the onset of sediment movement and figures as a parameter in various sediment transport equations (Ackers & White, 1973; Rettinger, et al., 2022a; Vollmer & Kleinhans, 2007; Wilcock, 1998). It also plays a role in the dissipation of wave energy along riverbanks and groynes (Chanda et al., 2023; Chwang & Chan, 1998; Ting et al., 2004), as well as in the internal friction angle (and steepness) of morphological features like dunes (Allen, 1985).

Ecologically, porosity determines the amount of void space within the hyporheic zone, which serves as a habitat for aquatic organisms. It plays a critical role in shaping the physical structure and ecological function of the hyporheic zone. By influencing the permeability of this zone, porosity controls the rate at which water flows through sediments, thereby affecting the delivery of oxygen and nutrients essential for biological processes (Boulton et al., 1998; Noack et al., 2017; Ping et al., 2020; Sawyer & Cardenas, 2009).

Geologically, porosity defines the economic value of gravel resources deposited by Quaternary rivers, while also determining the exploitable volumes of oil, gas, and groundwater stored within the pore spaces of sediments left by Mesozoic and Paleozoic rivers (e.g., Athy, 1930).

In riverbed-related research, sediment porosity is frequently assumed to be spatially uniform, a simplification that may not accurately reflect reality. Overlooking spatial variations in porosity could introduce systematic errors or biases in morphological, ecological, and geological analyses.

2.2 Porosity-controlling Factors

To understand or predict spatial variations in porosity along a riverbed, it is essential to identify the factors that control it. Insights into the porosity of sediment mixtures can be gained from studying artificial packings of spheres (Allen, 1985). These packings, which have been extensively explored in material science and chemistry (Nolan & Kavanagh, 1992; Scott, 1960; Song et al., 2008; Torquato et al., 2000; Yu & Standish, 1991), reveal that porosity is influenced by both material properties and packing methods. Similarly, the porosity of fluvial sediment mixtures must depend on (1) sediment properties and (2) depositional conditions.

Among sediment properties, grain size and shape are the most critical factors influencing porosity. Uniform sediments composed of nearly spherical grains typically have a porosity between 0.36 and 0.40 (Frings et al., 2011). However, mixing with different sized grains usually reduces pore space, with the degree of reduction depending on the mixing effect (joint interactions among particles) and the unmixing effect (filling or occupation) (Yu & Standish, 1991). Grain shape also plays a clear role on porosity. For instance, a slight deviation from a spherical shape can reduce the porosity of random packing, while a greater deviation in shape can lead to an increase in porosity (Chaikin et al., 2006; Delaney et al., 2011; Donev et al., 2004; Man et al., 2005; Williams & Philipse, 2003; Zou & Yu, 1996). Despite this, the effect of shape on porosity has received significantly less attention compared to grain size, mainly due to the challenges of measuring, characterizing, and controlling the complex shapes of fluvial sediments.

Depositional conditions are fundamental in determining whether a sediment mixture forms a loose or dense packing. When sediments are initially deposited, they are typically in a loosely packed state. However, various factors, such as vibrations occurring during or immediately after deposition, can induce the packing to become denser, leading to a significant decrease in porosity (Scott, 1960). While the exact mechanisms driving these changes are too a large degree unknown, the key variables appear to be sedimentation rate and flow velocity. The sedimentation rate influences the time and space available for grain rearrangement after initial deposition, with higher sedimentation rates typically resulting in lower porosity. The flow velocity also affects porosity by influencing the kinetic energy imparted to the grains during deposition. Higher flow velocities can provide more energy to the grains, promoting a more turbulent settling environment that may prevent optimal packing and result in increased porosity. On the other hand, lower flow velocities allow grains to settle more gently, reducing the kinetic energy available for agitation and thus facilitating closer grain packing.

2.3 Porosity Measurements

2.3.1 In-situ measurement

The primary reason for the limited knowledge about the spatial variations in porosity lies in the challenging of measuring porosity in fluvial sediment mixtures. Generally, in-situ porosity measurement techniques can be categorized into direct and indirect methods.

To directly measure the in-situ porosity of fluvial sediment mixtures, defined as ($n = 1 - V_s/V_t$), it is necessary to separately determine both the sediment volume (V_s) and the total volume (V_t) of a sediment sample. A traditional approach involves collecting a sample, measuring the volume of the sample pit (V_t), and then transporting the sample to a laboratory to determine the grain volume (V_s) using the water replacement method (Bear, 1972). The most challenging part of this process is accurately measuring V_t. A standard method, as proposed by the American Society for Testing and Materials (ASTM, 2021),

requires covering the sample pit with a plastic liner and measuring the amount of water needed to fill the pit (Fig. 2.1a&b). However, this method is time-consuming, labor-intensive, and prone to errors due to potential punctures in the liner caused by sharp sediment edges (Frings et al., 2011).

With technological advancements, modern techniques such as 3D scanning (Frings et al., 2012) and photogrammetry (e.g., Han & Endreny, 2014; Seitz et al., 2018) have been developed to measure V_t more efficiently. The structure-from-motion (SfM) photogrammetric method, in particular, has shown promise in estimating V_t due to its capability for high-resolution topographic reconstruction (Tabesh et al., 2019). This method involves creating two high-resolution digital elevation models (DEMs) before and after sediment excavation using multiple overlapping photographs and advanced tracking algorithms. The difference between the two DEMs provides the total volume of the sediment sample (Fig. 2.1c).

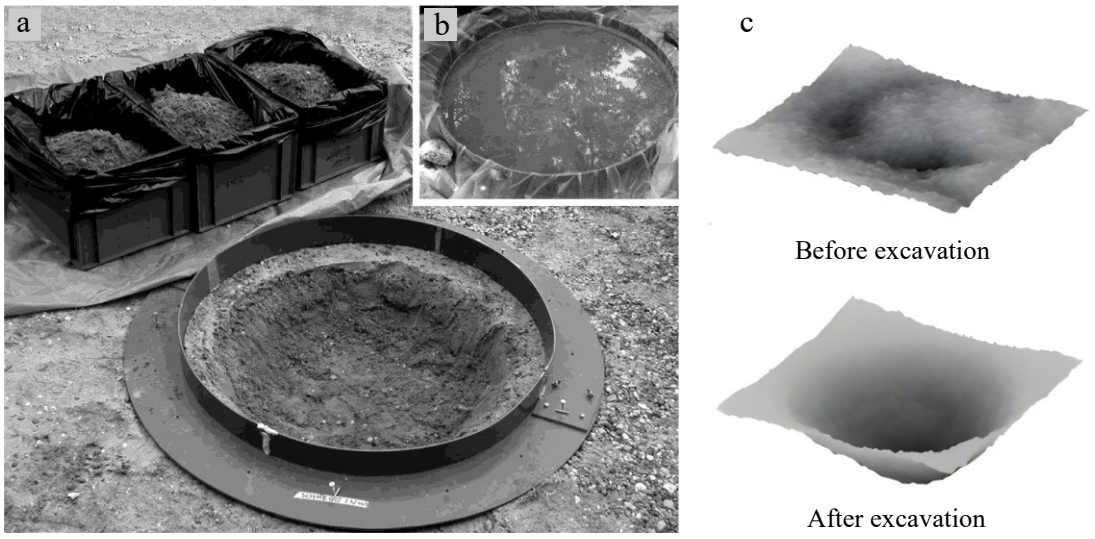

Figure 2.1. In-situ measurements of porosity: (a) sample pit and excavated sediments, (b) volume measurement of the pit using water, (c) digital elevation models before and after sediment excavation. Adapted from Frings et al. (2011) and Tabesh et al. (2019).

Indirect methods for determining porosity relate it to more easily measurable sediment properties, such as pore water content and wet sediment density, from which porosity can be calculated. Examples of such methods include nuclear density gauging (Tabesh et al., 2022), neutron probes, and gamma-gamma probes (Hallenburg, 1998). Typically, a Caesium-137 source that emits gamma radiation is used to measure the total wet sediment density based on the number of gamma particles passing through the sediment; denser sediments result in fewer gamma particles reaching the detector tubes. In addition, an Americium-241 source emitting neutron particles detects sediment moisture content based on the number of neutrons scattered back by hydrogen-containing sediment. Higher neutron counts indicate higher moisture content. While these techniques

are fast and relatively easy to implement, their accuracy is highly sensitive to environmental conditions, such as the chemical composition of the water and the elemental composition of the sediments. Consequently, neutron- and gamma-like probes require field calibration before measurements, a process that is quite challenging.

It is also important to note that in-situ measurements, whether by direct or indirect methods, are often impractical or prohibitively expensive (e.g., using a diving bell) when sediments are submerged beneath river water. As a result, their use is typically restricted to conditions where the riverbed surface is accessible, such as during periods of low flow (e.g., Tabesh et al., 2022).

2.3.2 Laboratory measurement

Several methods are available for measuring porosity in laboratory settings. Notable examples include the gas pycnometer, which is based on Boyle's law of volume-pressure relationships (e.g., Yan et al., 2018), the water desorption method, which involves saturating a sediment sample with water and then gradually desorbing the water while measuring the loss in weight (Klute, 1986), and the water replacement method (WRM) (Bear, 1972).

Among these, the WRM is frequently used for measuring the porosity of sediment samples. Sampled fluvial sediments, normally after drying in an oven, are added to a container (e.g., a cylindrical container) partially filled with a known volume of water (V_w), which is greater than the expected pore volume of the sediment to be added. The ultimate water level is recorded to determine the total accumulated volume (V_a), where $V_a = V_w + V_s$ (with V_s being the volume of the solid fraction). The total sediment volume (V_t), including pores, is obtained by measuring the height of the sediment packing. The porosity n $(= V_p/V_t)$ is then calculated, where V_p $(= V_t - (V_a - V_w))$ represents the pore volume of the particle packing (Fig. 2.2).

In WRM, errors associated with reading water levels and packing heights are the primary factors affecting accuracy (Liang et al., 2015). Additionally, a common issue in this method is the disturbance of packing near the container walls, resulting in larger pore spaces near the walls (Ridgway & Tarbuck, 1968). This wall effect is particularly evident in uniform sediment packings but less pronounced in multi-sized mixtures (Frings et al., 2011), as the open spaces near the container walls tend to be filled by finer grains from the size distribution.

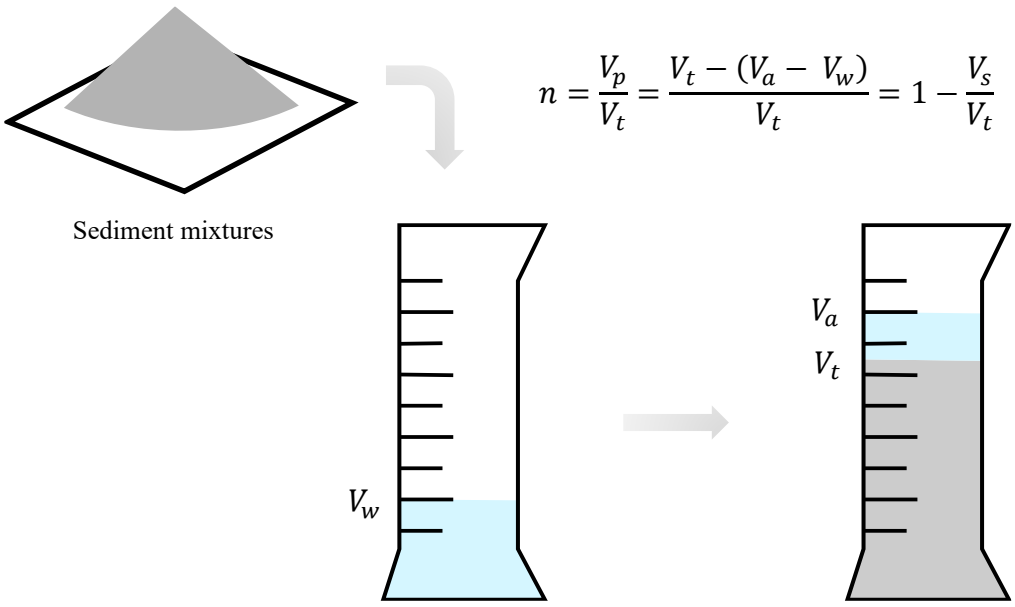

Figure 2.2. Schematic illustration of the water replacement method for measuring the porosity of fluvial sediment mixtures.

2.4 Porosity Simulations

In the past decades, numerical techniques have become more popular in the study of particle packing systems, advanced by robust computational algorithms and developments in the computer hardware industry. Accurate modeling of particle packing systems helps in understanding properties such as porosity. Packing simulation methods are classified into physics-based methods and non-physics-based methods.

2.4.1 Physics-based Method

Physics-based methods (PBMs) provide a way to model the packing systems by simulating particle interactions and capturing the underlying physics governing these interactions. The discrete element method (DEM) is perhaps the most widely used numerical method for studying particle packing systems, originally developed by Cundall and Strack (1979). DEM requires a certain overlap of particle geometries to determine the contact force explicitly. Intraparticle forces, such as normal and tangential contact forces, are calculated using a given penetration-force contact model, such as the Hertz-Mindlin model for normal contacts or the Mindlin-Deresiewicz model that computes tangential force. Particle motion is resolved by explicitly solving Newton's second law for translational (Eq. (2.1)) and rotational dynamics (Euler's Eq. (2.2)), with integration methods such as Verlet, velocity-Verlet or predictor-corrector.

$$m_i \frac{dv_i}{dt} = f_i^{ext} + \sum f_{ij}^{contact} \tag{2.1}$$

$$I_i \frac{d\omega_i}{dt} = T_i^{ext} + \sum T_{ij}^{contact} \tag{2.2}$$

where m_i is the mass of particle i, v_i is the translational velocity, I_i is the moment of inertia, ω_i is the angular velocity, f_i^{ext} and T_i^{ext} are external forces and torques, and $f_{ij}^{contact}$ and $T_{ij}^{contact}$ are contact forces and torques between particles i and j.

In DEM, particles are typically modeled as spheres or ellipsoids (e.g., An et al., 2011; Gan et al., 2016; Gan & Yu, 2020; Mori & Sakai, 2022), but more complex shapes can also be considered (Rettinger, et al., 2022b; Zhao et al., 2017). DEM requires small time steps to maintain numerical stability primarily due to the nature of the explicit time integration schemes and the need to accurately resolve particle interactions. While large-scale simulations involving millions of spherical particles have been performed, such as those by Horner et al. (2001), they are computationally very expensive. This is particularly true for simulations with large grain size ratios, where the timestep size often restricts both the spatial and temporal scales of the simulation.

Unlike DEM, which is based on the continuous integration of contact forces, non-smooth granular dynamics (NSGD) method, originally developed by Moreau (1977) and later Jean (1999), focuses on solving the problem in terms of contact constraints, making it particularly suitable for simulating systems with a large number of particles and rigid body dynamics. In NSGD, the contact between two particles i and j is governed by non-penetration and frictional constraints. For non-penetration:

$$g_{ij}(q) \geq 0 \tag{2.3}$$

where $g_{ij}(q)$ represents the gap distance between particles i and j. If $g_{ij}(q) = 0$, the particles are in contact.

The contact force $f_{ij}^{contact}$ must satisfy a Signorini condition:

$$0 \leq \lambda_{ij}^N \perp g_{ij}(q) \geq 0 \tag{2.4}$$

where λ_{ij}^N is the normal contact force, and $\perp$ denotes the complementarity condition: either there is a gap with zero force, or the particles are in contact with a force acting normally.

Frictional constraints are governed by Coulomb's friction law, which imposes a limit on the tangential force f_{ij}^T:

$$\| f_{ij}^T \| \leq \mu \lambda_{ij}^N \tag{2.5}$$

where μ is the coefficient of friction. This inequality constraint is also formulated as a complementarity problem.

NSGD does not explicitly resolve contact forces at every time step. Instead, it updates particle velocities to satisfy all constraints at each time step. A numerical solution algorithm is employed to ensure that all inequality constraints are met at the end of a time step, which involves solving a non-linear, and potentially over-determined, complementarity problem. Gauss-Jacobi and Gauss-Seidel methods are the preferred iterative solvers for this type of problem. Due to its implicit integration schemes, and non-smooth handling of collisions and contacts, NSGD allows for large time steps to maintain numerical stability. More details about the NSGD method can be found in Chapter 3.

Despite its more complex mathematical formulations in comparison to DEM, the NSGD approach is particularly well-suited for parallel processing, achieving high parallel efficiency (Preclik & Rüde, 2015). Similar to DEM, NSGD can accommodate a wide range of particle interactions, including dry friction, cohesive forces, cemented contacts, and compliant interactions (Radjaï & Dubois, 2011).

The PBMs, including both DEM and NSGD, have demonstrated great accuracy in reproducing the porosity of particle packing systems (e.g., Gan & Yu, 2020; Rettinger, et al., 2022b; Schruff et al., 2018).

2.4.2 Non-physics-based Method

While PBMs are commonly employed for modeling particle packing systems due to their ability to capture realistic interactions, non-physics-based methods (NPBMs) offer alternative approaches that are often more computationally efficient and conceptually simpler. Stochastic-based packing algorithms represent a typical class of NPBMs that utilize randomness and probabilistic processes to determine particle placement and arrangement. Examples of such methods include random sequential addition (RSA), ballistic deposition (BD), and Monte Carlo (MC) techniques. Among these, the random-walk algorithm proposed by Jia and Williams (2001) is one of the popular stochastic-based packing methods. This algorithm is designed to accommodate particles of arbitrary sizes and shapes within confined spaces of varying geometries.

In the random-walk algorithm, both the particles and the container are digitized and represented as a coherent collection of voxels. Unlike PBMs, the motion of particles in this method is not governed by physical forces; rather, it is entirely random. At each time step, a particle randomly moves one voxel in one of 26 possible translational directions, 6 orthogonal and 20 diagonal. This is followed by a rotational movement within a specified angular range until the rotation is impeded by the presence of another particle. Because both the container and the particles are voxelized, collision and overlap detection, normally the most time-consuming part of packing simulations, becomes significantly simplified. It can be efficiently performed by checking whether two particles occupy the same voxel sites at any given time. This voxel-based representation reduces

computational complexity and enables faster simulations for complex packing scenarios (see more in Chapter 4).

Another category of NPBMs for particle packing is optimization-based methods, which focus on finding optimal or near-optimal arrangements of objects within a given domain. These methods encompass a range of optimization techniques, including linear programming (LP), mixed-integer linear programming (MILP), and the nonlinear programming (NLP) algorithms (see Chapter 6). The optimization-based approach to packing problems requires the formulation of an objective function, such as maximizing packing density or minimizing potential energy, alongside a set of constraints that must be satisfied, such as non-overlapping conditions, boundary restrictions, or stability requirements.

The optimization problem is then solved using various techniques that can handle both the linear and nonlinear aspects of the objective functions and constraints. Commonly employed solvers include gradient-based approaches, interior-point methods, and sequential quadratic programming. These methods systematically explore the solution space to identify the most effective configurations that satisfy all imposed constraints. Optimization-based methods can address a wide range of packing problems, from arranging simple 2D and 3D geometric shapes such as rectangles, circles, and spheres, to dealing with more complex scenarios involving irregular shapes and mixed-size packing challenges (Birgin et al., 2016; Birgin & Lobato, 2019). However, they can be computationally expensive, especially for large-scale problems or problems with highly nonlinear constraints.

Unlike PBMs, NPBMs generally produce looser packings, which indicates higher porosity in particle packing simulations. This is particularly evident in stochastic-based methods (Liang et al., 2015; Sherwood, 1997).

2.5 Porosity Predictions

In-situ measurements, laboratory measurements, and numerical simulations all share the ability to directly evaluate porosity for specific cases, making them valuable sources of porosity data. However, field and laboratory studies require extensive sediment sampling, while numerical simulations need precise information about sediment properties, both of which are difficult to obtain on a large scale.

Given these constraints, mathematical porosity predictors have become an effective alternative. These predictors estimate porosity based on factors controlling sediment packing, such as grain size, grain shape, and depositional environment (leading to a loose or dense packing state). Current porosity predictors are generally classified into two categories: regression-based models and analytical models.

2.5.1 Regression-based Model

Regression-based models are created through statistical analysis by fitting mathematical formulas to specific datasets. Komura and Colby (1963) was the first to establish a relationship between median grain size (D_{50}, considered the characteristic parameter) and porosity (n) using fluvial sediments from various Japanese rivers. Similarly, Carling and Reader (1982) identified a clear correlation between D_{50} and porosity while studying the sedimentological properties of upland gravel-bedded streams in the U.K. Wu and Wang (2006) improved the correlation with D_{50} by modifying and adapting Komura and Colby's approach, based on existing literature data along with data from different reservoirs in China. Wooster et al. (2008) developed a relationship between logarithmic standard deviation (σ_φ) and porosity for unimodal sand-gravel mixtures using an exponential function. Frings et al. (2011) measured the porosity of fluvial sediment mixtures from the Rhine River and established a multivariate regression function involving σ_φ, the percentage of fines smaller than 0.5 mm ($f_{<0.5}$), and porosity. Table 2.1 lists the above-mentioned regression-based porosity predictors.

Table 2.1. Regression-based models for porosity prediction of fluvial sediment mixtures.

Ref	Statistical model	Application range
Komura and Colby (1963)	$n = 0.245 + \frac{0.0864}{(0.1D_{50})^{0.21}}$	$0.01 < D_{50} < 1000$ mm
Carling and Reader (1982)	$n = -0.0333 + \frac{0.4665}{(D_{50})^{0.21}}$	$5 < D_{50} < 200$ mm
Wu and Wang (2006)	$n = 0.13 + \frac{0.21}{(D_{50} + 0.002)^{0.21}}$	$10^{-3} < D_{50} < 100$ mm
Wooster et al. (2008)	$n = 0.621e^{-0.457\sigma_\varphi}$	$0.26 < \sigma_\varphi < 1.80$
Frings et al. (2011)	$n = 0.353 - 0.068\sigma_\varphi + 0.146f_{<0.5}$	$D = 0.02 - 125$ mm

While regression-based models are easy to apply due to their simple structure, their predictive accuracy is often unreliable outside the original study area. Research has indicated that the relationship between median grain size (D_{50}) and porosity fails to capture the observed variation in porosity. Although models based on logarithmic standard deviation (σ_φ) tend to perform better than those based on D_{50}, they still cannot account for the wide range of porosity values associated with a single σ_φ value, resulting in inaccurate porosity predictions for specific locations (Frings et al., 2011).

2.5.2 Analytical Model

Analytical models, in contrast, are established via theoretical frameworks that simulate the pairwise interactions among distinct particles and then combine them to obtain an estimation of the packing system's porosity. These methods mostly originate from industrial and engineering applications. Although some have been applied to packings

with distinct grain shapes, such as sphere-cylinder systems (Yu et al., 1996), the majority depend on grain size to differentiate the particles.

In general, analytical models are built up from an idealized binary mixture of spheres, where the size ratio ($r \in (0-1)$) between fine and coarse particles approaches zero, pioneered by Westman and Hugill (1930) and Furnas (1931) (see Fig. 2.3). In an ideal binary packing, small and large particles can be subject to two effects: filling and occupation. The filling effect occurs when fine particles percolate through the voids created by load-bearing coarse particles (seen on the right side in Fig. 2.3), while the occupation effect happens when coarse particles are scattered within a fine-grained matrix (seen on the left side in Fig. 2.3). Since neither interaction alters the structure of the mixture, they are later described as the unmixing effect (Yu & Standish, 1991). During the filling or occupation process, the porosity (n) of the ideal packing, i.e., the specific volume V ($= 1/(1-n)$, representing the reciprocal of packing density) to be more precise, decreases linearly as a function of the volume fraction of fine and coarse grains. Both linear functions provide an estimate for V, but only the higher estimate is correct (i.e., the solid lines in Fig. 2.3). A minimum porosity is achieved when the pore spaces among large grains is fully filled by fine particles.

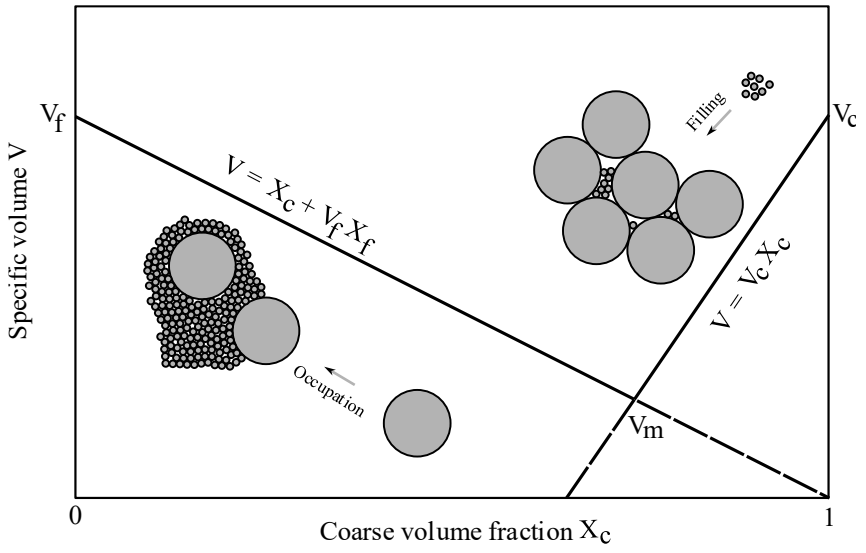

Figure 2.3. Schematic illustration of the ideal binary packing of spheres.

Given the linear relationship between V and X in an ideal two-fraction mixture, researchers assumed that the relationship between V and X in actual two- or multi-fraction mixtures would also be linear, which led to the development of linear packing models (LPMs) (e.g., Chang et al., 2015; Stovall et al., 1986; Yu & Standish, 1987). In LPMs, for each grain size fraction, a specific volume (V) value for its pairwise interaction with another grain is calculated iteratively, and the highest of these values is considered the correct one. During each iteration, the selected grain size is assumed as the dominant size forming the skeleton of the mixture. Grains larger than the dominant size fraction are

considered to have an occupation effect, reducing V (and porosity), while grains smaller than the dominant size faction are treated to reduce V through a filing effect. LPMs further evolved into non-linear packing models (NLPMs) when researchers realized that as the size ratio (r) between two components increases, the introduction of another particle can join the controlling component (the mixing effect) rather than simply filling or occupation. Such joint action causes the fabric of the original skeleton to change in a non-linear manner. Even with small size ratios, non-linear changes may still occur, such as by wedging of small particles between the large ones or by inducing a wall effect over the small particles (Dias et al., 2004; Kwan et al., 2013). The main difference from LPMs lies in the type of intraparticle interaction functions utilized, such as the quadratic and cubic terms introduced by Yu and Standish (1988), to account for the complex non-linear packing behavior.

However, most of these models are designed for binary (Chang & Deng, 2017; Kamann et al., 2007; Koltermann & Gorelick, 1995; Roquier, 2017; Westman, 1936; Wu & Li, 2017; Zhang et al., 2011) and ternary (Esselburn et al., 2011; Kwan et al., 2015; Perera et al., 2022) packing, with only a few capable of addressing large-component packing systems, such as those found in fluvial sediment mixtures (Chang & Deng, 2018; De Larrard, 1999; Liu et al., 2019; Yu & Standish, 1991). Among them, the linear-mixture packing model (LMPM) is the most popular one used for estimating the porosity of fluvial sediment mixtures (Yu & Standish, 1991). The LMPM takes into account both the linear and non-linear (mixture) interparticle interactions according to a critical-entrance ratio (r_c), typically set at 0.154. Above this ratio, particles experience a mixing effect, while below it, they undergo filling and occupation. The model has shown significant potential in estimating porosity for unimodal gravel deposits. However, for more complex sediment packings, such as bimodal gravel mixtures, this model tends to underpredict porosity (Frings et al., 2011; Rettinger et al., 2023), probably due to the rigid transition between mixing and unmixing interactions at the r_c value (more on this in Chapter 3).

While analytical models provide broader generality than the regression-based ones, there is a clear trend toward underestimation of porosity for complex or heterogeneous sediment packings. Besides, they are computationally rather complex, with the number of equations to be solved proportional to $4h^2$, with h being the number of grain size fractions.

2.6 Conclusions

Porosity is a fundamental property that remains poorly known on a large scale over the spatial variation of riverbeds. This chapter briefly reviews the endeavor that lasts almost a century aimed at the understanding of packing porosity. Various methods have been developed, each with its own cons and pros. Direct methods, including in-situ and laboratory measurements, as well as numerical simulations, can provide first-hand

estimates on porosity but are impractical for large-scale applications. Existing mathematical methods, on the other hand, struggle to produce accurate predictions due to the locality embedded in regression-based models and inappropriate assumptions underlying analytical ones. Nevertheless, mathematical models remain an appealing approach and have the potential to be leveraged on a broad scale. This leads to the main objective of this thesis: to establish an accurate, general, and simple porosity predictor, as explored in the following chapters.

References

Ackers, P., & White, W.R. (1973). Sediment transport: new approach and analysis. Journal of the Hydraulics Division, 99, 2041-2060.

Allen, J.R.L. (1985). Principles of physical sedimentology. George Allen & Unwin, London.

An, X., Yang, R., Dong, K., & Yu, A. (2011). DEM study of crystallization of monosized spheres under mechanical vibrations. Computer Physics Communications, 182(9), 1989-1994.

ASTM (2021 EDITION) Standard Test Methods for Density of Soil and Rock in Place by the Water Replacement Method in a Test Pit, D5030. American Society of Testing and Materials.

Athy, L.F. (1930). Density, Porosity, and Compaction of Sedimentary Rocks. AAPG Bulletin, 14(1), 1-24.

Bear, J. (1972). Dynamics of fluids in porous media. Elsevier, 764.

Birgin, E.G., & Lobato, R.D. (2019). A matheuristic approach with nonlinear subproblems for large-scale packing of ellipsoids. European Journal of Operational Research, 272(2), 447-464.

Birgin, E.G., Lobato, R.D., & Martínez, J. M. (2016). Packing ellipsoids by nonlinear optimization. Journal of Global Optimization, 65(4), 709-743.

Boulton, A.J., Findlay, S., Marmonier, P., Stanley, E.H., & Maurice Valett, H. (1998). The functional significance of the hyporheic zone in streams and rivers. Annual Review of Ecology and Systematics, 29, 59-81.

Carling, P.A., & Reader, N.A. (1982). Structure, composition and bulk properties of upland stream gravels. Earth Surface Processes and Landforms, 7(4), 349-365.

Chaikin, P.M., Donev, A., Man, W., Stillinger, F.H., & Torquato, S. (2006). Some Observations on the Random Packing of Hard Ellipsoids. Industrial and Engineering Chemistry Research, 45(21), 6960-6965.

Chanda, A., Pramanik, S., Chanda, A., & Pramanik, S. (2023). Effects of a thin vertical porous barrier on the water wave scattering by a porous breakwater. Physics of Fluids, 35(6), 062120.

Chang, C.S., & Deng, Y. (2017). A particle packing model for sand–silt mixtures with the effect of dual-skeleton. Granular Matter, 19(4), 1-15.

Chang, C.S., & Deng, Y. (2018). A nonlinear packing model for multi-sized particle mixtures. Powder Technology, 336, 449-464.

Chang, C.S., Wang, J. Y., & Ge, L. (2015). Modeling of minimum void ratio for sand–silt mixtures. Engineering Geology, 196, 293-304.

Chwang, A.T., & Chan, A.T. (1998). Interaction between porous media and wave motion. Annual Review of Fluid Mechanics, 30, 53-84.

Coleman, S.E., & Nikora, V.I. (2009). Exner equation: A continuum approximation of a discrete granular system. Water Resources Research, 45(9), 9421.

Cundall, P. A., & Strack, O.D.L. (1979). A discrete numerical model for granular assemblies. Géotechnique, 29, 47-65.

De Larrard, F. (1999). Concrete mixture proportioning: a scientific approach. Concrete Mixture Proportioning.

Delaney, G.W., Hilton, J.E., & Cleary, P.W. (2011). Defining random loose packing for nonspherical grains. Physical Review E, 83(5), 051305.

Dias, R.P., Teixeira, J.A., Mota, M.G., & Yelshin, A.I. (2004). Particulate binary mixtures: dependence of packing porosity on particle size ratio. Industrial and Engineering Chemistry Research, 43(24), 7912-7919.

Donev, A., Cisse, I., Sachs, D., Variano, E.A., Stillinger, F.H., Connelly, R., Torquato, S., & Chaikin, P.M. (2004). Improving the Density of Jammed Disordered Packings Using Ellipsoids. Science, 303(5660), 990-993.

Esselburn, J.D., Ritzi, R.W., & Dominic, D.F. (2011). Porosity and Permeability in Ternary Sediment Mixtures. Ground Water, 49(3), 393-402.

Frings, R.M., Gehres, N., Promny, M., Middelkoop, H., Schüttrumpf, H., & Vollmer, S. (2014). Today's sediment budget of the Rhine River channel, focusing on the Upper Rhine Graben and Rhenish Massif. Geomorphology, 204, 573-587.

Frings, R.M., Kirsch, F., & Schüttrumpf, H. (2012). The transition between gravel-bed rivers and sand-bed rivers. River Flow. Taylor and Francis, London, 629-634.

Frings, R.M., Kleinhans, M.G., & Vollmer, S. (2008). Discriminating between pore-filling load and bed-structure load: a new porosity-based method, exemplified for the river Rhine. Sedimentology, 55(6), 1571-1593.

Frings, R.M., Schüttrumpf, H., & Vollmer, S. (2011). Verification of porosity predictors for fluvial sand-gravel deposits. Water Resources Research, 47(7), 7525.

Furnas, C.C. (1931). Grading Aggregates: I—Mathematical Relations for Beds of Broken Solids of Maximum Density. Industrial and Engineering Chemistry, 23(9), 1052-1058.

Gan, J.Q., Yu, A.B., & Zhou, Z.Y. (2016). DEM simulation on the packing of fine ellipsoids. Chemical Engineering Science, 156, 64-76.

Gan, J.Q., & Yu, A. B. (2020). DEM study on the packing density and randomness for packing of ellipsoids. Powder Technology, 361, 424-434.

Hallenburg, J.K. (1998). Standard methods of geophysical formation evaluation (1st edition). CRC Press.

Han, B., & Endreny, T.A. (2014). River surface water topography mapping at sub-millimeter resolution and precision with close range photogrammetry: Laboratory scale application. IEEE Journal of Selected Topics in Applied Earth Observations and Remote Sensing, 7(2), 602-608.

Horner, D.A., Peters, J.F., & Carrillo, A. (2001). Large Scale Discrete Element Modeling of Vehicle-Soil Interaction. Journal of Engineering Mechanics, 127(10), 1027-1032.

Jean, M. (1999). The non-smooth contact dynamics method. Computer Methods in Applied Mechanics and Engineering, 177, 235-257.

Jia, X., & Williams, R.A. (2001). A packing algorithm for particles of arbitrary shapes. Powder Technology, 120(3), 175-186.

Kamann, P.J., Ritzi, R.W., Dominic, D.F., & Conrad, C.M. (2007). Porosity and Permeability in Sediment Mixtures. Groundwater, 45(4), 429-438.

Klute, A. (1986). Methods of Soil Analysis: Part 1 Physical and Mineralogical Methods. In Methods of Soil Analysis, Part 1: Physical and Mineralogical Methods (Second Edition). American Society of Agronomy, USA.

Koltermann, C.E., & Gorelick, S.M. (1995). Fractional packing model for hydraulic conductivity derived from sediment mixtures. Water Resources Research, 31(12), 3283-3297.

Komura, S., & Colby, B.R. (1963). Discussion of "Sediment Transportation Mechanics: Introduction and Properties of Sediment, Progress Report by the Task Committee on Preparation of Sedimentation Manual of the Committee on Sedimentation of the Hydraulics Division." Journal of the Hydraulics Division, 89(1), 263-268.

Kwan, A.K.H., Chan, K.W., & Wong, V. (2013). A 3-parameter particle packing model incorporating the wedging effect. Powder Technology, 237, 172-179.

Kwan, A.K.H., Wong, V., & Fung, W.W.S. (2015). A 3-parameter packing density model for angular rock aggregate particles. Powder Technology, 274, 154-162.

Liang, R., Schruff, T., Jia, X., Schüttrumpf, H., & Frings, R.M. (2015). Validation of a stochastic digital packing algorithm for porosity prediction in fluvial gravel deposits. Sedimentary Geology, 329, 18-27.

Liu, Z.R., Ye, W.M., Zhang, Z., Wang, Q., Chen, Y.G., & Cui, Y.J. (2019). A nonlinear particle packing model for multi-sized granular soils. Construction and Building Materials, 221, 274-282.

Lokin, L.R., Warmink, J.J., & Hulscher, S.J.M.H. (2023). The Effect of Sediment Transport Models on Simulating River Dune Dynamics. Water Resources Research, 59(12), 34607.

Man, W., Donev, A., Stillinger, F.H., Sullivan, M.T., Russel, W.B., Heeger, D., Inati, S., Torquato, S., & Chaikin, P.M. (2005). Experiments on random packings of ellipsoids. Physical Review Letters, 94(19).

Moreau, J.J. (1977). Evolution problem associated with a moving convex set in a Hilbert space. Journal of Differential Equations, 26(3), 347-374.

Mori, Y., & Sakai, M. (2022). Advanced DEM simulation on powder mixing for ellipsoidal particles in an industrial mixer. Chemical Engineering Journal, 429.

Noack, M., Ortlepp, J., & Wieprecht, S. (2017). An Approach to Simulate Interstitial Habitat Conditions During the Incubation Phase of Gravel-Spawning Fish. River Research and Applications, 33(2), 192-201.

Nolan, G.T., & Kavanagh, P.E. (1992). Computer simulation of random packing of hard spheres. Powder Technology, 72(2), 149-155.

Núñez-González, F., Martín-Vide, J.P., & Kleinhans, M.G. (2016). Porosity and size gradation of saturated gravel with percolated fines. Sedimentology, 63(5), 1209-1232.

Perera, C., Wu, W., & Knack, I. (2022). Porosity of bimodal and trimodal sediment mixtures. International Journal of Sediment Research, 37(2), 258-271.

Ping, X., Jin, M., & Xian, Y. (2020). Effect of bioclogging on the nitrate source and sink function of a hyporheic zone. Journal of Hydrology, 590, 125425.

Preclik, T., & Rüde, U. (2015). Ultrascale simulations of non-smooth granular dynamics. Computational Particle Mechanics, 2(2), 173-196.

Radjaï, F., & Dubois, F. (2011). Discrete-element modeling of granular materials. ISTE，Wiley.

Rettinger, C., Eibl, S., Rüde, U., & Vowinckel, B. (2022a). Rheology of mobile sediment beds in laminar shear flow: effects of creep and polydispersity. Journal of Fluid Mechanics, 932, A1.

Rettinger, C., Rüde, U., Vollmer, S., & Frings, R.M. (2022b). Effect of sediment form and form distribution on porosity: a simulation study based on the discrete element method. Granular Matter, 24(4), 1-23.

Rettinger, C., Tabesh, M., Rüde, U., Vollmer, S., & Frings, R.M. (2023). On the use of packing models for the prediction of fluvial sediment porosity. Earth Surface Dynamics, 11(6), 1097-1115.

Ridgway, K., & Tarbuck, K.J. (1968). Voidage fluctuations in randomly-packed beds of spheres adjacent to a containing wall. Chemical Engineering Science, 23(9), 1147-1155.

Roquier, G. (2017). The 4-parameter Compressible Packing Model (CPM) for crushed aggregate particles. Powder Technology, 320, 133-142.

Sawyer, A.H., & Cardenas, M.B. (2009). Hyporheic flow and residence time distributions in heterogeneous cross-bedded sediment. Water Resources Research, 45(8).

Schruff, T., Liang, R., Rüde, U., Schüttrumpf, H., & Frings, R.M. (2018). Generation of dense granular deposits for porosity analysis: assessment and application of large-scale non-smooth granular dynamics. Computational Particle Mechanics, 5(1), 59-70.

Scott, G.D. (1960). Packing of Spheres: Packing of Equal Spheres. Nature 1960, 188, 908-909.

Seitz, L., Haas, C., Noack, M., & Wieprecht, S. (2018). From picture to porosity of river bed material using Structure-from-Motion with Multi-View-Stereo. Geomorphology, 306, 80-89.

Sherwood, J.D. (1997). Packing of spheroids in three-dimensional space by random sequential addition. Journal of Physics A: Mathematical and General, 30, 839-843.

Song, C., Wang, P., & Makse, H.A. (2008). A phase diagram for jammed matter. Nature, 453, 629-632.

Stovall, T., de Larrard, F., & Buil, M. (1986). Linear packing density model of grain mixtures. Powder Technology, 48(1), 1-12.

Tabesh, M., Hoffmann, T., Vollmer, S., Schüttrumpf, H., & Frings, R.M. (2019). In-situ measurement of river-bed sediment porosity using Structure-from-Motion image analysis. Geomorphology, 338, 61-67.

Tabesh, M., Vollmer, S., Schüttrumpf, H., & Frings, R.M. (2022). Spatial variability in river bed porosity determined by nuclear density gauging: A case study from a French gravel-bed river. Sedimentology, 69(2), 823-844.

Ting, C.L., Lin, M.C., & Cheng, C.Y. (2004). Porosity effects on non-breaking surface waves over permeable submerged breakwaters. Coastal Engineering, 50(4), 213-224.

Torquato, S., Truskett, T.M., & Debenedetti, P.G. (2000). Is Random Close Packing of Spheres Well Defined? Physical Review Letters, 84, 2064.

Vollmer, S., & Kleinhans, M.G. (2007). Predicting incipient motion, including the effect of turbulent pressure fluctuations in the bed. Water Resources Research, 43(5), 5410.

Westman, A.E.R. (1936). The packing of particles: empirical equations for intermediate diameter ratios. Journal of the American Ceramic Society, 19, 127-129.

Westman, A.E.R., & Hugill, H.R. (1930). The packing of particles. Journal of the American Ceramic Society, 13(10), 767-779.

Wilcock, P.R. (1998). Two-Fraction Model of Initial Sediment Motion in Gravel-Bed Rivers. Science, 280, 410-412.

Williams, S.R., & Philipse, A.P. (2003). Random packings of spheres and spherocylinders simulated by mechanical contraction. Physical Review E, 67(5), 051301.

Wooster, J.K., Dusterhoff, S.R., Cui, Y., Sklar, L.S., Dietrich, W.E., & Malko, M. (2008). Sediment supply and relative size distribution effects on fine sediment infiltration into immobile gravels. Water Resources Research, 44(3), 3424.

Wu, W., & Li, W. (2017). Porosity of bimodal sediment mixture with particle filling. International Journal of Sediment Research, 32(2), 253-259.

Wu, W., & Wang, S.S.Y. (2006). Formulas for sediment porosity and settling velocity. Journal of Hydraulic Engineering, 132(8), 858-862.

Yan, Y., Zhang, L., Luo, X., Li, C., & Hu, F. (2018). A new method for calculating the primary porosity of unconsolidated sands based on packing texture: Application to modern beach sand. Marine and Petroleum Geology, 98, 384-396.

Yu, A.B., & Standish, N. (1987). Porosity calculations of multi-component mixtures of spherical particles. Powder Technology, 52(3), 233-241.

Yu, A.B., & Standish, N. (1988). An analytical—parametric theory of the random packing of particles. Powder Technology, 55(3), 171-186.

Yu, A.B., & Standish, N. (1991). Estimation of the porosity of particle mixtures by a linear-mixture packing model. Industrial and Engineering Chemistry Research, 30(6), 1372-1385.

Yu, A.B., Zou, R.P., & Standish, N. (1996). Modifying the Linear Packing Model for Predicting the Porosity of Nonspherical Particle Mixtures. Industrial & Engineering Chemistry Research, 35(10), 3730-3741.

Zhang, Z.F., Ward, A.L., & Keller, J.M. (2011). Determining the Porosity and Saturated Hydraulic Conductivity of Binary Mixtures. Vadose Zone Journal, 10(1), 313-321.

Zhao, B., An, X., Wang, Y., Qian, Q., Yang, X., & Sun, X. (2017). DEM dynamic simulation of tetrahedral particle packing under 3D mechanical vibration. Powder Technology, 317, 171-180.

Zou, R.P., & Yu, A.B. (1996). Evaluation of the packing characteristics of mono-sized non-spherical particles. Powder Technology, 88, 71-79.

3

A Binary-Unit Conceptual Packing Model

The porosity of fluvial sediments is significant to virtually every inquiry into the riverbed. In this study, we propose a novel porosity predictor, namely the binary-unit conceptual (BUC) packing model, that is both simple and general to use. The core of the BUC model is based on a newly proposed binary-unit concept, which enables to transform any multi-sized (or continuous) sediment mixture into an equivalent binary-unit mixture through the link of identical grain size statistics of mean, standard deviation and skewness. It was found that the binary-unit mixture can be viewed as the most elementary packing unit that embodies the equivalent particle-particle interactions in the original mixture. With this concept, the porosity of fluvial sediments, no matter how labyrinthine their grain size distributions are, can be readily computed through the utilization of models capable of predicting the porosity of a binary particle packing. The Westman equation is highly recommended as the prime option for this purpose. Remarkable outcomes were achieved in the validation against a range of sediment mixtures generated through numerical simulations and laboratory experiments, producing a root-mean-square error of 0.01 ~ 0.03. In comparison to other analytical models, the BUC model surpassed them with both efficiency and accuracy.

3.1 Introduction

Porosity, a key property of fluvial sediments, is defined as the ratio of pore volume to total volume. The porosity of fluvial sediments is significant to many investigations associated with riverbeds. At surface riverbeds, porosity acts as a critical input in the computation of sediment concentration, dictating the rate of bed level changes (Coleman & Nikora, 2009; Frings et al., 2008; Núñez-González et al., 2016). Additionally, porosity affects the mobility of particles, as being a parameter in various sediment transport equations (Ackers & White, 1973; Rettinger et al., 2022a; Vollmer & Kleinhans, 2007). Sub-surface riverbeds, on the other hand, present a different set of challenges, where porosity governs the void space of the hyporheic zone that harbors aquatic organisms. It also exerts significant control on the permeability of the hyporheic zone, which, in turn, regulates the rate of water exchange, oxygen, nutrient supply, and pollutant removal, crucial factors for the sustainability of a healthy aquatic environment (Boulton et al., 1998; Noack et al., 2017; Sawyer & Cardenas, 2009).

The current information of riverbed porosity is scarce, despite its important role in riverbed-related research. The primary reason is that riverbeds are often inundated by surging waters of the river itself, hampering the use of remote monitoring techniques, and rendering direct field measurements both costly and arduous. In order to obtain the porosity of sediment packings, researchers have proposed an alternative method that relies on estimates from a host of factors governing porosity. These factors are mainly identified as grain size, grain shape, and depositional condition (leading to a loose or dense packing state) (Chang et al., 2018; Fraser, 1935; Gaither, 1953; Liang et al., 2015; Rettinger, et al., 2022b; Tabesh et al., 2019, 2022). At present, the available porosity predictors can be broadly sorted into two categories: regression-based models and analytical models.

Regression-based models are a mere outcome of statistical analysis via the fitting process on a specific dataset. These models usually take on the form of a concise mathematical formula, requiring a minimal amount of information regarding the system, thus making them easily implementable. As demonstrated by Carling and Reader (1982), Wu and Wang (2006), and Wooster et al. (2008), porosity is formulated with either median grain size or logarithmic standard deviation. Similarly, Frings et al. (2011) developed a porosity predictor that combines two grain size characteristics: logarithmic standard deviation and the percentage of fine grains smaller than 0.5 mm. Despite the apparent simplicity of these models, their predictive quality is often insufficient when utilized in regions outside of the original dataset (Frings et al., 2011).

On the other hand, analytical models emerge through a theoretical framework that conceptualizes the packing system as a finite ensemble of distinct particle classes. These models, in turn, simulate the interclass pairwise particle interactions which are amalgamated to infer the system's porosity. These models are typically derived from the

study of binary mixtures of spheres, and then extrapolated to encompass arbitrary mixtures (Chang & Deng, 2018; De Larrard, 1999; Liu et al., 2019; Stovall et al., 1986; Yu & Standish, 1991). Although such models are endowed with greater generality and flexibility than the regression-based ones, their implementation requires a considerable number of parameters as input, making them difficult to apply and computationally burdensome.

In this context, the objective of this study was to develop a novel porosity predictor that is both straightforward and generally applicable. To achieve this, the Westman equation (Westman, 1936), developed to estimate porosity for binary mixtures of spheres, was employed as a solid foundation for establishing our model, namely the binary-unit conceptual (BUC) packing model. Unlike the traditional analytical models that expand into complex models to suit multi-component mixtures, our approach reverses this process by compressing the multi-component mixture into a binary-unit packing. Following a description of the Westman equation in section 3.2, we explicate how to develop the binary-unit conceptual packing model based on the Westman equation in section 3.3. Then, we validate our model using datasets from different sources in section 3.4, followed by discussion and conclusions (sections 3.5 & 3.6).

3.2 The Westman Equation

The Westman equation is a simple conic equation that possesses the ability to provide a broad estimation of porosity for binary packing systems of spherical particles (Westman, 1936). It is worth mentioning that the use of specific volume, which represents the reciprocal of packing density, in its expression is a numerically convenient tactic that streamlines the governing equations into linear forms at extreme cases, shown below:

$$\left(\frac{V - V_c X_c}{V_f}\right)^2 + 2G\left(\frac{V - V_c X_c}{V_f}\right)\left(\frac{V - X_c - V_f X_f}{V_c - 1}\right) + \left(\frac{V - X_c - V_f X_f}{V_c - 1}\right)^2 = 1 \quad (3.1)$$

Where V represents the total specific volume, which can be easily converted to the total porosity (n) by $n = 1 - 1/V$. V_c and V_f are the initial specific volume of the coarser and finer particles separately, with X_c, X_f being the volume percentage of the coarser and finer components that satisfy the constraint $X_c + X_f = 1$.

The coefficient G in Eq. (3.1) is the only unknown parameter, which was later found to be dependent solely on the size ratio r $(= d_f/d_c)$ between finer and coarser particles (Yu et al., 1993):

$$\frac{1}{G} = \begin{cases} 1.355\, r^{1.566} & (r \le 0.824) \\ 1 & (r > 0.824) \end{cases} \quad (3.2)$$

Then, the Westman equation can be solved analytically by rewriting it in the form of a quadratic equation with its positive square root being the solution:

$$V = \frac{-B + \sqrt{B^2 - 4AC}}{2A} \tag{3.3}$$

Where

$$A = \left(\frac{1}{V_f}\right)^2 + \frac{2G}{V_f(V_c - 1)} + \frac{1}{(V_c - 1)^2}$$

$$B = -\frac{2V_cX_c}{(V_f)^2} + \frac{2G}{V_f(V_c - 1)}(V_fX_c - V_f - X_c - V_cX_c) + \frac{2(V_fX_c - V_f - X_c)}{(V_c - 1)^2}$$

$$C = \left(\frac{V_cX_c}{V_f}\right)^2 - \frac{2G}{V_f(V_c - 1)}V_cX_c(V_fX_c - V_f - X_c) + \left(\frac{(V_fX_c - V_f - X_c)^2}{(V_c - 1)^2}\right) - 1$$

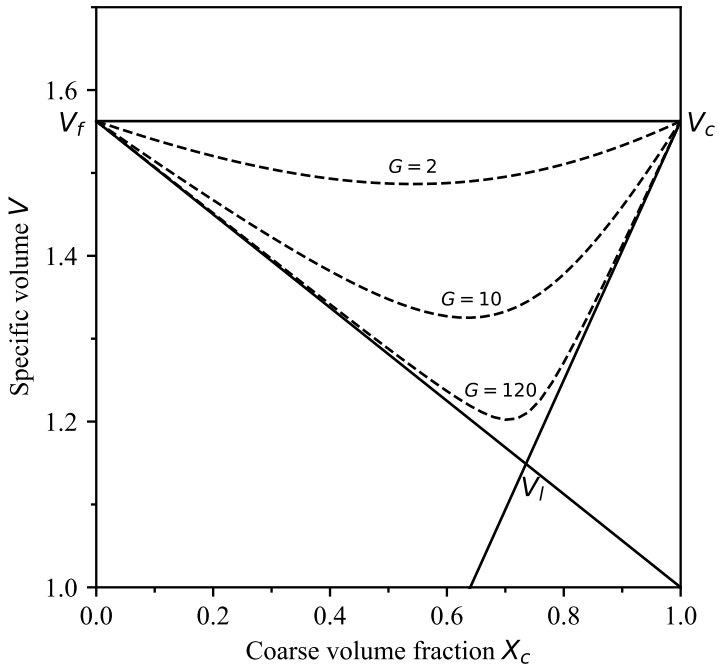

Figure 3.1. Graphical representation of the Westman equation.

Fig. 3.1 shows the Westman equation visually by setting the initial specific volume of each component to be equal to 1.56, i.e., $n = 0.36$, representing a random dense packing state of spheres (Song et al., 2008). It should be noted that the initial specific volume of each component remains unchanged during the entire mixing process, which is the underlying assumption in the Westman equation.

When $G = 1$, i.e., the two components have the same diameter, the Westman equation resolves itself into a linear equation (line $V_f V_c$), showing no shrinkage on mixing.

$$V = V_c X_c + V_f X_f \tag{3.4}$$

When $G = \infty$, i.e., the coarse particles with a diameter infinitely larger than that of the fines, the Westman equation simplifies into the linear form:

$$V = X_c + V_f X_f \tag{3.5}$$

$$V = V_c X_c \tag{3.6}$$

Eq. (3.5) represents the line connecting V_f to the right corner of the diagram. It reflects the occupation process when adding coarse particles into a matrix of fines, the coarse particles are immersed in the fines, reducing the specific volume (or porosity) by occupying with solid volumes. Eq. (3.6) indicates the line connecting V_c to the origin point at the left side of the diagram. It reflects the filling process when adding fine particles into a framework of coarse particles, the fines percolate through the pores, reducing the specific volume (or porosity) by filling the voids among large particles. The intersection point, V_l, of the two straight lines produces the lowest value of the specific volume (or porosity) when the fines fully fill in the voids of the coarse particles. The shape triangle, $V_f V_l V_c$, forms the boundary (limiting cases) for the entire packing scenarios of binary mixtures.

When $1 < G < \infty$, i.e., for size ratios intermediate within the above limits, the Westman equation takes its whole form, exhibiting a festoon-like curve across the values of specific volume. As G becomes larger, or the size ratio r gets smaller, the curve becomes steeper, suggesting more shrinkage on mixing as shown in Fig. 3.1.

3.3 The Binary-Unit Conceptual Packing Model

In this section, we show how to establish the binary-unit conceptual (BUC) packing model with the foundation of the Westman equation. To do so, we re-evaluated the three dominant factors that govern the specific volume of a binary mixture: initial specific volume, coefficient G, and fractional solid volume. These factors were originally proposed to depict only binary components, which cannot be directly applied to multiple or continuous components. Therefore, a hypothesis was proposed that if the three factors could be revamped in connection with arbitrary components, the Westman equation should be empowered to estimate the porosity of arbitrary mixtures in a general manner.

To tackle this task, we viewed the three factors from a different perspective. The initial specific volume, which mirrors the initial packing state of each component, essentially depicts the final packing state of a binary mixture since it remains unchanged throughout

the mixing process (underlying assumption). The coefficient G, which is influenced by size ratio, roughly indicates the degree of dispersion of the two components' sizes, while the fractional solid volume highlights the asymmetry (or imbalance) of the two components in terms of volume content. After reconsidering these factors, it was expected that the coefficient G and fractional solid volume could be substituted reasonably by standard deviation and skewness, which statistically reflect the dispersion and asymmetry of any grain constituents involved in a packing.

With this in mind, we proceeded to perform the statistical calculations with respect to the coefficient G and the fractional solid volume, and subsequently visualized our findings (Fig. 3.2). The outcome shows that the logarithmic skewness (SK_ϕ) is only determined by the percentage of the coarser particle (X_c) with no impact from the coefficient G (i.e., the grain size ratio), providing a one-to-one corresponding relationship where as X_c varies from 0 to 1, SK_ϕ traverses from negative infinity to positive infinity (Fig. 3.2a). Taking nine SK_ϕ values from -2.67 to 2.67 for illustration (corresponding to X_c values from 0.1 to 0.9, at 0.1 step), the coefficient G depicts a discernable correlation with the logarithmic standard deviation (σ_ϕ) under various SK_ϕ settings. Specifically, the σ_ϕ value increases as the coefficient G increases, with identical absolute values of SK_ϕ (i.e., $\pm SK_\phi$) resulting in identical σ_ϕ values (Fig. 3.2b).

The logarithmic method of moments (Blott & Pye, 2001) was used to calculate the statistics shown as:

$$\mu_\phi = \sum f x_\phi \tag{3.7}$$

$$\sigma_\phi = \sqrt{\sum f(x_\phi - \mu_\phi)^2} \tag{3.8}$$

$$SK_\phi = \frac{\sum f(x_\phi - \mu_\phi)^3}{(\sigma_\phi)^3} \tag{3.9}$$

Where μ_ϕ is the logarithmic mean. f represents the weights, i.e., the factional solid volume in this case, while x_ϕ denotes the particle size in phi unit.

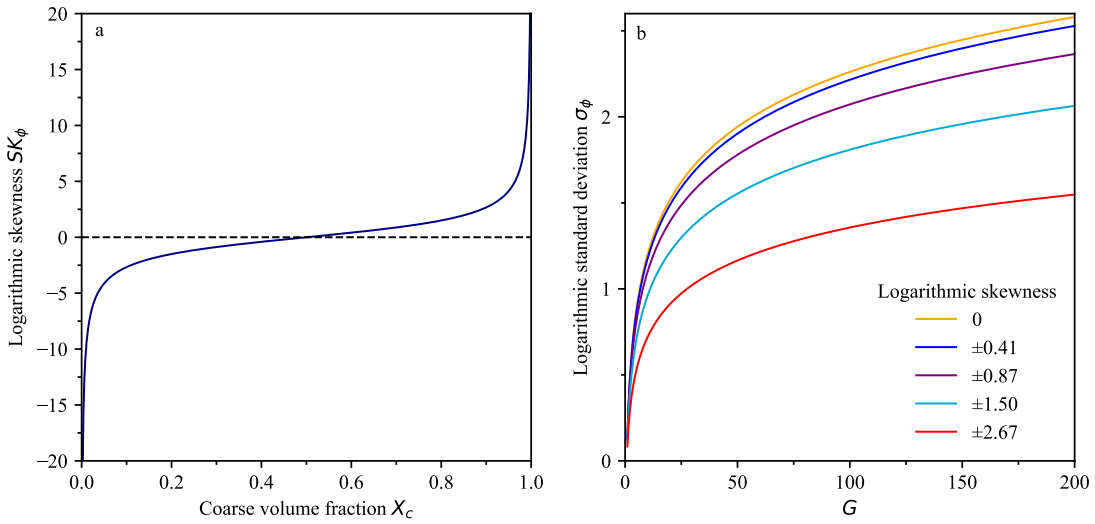

Figure 3.2. Relationship between (a) coarse volume fraction (X_c) and logarithmic skewness (SK_ϕ), (b) the coefficient G and logarithmic standard deviation (σ_ϕ).

It is noteworthy that we employed logarithmic statistical measures of mean, standard deviation and skewness, the commonly used scale for characterizing natural sediments. However, the application of other statistical scales, such as the arithmetic or geometric ones, is also viable, providing commensurate trends with their respective calculations.

Realizing the existence of such relationships, the Westman equation scheme can be reconfigured. Fig. 3.3 (a) replots the Westman equation using SK_ϕ as the x-axis, with vertical dotted lines indicating the change of specific volume as σ_ϕ shifts. Fig. 3.3 (b & c) show exactly how the specific volume (or porosity) shift with σ_ϕ along these vertical dotted lines. It is thus convinced that initial specific volume, logarithmic standard deviation, and logarithmic skewness can be viewed as the equivalent factors controlling the specific volume (or porosity) for any binary mixture of spheres.

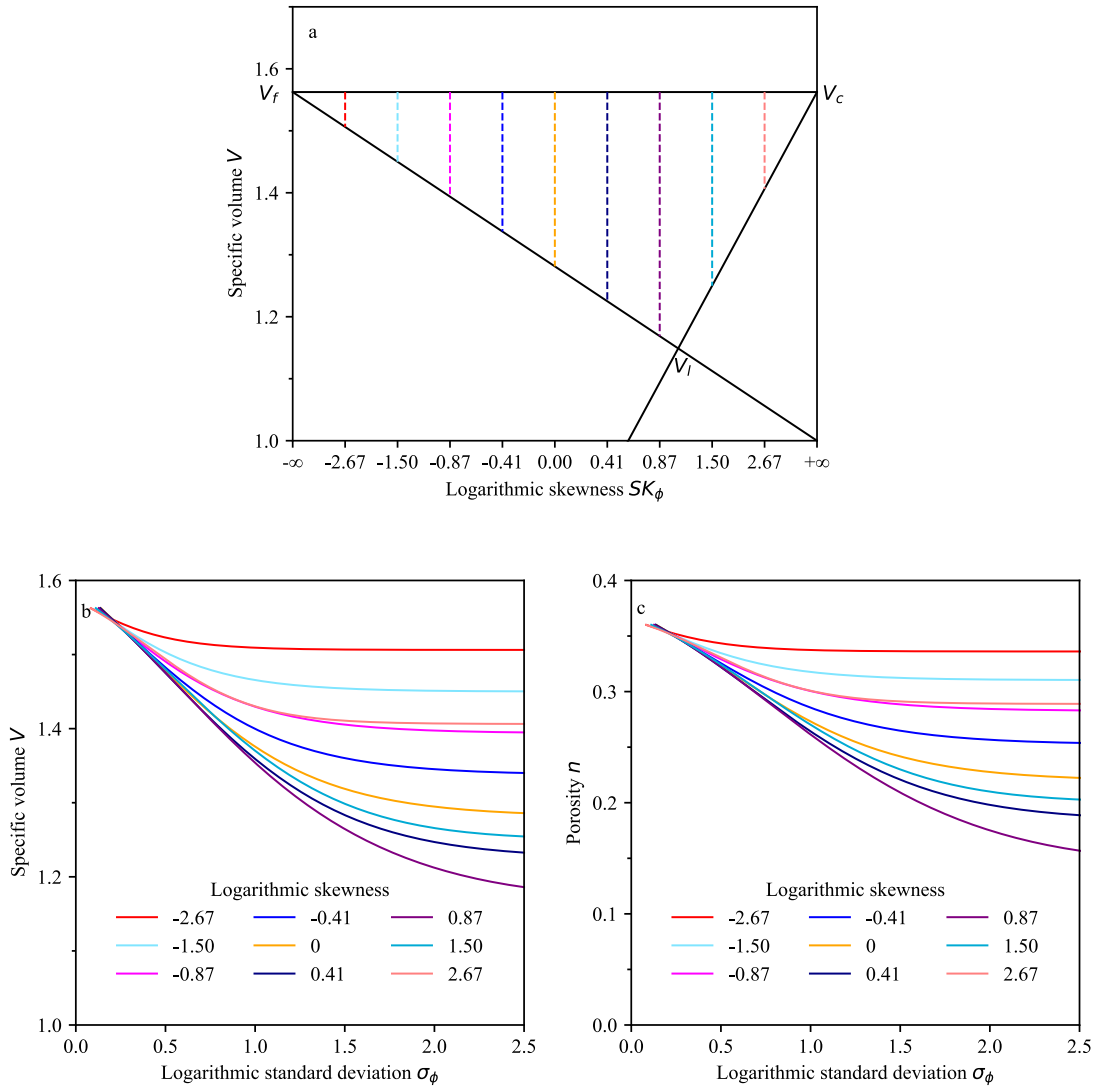

Figure 3.3. An equivalent graphical representation of the Westman equation delineating how specific volume or porosity varies in terms of logarithmic standard deviation (σ_ϕ) and logarithmic skewness (SK_ϕ).

Specifically, as shown in Fig. 3.3 (c), all the curves exhibit a decrease trend in porosity with an increase of σ_ϕ, which is not surprising, since σ_ϕ determines the width of the grain size distribution and hence, the intensity of the joint action among particles (i.e., the mixing effect). Although the correlation between σ_φ and porosity is quite straightforward, their relation with SK_ϕ is considerably more complex. When SK_φ possesses the same absolute value, negatively skewed ($+SK_\phi$) grain size distributions generally exhibit a lower porosity than their positively skewed counterparts. This is because the former encompasses a greater quantity of coarse particles, where the filling effect is dominating that diminishes the pore volume more efficiently than the occupation

effect, which is predominant in the latter. However, when SK_ϕ has different absolute values, this trend dissipates, as porosity does not vary linearly with SK_ϕ. For instance, the curve with a SK_ϕ of 2.67 that should rightfully occupy the base of the other curves within the trend, instead resides in the third place. This observation signifies that a grain size distribution with a more substantial proportion of larger particles does not necessarily guarantee a higher degree of filling effect, due to the paucity of smaller particles that are required to facilitate introduction. In fact, the order of the curves of different SK_ϕ values follow roughly with the order of their distance to the particular value of SK_ϕ ($= 1.067$ in this case) producing the lowest porosity where the particle-particle interactions are most intensive (Fig. 3.3a&c)).

According to the aforementioned hypothesis, the Westman equation should be applicable to arbitrary mixtures, with an assumption that all the components in the ultimate mixture are packed at the same level. In other words, the initial specific volume (or porosity) for each component should be taken equally to reflect the average packing level.

In the quest to compute the porosity of arbitrary mixtures, one may attempt to establish the explicit mathematical form of the relationship shown in Fig. 3.3 (c), but this endeavor is far from straightforward and may prove infeasible due to the interdependence of many parameters. Alternatively, a binary-unit concept is proposed here. It refers to that any multi-sized (or continuous) spherical packing system can be transformed into an equivalent binary spherical packing system, through the link of the identical grain size statistics of mean, standard deviation and skewness. By inverting Eqs. (3.7-3.9), one can derive the sizes of the equivalent binary-unit mixture as well as their respective proportions from the input data on mean, standard deviation, and skewness of the original mixture. Again, there is no restrictions on the scales used for statistics. Analytical solution of these equations is theoretically possible, but numerical analysis may be more straightforward, requiring specification of rational initial values for the sizes of the two components and one of their proportions, as well as a termination tolerance which is normally set as $1e^{-8}$ to ensure highly accurate outcomes. More details on the binary-unit concept are discussed in section 3.5.2.

With the proposed binary-unit concept, alongside the Westman equation, the so-called binary-unit conceptual (BUC) packing model has been established that should be able to estimate the porosity of any arbitrary mixtures of spherical particles.

3.4 Validation of the BUC Packing Model

3.4.1 Validation against Binary Mixtures

As the BUC packing model is built upon the Westman equation, it is essential to verify the Westman equation in the first place. Through a search of literatures reporting datasets

related to binary packings of spherical particles, we found a considerable amount of 189 experimental measurements to verify the Westman equation. Specifically, these datasets (extracted from Dias et al., 2004; Mcgeary, 1961; Mota et al., 2001; Westman & Hugill, 1930; Yerazunis et al., 1965; Yu et al., 1992) cover binary packings with a wide range of size ratios, containing diverse materials, and varying in stage from loosely to densely packed.

To evaluate porosity estimates quantitatively, the squared Pearson correlation coefficient (R^2) and the root-mean-square error ($RMSE$) are calculated as follows:

$$R^2 = \left(\frac{\sum(x_i - \bar{x})(y_i - \bar{y})}{\sqrt{\sum(x_i - \bar{x})^2}\sqrt{\sum(y_i - \bar{y})^2}} \right)^2 \tag{3.10}$$

$$RMSE = \sqrt{\frac{\sum(x_i - y_i)^2}{N}} \tag{3.11}$$

Where N is sample size. x_i, y_i are the individual sample points, i.e., the measured and estimated porosity values in this case while $\bar{x}$, $\bar{y}$ are the means of sample x_i and y_i respectively.

The metric R^2 normally spanning from 0 to 1, reflects the magnitude of the linear correlation between two datasets. A greater value of R^2 stands for a stronger linear correlation between the two sets. Meanwhile, $RMSE$, a non-negative quantity, measures the dissimilarities between predicted and actual values. In evaluating models, a lower $RMSE$ value is superior, as it suggests better overall performance.

Upon visualization of the comparison results (Fig. 3.4), the Westman equation is remarkably successful at estimating porosity of binary packings of spherical particles, boasting a high R^2 score of 0.947 and a low $RMSE$ value of 0.012.

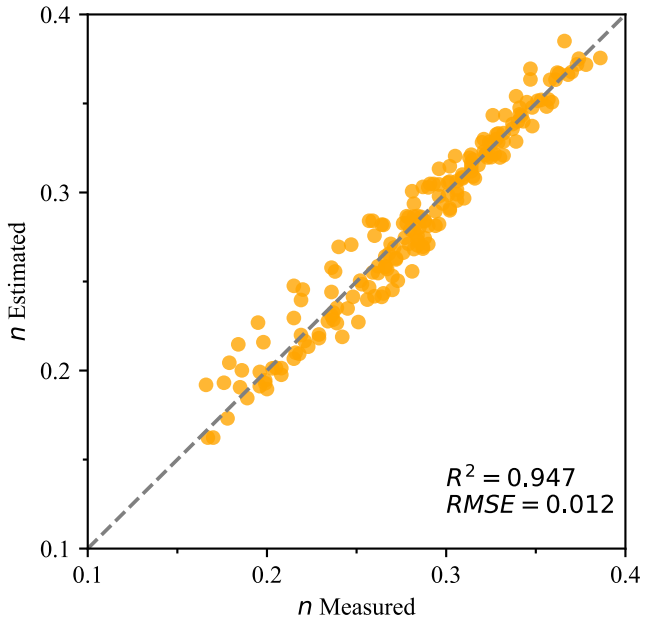

Figure 3.4. Comparison of the measured and estimated porosity for 189 spherical binary packings.

3.4.2 Validation against Multi-component Mixtures

3.4.2.1 Dataset from Numerical Simulations

In this study, multi-component mixtures of digital sediment deposits were simulated, with the aim of comparing their porosity values against those estimated by the BUC packing model. The numerical simulations were conducted using the non-smooth granular dynamics (NSGD) algorithm, following the pioneering work of Schruff et al. (2018), who had extensively validated the NSGD algorithm by producing promising results in porosity prediction of large granular systems. Here, we merely provide a brief summary of the features and particulars of the numerical method and the simulation setup, and direct the reader to peruse the original work for a comprehensive discussion of all components thereof.

NSGD Algorithm

The NSGD algorithm used herein is implemented in the open-source waLBerla framework for multi-physics simulations (Bauer et al., 2021). The basic principle of the NSGD method can be viewed as a global numerical treatment of non-smooth and multi-contact granular systems at the scale of particle rearrangements in which their micro-dynamics are neglected. Interactions between particles are modeled with hard contact laws that are subject to inequality constraints in order to eliminate the necessity of resolving small elastic responses. Consequently, reaction forces from collisions are impulsive, resulting in velocity discontinuities or jumps during time-stepping evolution. For such a non-smooth motion, second or higher order integrators for smooth (continuous)

motions are unhelpful, and instead first order integrators of the discrete-time Newton-Euler equations of dynamics are applied. Solving the multi-contact dynamical granular system entails the simultaneous fulfillment of inequality constraints given by all potential contacts at each time step. This is an incredibly complex mathematical task that requires the use of iterative methods. In the present work, the non-linear block Gauss-Seidel algorithm (Preclik & Rüde, 2015) was utilized to solve this challenging problem. The algorithm uses a mild under-relaxation value ($0 < w < 1$) to calculate a weighted mean between the approximation of the previous and new iteration. A value of 0 means only the approximation of the previous iteration is taken into account, while a value of 1 means the current approximation is of consideration. Each iteration procedure yields an updated set of contact reaction impulses and velocities that may give rise to new violations of inequality constraints at all potential contacts. Iterations proceed until the violations are less than a prescribed precision threshold or the maximum number of iterations is surpassed.

Simulation Setup

The formation of digital packings was simulated by rain-dropping a certain number of particles at a certain height into a box container with periodic boundaries along the lateral x and y axes (z axis pointing upward) and a solid plane at the bottom (at $z = 0$). To ensure the complete randomness of the process, the particles, with varying sizes, were systematically introduced at regular intervals, each possessing a small range of velocities along with randomized directions and orientations. These particles were then subject to the force of gravity and eventually deposited within the container box. After the requisite particles needed for the formation of packings were added, a certain period of time was allotted for the stabilization of the entire packing to occur. During this period, no further particles were introduced, leading to the formation of a dense and random packing structure.

The simulation parameters used are similar to those tested by Schruff et al. (2018) (see Table 3.1). A total of eleven parameters are present, which are classified into three distinct groups. The “General” parameters offer a sweeping overview of the simulation environment: gravity, which was reduced to 6.11 m/s^2, aimed to incorporate the buoyancy effect of water, according to $g' = g(1 - \rho_w/\rho_p)$, where g, g' are the default gravity and reduced gravity, ρ_w, ρ_p are the density of water and particle respectively. Damping coefficient was set to 0.001 in order to simulate the energy loss stemming from collisions between particles or particle-water interactions during the packing process. Simulation length is the parameter that dictates the real-time duration, expressed in seconds, taken for the formation of packings, which is equal to the single timestep (in seconds) multiplied by the total timesteps. The “Solution” parameters, the second group, are used to resolve multi-contact issues numerically as previously mentioned. Finally, the third group, the “Material” parameters, describe the particle material properties used in the simulation.

Here, only the particle density and friction coefficient are required since the microscopic collision processes are not explicitly modeled in the hard-contact approach. The particle density was set to 2650 kg/m^3, mimicking the mineral density of quartz.

The width of box containers for all simulations was set at least 25 times larger than the size of a representative particle to mitigate the so-called “relative size effect” that likely leads to an overestimation of the total packing porosity (Schruff et al., 2018). In this case, the geometric mean of the grain size distributions was employed as the representative particle size.

Table 3.1. An overview of the set-up parameters used in the NSGD simulations.

Category	Parameters	Opted values
General	Gravity	9.81 m/s^2
	Reduced gravity	6.11 m/s^2
	Water density	1000 kg/m^3
	Damping coefficient	0.001
	Timestep	10^{-3} s
	Total timesteps	10,000-200,000
	Simulation length	10 - 200 s
Solution	Relaxation	0.75
	Maximum iterations	10-50
Material	Solid density	2650 kg/m^3
	Friction coefficient	0.5

3.4.2.2 Evaluation

Packing simulations become increasingly challenging for larger size ratios as the number of particles grows cubically. To mitigate the computational cost, we limited our validation study to a narrow size range that corresponds solely to gravels. The discrete size classes used for constructing multi-sized sediment mixtures were 2, 2.83, 4, 5.66, 8, 11.31, 16, 22.63, 32, 45.25 and 64 mm, sorted by a width of 0.5 phi, with the grain shape assumed to be spherical. Overall, we generated a total of 85 digital sediment deposits, ranging from ternary to 11 muti-sized mixtures (Fig. 3.5). These deposits spanned from well sorted to poorly sorted ($0.35 \leq \sigma_\phi \leq 1.72$), and from very coarse skewed to very fine skewed ($-1.34 \leq Sk_\phi \leq 1.34$) based on the descriptive terminology proposed by Blott and Pye (2001).

As detailed in Schruff et al. (2018), the bulk porosity of the digital packings was determined through a voxelization approach as the ratio of the number of empty voxels (voids) to the total number of voxels and calculated for the lower 90% of the mixture to discount surface irregularities. It should be noted that the digital packings contained a few instances of particle overlap, but since the impact on bulk porosity was so minuscule and thus overlooked.

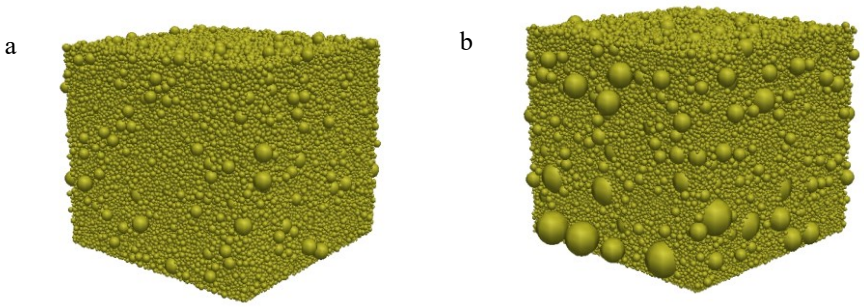

Figure 3.5. Examples of generated digital sediment deposits composed of (a) six-size fractions, and (b) nine-size fractions.

In order to evaluate the BUC packing model, we first performed a calculation of the logarithmic mean, standard deviation and skewness of the 85 grain size distributions. Based on which, we obtained the equivalent binary-unit mixtures. Finally, we employed the Westman equation to directly calculate the porosity of the obtained binary-unit mixtures. The initial porosity of each component was set equal to 0.36, indicating a random dense packing state present in these simulations.

The outcome is visualized in Fig. 3.6, showing the BUC model is able to produce accurate porosity values for multi-component packings of spherical particles, exhibiting a high R^2 score of 0.824 and a low $RMSE$ value of 0.014, despite involving the absolute errors (around ± 0.01) in estimating porosity with the NSGD algorithm (Schruff et al., 2018).

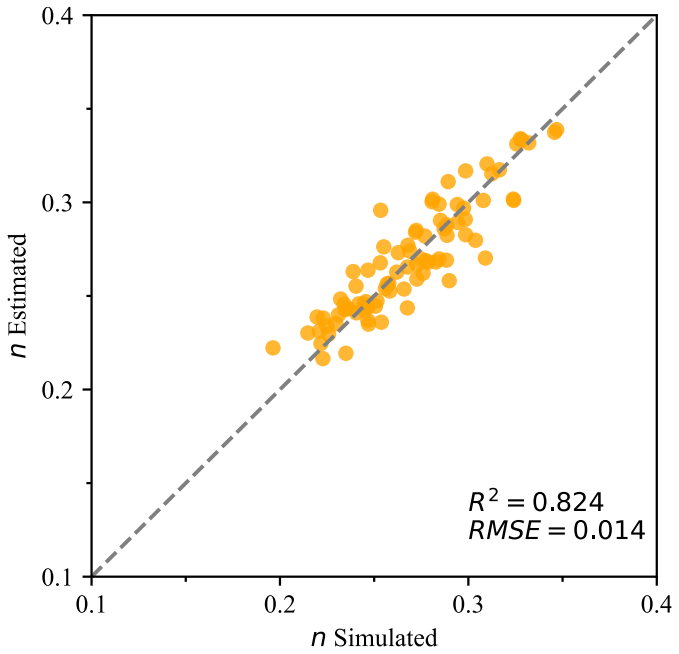

Figure 3.6. Comparison of the simulated and estimated porosity for the generated 85 digital sediment mixtures.

3.4.3 Dataset from the Rhine River

At the final step, the BUC packing model was validated against laboratory measurement data of fluvial sediment mixtures. Frings et al. (2011) executed 46 laboratory measurements on sediment samples sourced from sub-surface layers of the channel bed and river bank in the Rhine River. The sediment's dimensions range from 0.02 up to 200 mm, spanning from silt to cobbles, thus signifying a significant extension of the size range in comparison to the previous validation. The sediment's shape generally takes on a sub-spherical form, exhibiting an average of intercept sphericity hovering around 0.74 according to Liang et al. (2015). The measured sediment mixtures spread from well sorted to very poorly sorted ($0.40 \leq \sigma_{\phi} \leq 2.97$), from very coarse skewed to very fine skewed ($-2.33 \leq Sk_{\phi} \leq 6.35$), underscoring the striking heterogeneity of the samples. Porosity of the sediment mixtures was measured using the water displacement method (Bear, 1972).

To evaluate the BUC model, again, the equivalent binary-unit mixtures were first obtained based on the statistics of mean, standard deviation and skewness calculated from the 46 samples, after which their porosity values were acquired using the Westman equation. The initial porosity was taken as 0.37 for all size classes, based on the average of the laboratory measurements conducted with uniform packings with analogous sediments (Frings et al., 2011).

The comparison is shown in Fig. 3.7, where the outcome is not up to par with previous estimations, exhibiting a relatively low R^2 score of 0.692 and a relatively high $RMSE$ value of 0.032.

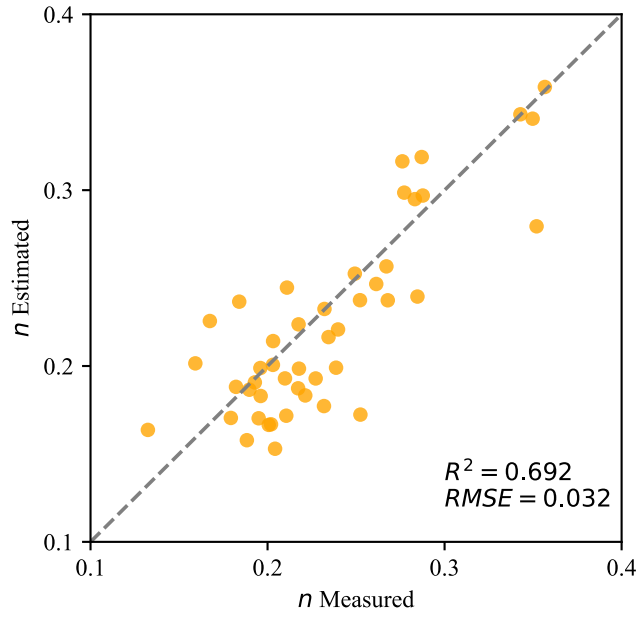

Figure 3.7. Comparison of the measured and estimated porosity for the 46 Rhine sediment mixtures.

Given the remarkable precision of the BUC model in gauging the porosity of spherical particle packings, the relatively sizeable disparities for fluvial sediment mixtures can be attributed to two primary factors, namely (1) measurement inaccuracies, and (2) grain shape effect. Within laboratory settings, the reading errors associated with water levels and packing heights dominate the accuracy of outputs, yielding an absolute error of ~0.01 for porosity measurements (Liang et al., 2015). The grain shape effect remains evident since the shape of sediment is not entirely spherical. The impact of this can be assessed by plotting measured porosity against the theoretical limits of random packing of spheres. To accomplish this, the initial porosity was fixed at 0.36 and 0.4 (Allen, 1985), corresponding to the state of random loose packing and dense packing of spheres, respectively. In the hypothetical scenario that sediment shape was truly spherical, the measured porosity values should lie within the range demarcated by the two limiting values, or at least, close to this region, taking into account the errors introduced by measurements. However, as Fig. 3.8 clearly illustrates, certain measurements, for example, IDs 5, 20, 21, 40 and 42, stray far beyond the limiting bounds, indicating the grain shape effect becomes marked for situations where grain shape is likely much deviated from spherical.

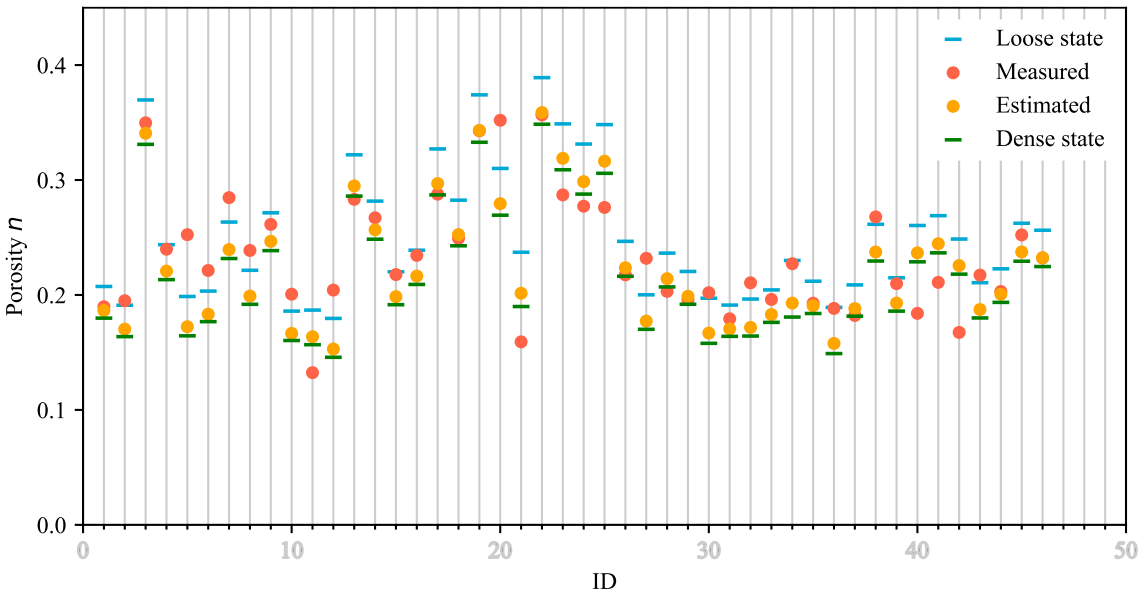

Figure 3.8. Measured against estimated porosity for different packing states of the 46 Rhine sediment mixtures.

3.5 Discussion

3.5.1 Performance over Other Analytical Models

In the present analysis, we focus on the BUC model's comparison to the generally applicable models, i.e., the analytical porosity predictors as mentioned in section 3.1. A recent paper from Rettinger et al. (2023) sheds light on the evaluation of several universal models predicting porosity for multi-sized mixtures of fluvial sediments. Within their evaluation, two of the models were scrutinized using the same dataset of the Rhine sediment, thereby providing an opportunity to discern the performance of the BUC model in comparison. Specifically, the two packing models being evaluated were the linear mixture packing model (LMPM) (Yu and Standish, 1991), and the compressible packing Model (CPM) (De Larrard, 1999).

In Table 3.2, the comparative performance of the BUC model against the LMPM and CPM is presented. From the results, it can be clearly seen that our model outperforms the other two models in porosity prediction accuracy. A careful inspection of their data reveals that both LMPM and CPM models have consistently underestimated the porosity of the packings, despite using the same initial porosity value of 0.37 as the BUC model. The underlying reason for the poor performance of these models can be attributed to their fundamental principles.

Table 3.2. Comparison of porosity estimation performance of packing models for the Rhine sediment mixtures.

Packing model	Original			With cohesion model		
	R^2	RMSE	MAE[a]	R^2	RMSE	MAE[a]
LMPM	-0.023	0.068	0.180	0.384	0.053	0.094
CPM	0.356	0.054	0.187	0.689	0.038	0.096
BUC	**0.692**	**0.032**	**0.080**			

[a] maximum absolute error MAE

The central idea of the LMPM is to category the particles of a packing into three groups, each lined to a different packing mechanism (Fig. 3.9). The central group consists of particles that form the skeleton of a packing, in which the size range of the particles are relatively small, thus reducing porosity by occupying each other's pore space (mixing effect). The first and the third groups, on the other hand, include particles that are either too small or too large, respectively, when compared to the middle size of the central group, namely the dominant size (d_i). These particles reduce porosity by either filling into the pores in the skeleton of a packing, or completely occupying them with solid volumes. Since both mechanisms reduce porosity without changing the skeleton of a mixture, they are referred to unmixing effect (Yu and Standish, 1991). Normally, the critical size ratio r of 0.154 is used in the LMPM to separate the three particle groups.

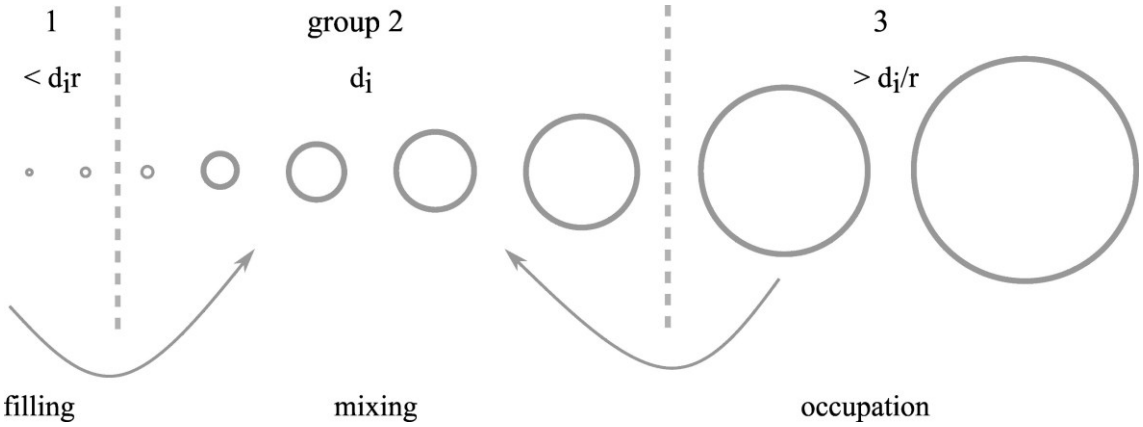

Figure 3.9. Schematic diagram showing the mechanism of the LMPM in estimating porosity of multi-size mixtures.

The defect of the LMPM is apparent, since it takes into account solely the interactions between the dominant size and one of the other sizes, while casting aside the interactions among more than two size fractions at once. Reality, however, proves to be markedly different. Tiny particles, for instance, which per the LMPM ought to percolate through the pores of the skeleton of group 2 mixture, instead mix with them to a significant extent, as group 2 particles encompass numerous smaller-than-the-dominate-size particles with sizes closely aligned with those of the tiny particle. Similarly, with regards to the occupation effect, larger particles cannot occupy a position with ease without transforming the structure of group 2 mixture, given that many larger-than-the-dominate-size particles are present. The LMPM's underlying assumption treats the supposed mixing effect wrongly as the unmixing one, thus inevitably introducing systematic underestimation of porosity, a phenomenon observed elsewhere as well (e.g., Frings et al., 2011).

The CPM distinguishes itself from the LMPM by classifying all particles within a mixture as belonging to one group. This model considers solely the unmixing effect between particle interactions. Once more, the CPM merely accounts for two-fraction interactions between the dominant size and a single other size. However, the CPM incorporates a relaxation-like parameter, denoted as $K \in (0, \infty)$, that serves to lessen the effect of unmixing interactions that lead to the reduction of porosity. The magnitude of the relaxation effect is inversely related to the K value; a higher K value implies a weaker relaxation effect. In general, a K value of 4 is advised for dealing with loose packing, whereas a K value of 9 is preferable for dense packing (De Larrard, 1999). The addition of the relaxation parameter K might plausibly account for why the CPM underpredicted the porosity to a lesser extent than the LMPM for the Rhine sediment mixtures.

The systematic underestimation of porosity introduced by the two packing models led those authors to speculate that such an issue was likely attributable to the oversight of the

cohesion effect among fine particles, which might augment porosity by means of van der Waals or electrostatic forces between diminutive grains (Yu et al., 2003; Zou et al., 2011). Consequently, they reexamined the two packing models, this time incorporating the influence of cohesion by elevating the initial porosity of small particles and redefining the size ratio according to Yu et al. (1997) and Zou et al. (2011). The size of 0.5 mm was identified as the demarcation threshold, below which fine grains were presumed to be affected by the cohesion effect based on the laboratory measurements of uniform packings of Rhine sediments (Frings et al., 2011). Unsurprisingly, this approach yielded marked improvements in the results (see Table 3.2), as increasing the initial porosity was bound to increase the final porosity.

The query that demands scrutiny is whether the influence of cohesion is truly vital in those arbitrary packings. We can delve into this by using the equivalent binary-unit mixtures derived from our BUC packing model. The binary-unit mixtures not only facilitate the computation of the final porosity but can also reflect the attribute of the multi-sized packing system with the binary (small and large) size fractions representing all the fine and coarse particles involved in a packing, respectively. The assessment of the 46 binary-unit mixtures reveals the presence of 12 mixtures containing fine grains that are smaller than the 0.5 mm threshold size (Fig. 3.10). We then compare the measured and estimated porosity values of these 12 sediment packings (Fig. 3.11). The outcome indicates that the cohesion effect is not a significant factor in these packings. The measured porosity is only notably greater than the estimated value when the content of fine grains is approximately 30%. As the fine grain fraction increases, the disparity between them shrinks to near equivalence, which is contrary to what would be expected if the cohesion effect were operative.

The query that remains unresolved is why the cohesive effect was only observed in the uniform packings but not significant in the multi-sized mixtures. One possibility is that the cohesive force is most effective among like-sized particles with similar composition. When different-sized particles of varying compositions are mixed, the microscopic interaction force weakens and may eventually dissipate. However, this is merely a hypothesis that requires further investigation, which surpasses the scope of this study.

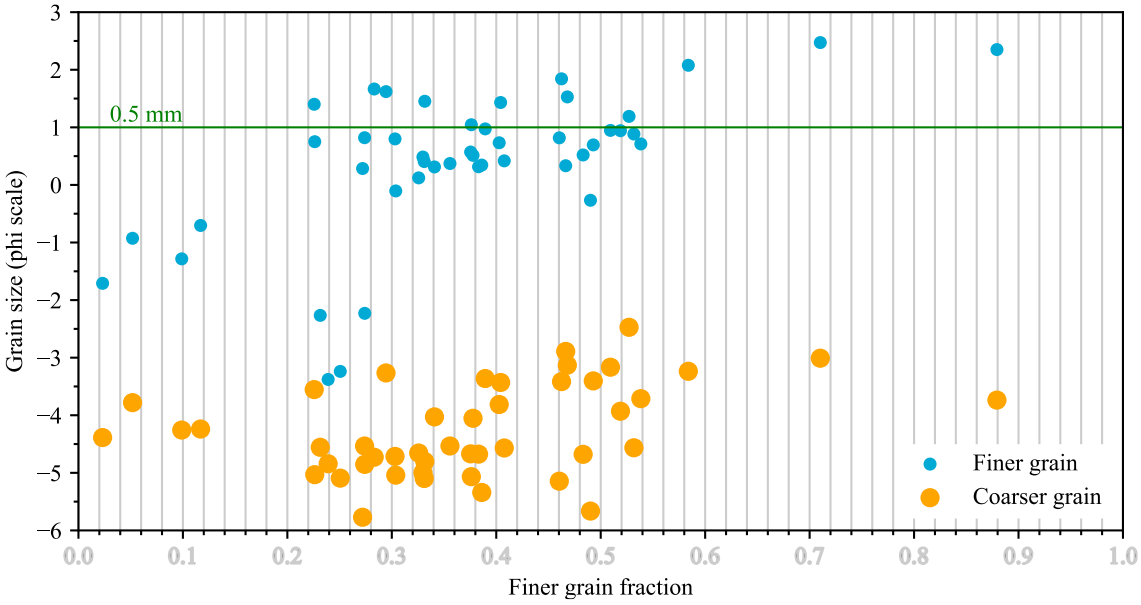

Figure 3.10. The obtained equivalent binary-unit mixtures for the 46 Rhine sediment mixtures.

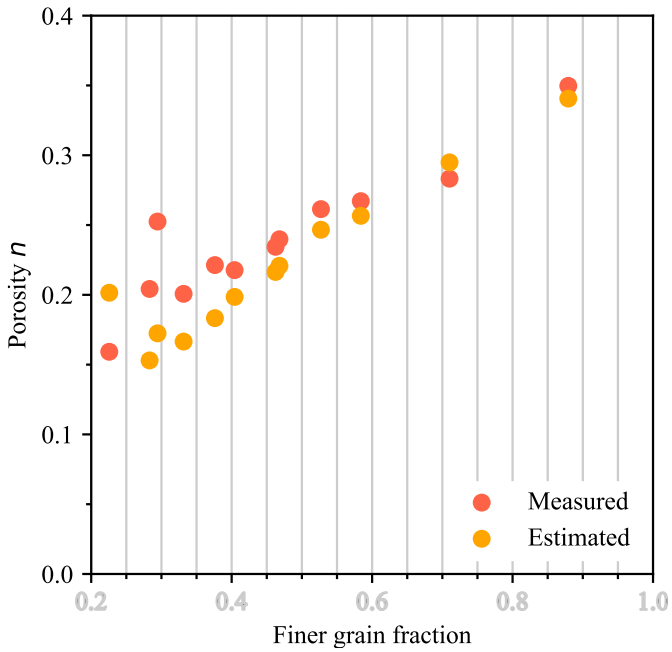

Figure 3.11. Comparison of the measured and estimated porosity for the 12 Rhine sediment mixtures consisting of the representative fines smaller than the size of 0.5 mm.

3.5.2 Flexibility and Limitation of the BUC Packing Model

The BUC packing model, while originating from the Westman equation, is not dependent on it, for the essence of the BUC model lies in the binary-unit concept. The idea of utilizing equivalent binary-unit mixtures to represent original mixtures extends beyond a mere interface for porosity calculation. Given the high precision in estimating porosity for spherical packing systems (see section 3.4.2), it demonstrates that the grain size

statistics of mean, standard deviation, and skewness are the fundamental factors that control the porosity of arbitrary spherical packings, including binary mixtures. Specifically, the standard deviation, which measures the spread of grain sizes around the mean, primarily reflects the mixing effect between particles. Skewness, which measures the asymmetry of grain sizes about its mean, mainly captures the unmixing intraparticle interactions. The mean, however, merely plays a role in determining the specific values within the grain size distribution. Therefore, the obtained binary mixture can be viewed as the most elementary packing unit that equivalently represents the diversity of particle-particle interactions in multi-component (or continuous) mixtures. This theoretical foundation is what makes binary-unit mixtures highly useful for evaluating complex mixtures.

With the binary-unit concept, the BUC packing model possesses the flexibility to make use of any other existing models able to predict the porosity of spherical binary mixtures, such as the mentioned analytical models and many others (e.g., Dias et al., 2004; Koltermann & Gorelick, 1995). However, the Westman equation is still our recommended option, due to its ability to consider all possible interparticle interactions in an implicit manner. This feature allows the Westman equation to deliver promising predictions, as demonstrated in section 3.4.1. Furthermore, the binary-unit concept transcends the realm of porosity estimation, as the interparticle interactions exert a far-reaching impact than mere porosity. Accordingly, the binary-unit concept has the potential to gauge solutions for numerous problems associated with particle packing systems, such as the estimation of permeability in sediment mixtures (Masch & Denny, 1966), determination of the cut-off grain size for morphological changes (Frings et al., 2008), and even prediction regarding the onset of sediment transport (Wilcock & Kenworthy, 2002).

The BUC model's limit is apparent due to its incapacity to capture the effect of complex grain shape, which has a marked influence on porosity as evident in this study and others (e.g., Liang, et al., 2015; Rettinger et al., 2022b). So far, the BUC packing model is only suitable for estimating packings with spherical or sub-spherical particles. Therefore, incorporating the non-spherical grain shape effect into the BUC model is a future necessity to enhance its functionality, which will enable accurate porosity estimation for fluvial sediment mixtures.

3.6 Conclusions

The BUC packing model has been established from the re-analysis of the conic Westman equation. The core of the BUC packing model lies in the newly proposed binary-unit concept, which states that any arbitrary mixture can be transformed into an equivalent binary-unit mixture for spherical packings, through the link of identical statistics of mean, standard deviation and skewness. The BUC model's versatility stems from the binary-unit mixture's ability to capture all the feasible particle-particle interactions that impact

porosity in arbitrary packing systems. Leveraging the Westman equation, the BUC model can provide general and precise porosity estimation for arbitrary sediment mixtures of spherical or sub-spherical shapes. Not only does the BUC model surpass other analytical packing models in terms of efficiency and accuracy, but it also highlights the negligible role of the cohesion effect in multi-sized packings. Besides, the binary-unit concept makes it possible to tackle other particle-related issues beyond porosity estimation. The next phase entails integrating the non-spherical grain shape effect into the BUC packing model to offer comprehensive porosity prediction for fluvial packing systems.

References

Ackers, P., & White, W.R. (1973). Sediment transport: new approach and analysis. Journal of the Hydraulics Division, 99, 2041-2060.

Allen, J.R.L. (1985). Principles of physical sedimentology. George Allen and Unwin, London.

Bauer, M., Eibl, S., Godenschwager, C., Kohl, N., Kuron, M., Rettinger, C., et al. (2021). waLBerla: A block-structured high-performance framework for multiphysics simulations. Computers & Mathematics with Applications, 81, 478-501.

Bear, J. (1972). Dynamics of fluids in porous media. Elsevier, 764.

Blott, S.J., & Pye, K. (2001). Gradistat: A grain size distribution and statistics package for the analysis of unconsolidated sediments. Earth Surface Processes and Landforms, 26(11), 1237-1248.

Boulton, A.J., Findlay, S., Marmonier, P., Stanley, E.H., & Valett, H.M. (1998). The functional significance of the hyporheic zone in streams and rivers. Annual Review of Ecology, 29, 59-81.

Carling, P.A., & Reader, N.A. (1982). Structure, composition and bulk properties of upland stream gravels. Earth Surface Processes and Landforms, 7(4), 349-365.

Chang, C.S., & Deng, Y. (2018). A nonlinear packing model for multi-sized particle mixtures. Powder Technology, 336, 449-464.

Chang, C.S., Deng, Y., & Meidani, M. (2018). A multi-variable equation for relationship between limiting void ratios of uniform sands and morphological characteristics of their particles. Engineering Geology, 237, 21-31.

Coleman, S.E., & Nikora, V.I. (2009). Exner equation: A continuum approximation of a discrete granular system. Water Resources Research, 45(9), 9421.

De Larrard, F. (1999). Concrete mixture proportioning: a scientific approach. Concrete Mixture Proportioning.

Dias, R.P., Teixeira, J.A., Mota, M.G., & Yelshin, A.I. (2004). Particulate binary mixtures: dependence of packing porosity on particle size ratio. Industrial and Engineering Chemistry Research, 43(24), 7912-7919.

El-Husseiny, A. (2020). Improved Packing Model for Functionally Graded Sand-Fines Mixtures-Incorporation of Fines Cohesive Packing Behavior. Applied Sciences, 10(23), 562.

Fraser, H.J. (1935). Experimental Study of the Porosity and Permeability of Clastic Sediments. The Journal of Geology, 43(8, Part 1), 910-1010.

Frings, R.M., Kleinhans, M.G., & Vollmer, S. (2008). Discriminating between pore-filling load and bed-structure load: a new porosity-based method, exemplified for the river Rhine. Sedimentology, 55(6), 1571-1593.

Frings, R.M., Schüttrumpf, H., & Vollmer, S. (2011). Verification of porosity predictors for fluvial sand-gravel deposits. Water Resources Research, 47(7), 7525.

Gaither, A. (1953). A study of porosity and grain relationships in experimental sands. Journal of Sedimentary Research, 23(3), 180-195.

Koltermann, C.E., & Gorelick, S.M. (1995). Fractional packing model for hydraulic conductivity derived from sediment mixtures. Water Resources Research, 31(12), 3283-3297.

Liang, R., Schruff, T., Jia, X., Schüttrumpf, H., & Frings, R.M. (2015). Validation of a stochastic digital packing algorithm for porosity prediction in fluvial gravel deposits. Sedimentary Geology, 329, 18-27.

Liu, Z.R., Ye, W.M., Zhang, Z., Wang, Q., Chen, Y.G., & Cui, Y.J. (2019). A nonlinear particle packing model for multi-sized granular soils. Construction and Building Materials, 221, 274-282.

Masch, F.D., & Denny, K.J. (1966). Grain size distribution and its effect on the permeability of unconsolidated sands. Water Resources Research, 2(4), 665-677.

Mcgeary, R.K. (1961). Mechanical packing of spherical particles. Journal of the American Ceramic Society, 44(10), 513-522.

Mota, M., Teixeira, J., Bowen, W., & Yelshin, A. (2001). Binary spherical particle mixed beds: porosity and permeability relationship measurement.

Noack, M., Ortlepp, J., & Wieprecht, S. (2017). An Approach to Simulate Interstitial Habitat Conditions During the Incubation Phase of Gravel-Spawning Fish. River Research and Applications, 33(2), 192-201.

Núñez-González, F., Martín-Vide, J.P., & Kleinhans, M.G. (2016). Porosity and size gradation of saturated gravel with percolated fines. Sedimentology, 63(5), 1209-1232.

Preclik, T., & Rüde, U. (2015). Ultrascale simulations of non-smooth granular dynamics. Computational Particle Mechanics, 2(2), 173-196.

Rettinger, C., Rüde, U., Vollmer, S., & Frings, R.M. (2022b). Effect of sediment form and form distribution on porosity: a simulation study based on the discrete element method. Granular Matter, 24(4), 1-23.

Rettinger, C., Eibl, S., Rüde, U., & Vowinckel, B. (2022a). Rheology of mobile sediment beds in laminar shear flow: effects of creep and polydispersity. Journal of Fluid Mechanics, 932, A1.

Sawyer, A.H., & Cardenas, M.B. (2009). Hyporheic flow and residence time distributions in heterogeneous cross-bedded sediment. Water Resources Research, 45(8).

Schruff, T., Liang, R., Rüde, U., Schüttrumpf, H., & Frings, R.M. (2018). Generation of dense granular deposits for porosity analysis: assessment and application of large-scale non-smooth granular dynamics. Computational Particle Mechanics, 5(1), 59-70.

Song, C., Wang, P., & Makse, H.A. (2008). A phase diagram for jammed matter. Nature 2008 453:7195, 453(7195), 629-632.

Stovall, T., de Larrard, F., & Buil, M. (1986). Linear packing density model of grain mixtures. Powder Technology, 48(1), 1-12.

Tabesh, M., Hoffmann, T., Vollmer, S., Schüttrumpf, H., & Frings, R.M. (2019). In-situ measurement of river-bed sediment porosity using Structure-from-Motion image analysis. Geomorphology, 338, 61-67.

Tabesh, M., Vollmer, S., Schüttrumpf, H., & Frings, R.M. (2022). Spatial variability in river bed porosity determined by nuclear density gauging: A case study from a French gravel-bed river. Sedimentology, 69(2), 823-844.

Vollmer, S., & Kleinhans, M.G. (2007). Predicting incipient motion, including the effect of turbulent pressure fluctuations in the bed. Water Resources Research, 43(5), 5410.

Westman, A.E.R. (1936). The packing of particles: empirical equations for intermediate diameter ratios. Journal of the American Ceramic Society, 19, 127-129.

Westman, A.E.R., & Hugill, H.R. (1930). The packing of particles. Journal of the American Ceramic Society, 13(10), 767-779.

Wilcock, P.R., & Kenworthy, S.T. (2002). A two-fraction model for the transport of sand/gravel mixtures. Water Resources Research, 38(10), 1194.

Wooster, J.K., Dusterhoff, S.R., Cui, Y., Sklar, L.S., Dietrich, W.E., & Malko, M. (2008). Sediment supply and relative size distribution effects on fine sediment infiltration into immobile gravels. Water Resources Research, 44(3), 3424.

Wu, W., & Wang, S.S.Y. (2006). Formulas for sediment porosity and settling velocity. Journal of Hydraulic Engineering, 132(8), 858-862.

Yerazunis, S., Cornell, S.W., & Wintner, B. (1965). Dense random packing of binary mixtures of spheres. Nature 1965 207:4999, 207(4999), 835-837.

Yu, A.B., & Standish, N. (1991). Estimation of the porosity of particle mixtures by a linear-mixture packing model. Industrial and Engineering Chemistry Research, 30(6), 1372-1385.

Yu, A.B., Zou, R.P., & Standish, N. (1992). Packing of ternary mixtures of nonspherical particles. Journal of the American Ceramic Society, 75(10), 2765-2772.

Yu, A.B., Standish, N., & McLean, A. (1993). Porosity calculation of binary mixtures of nonspherical particles. Journal of the American Ceramic Society, 76(11), 2813-2816.

Yu, A.B., Bridgwater, J., & Burbidge, A. (1997). On the modelling of the packing of fine particles. Powder Technology, 92(3), 185-194.

Yu, A.B., Feng, C.L., Zou, R.P., & Yang, R.Y. (2003). On the relationship between porosity and interparticle forces. Powder Technology, 130(1-3), 70-76.

Zou, R.P., Gan, M.L., & Yu, A.B. (2011). Prediction of the porosity of multi-component mixtures of cohesive and non-cohesive particles. Chemical Engineering Science, 66(20), 4711-4721.

4

Validation of A Stochastic Digital Packing Algorithm

Porosity as one of the key properties in sediment mixtures is poorly understood. Most of the existing porosity predictors based upon grain size characteristics have been unable to produce satisfying results for fluvial sediment porosity, due to the lack of consideration of other porosity-controlling factors like grain shape and depositional condition. Considering this, a stochastic digital packing algorithm was applied in this work, which provides an innovative way to pack particles of arbitrary shapes and sizes based on digitization of both particles and packing space. The purpose was to test the applicability of this packing algorithm in predicting fluvial sediment porosity by comparing its predictions with the outcomes obtained from laboratory measurements. Laboratory samples examined were two natural fluvial sediments from the Rhine River and Kall River (Germany), and commercial glass beads (spheres). All samples were artificially combined into seven grain size distributions: four unimodal distributions and three bimodal distributions. Our study demonstrates that apart from grain size, grain shape also has a clear impact on porosity. The stochastic digital packing algorithm successfully reproduced the measured variations in porosity for the three different particle sources. However, the packing algorithm systematically overpredicted the porosity measured in random dense packing conditions, mainly because the random motion of particles during settling introduced unwanted kinematic sorting and shape effects. The results suggest that the packing algorithm produces loose packing structures, and is useful for trend analysis of packing porosity.

4.1 Introduction

Porosity prediction of sedimentary deposits is of interest in a fluvial environment. Previous studies have shown that porosity, as a key structural property, plays an important role in the morphological, ecological and geological characteristics of fluvial systems. Morphologically, porosity governs the initiation of sediment motion and bank collapse (e.g., Wilcock, 1998; Vollmer & Kleinhans, 2007). Ecologically, porosity determines the interstitial space of the hyporheic zone for aquatic habitats (e.g., Boulton et al., 1998). Geologically, porosity dominates the exploitable reserve of oil, gas, and groundwater stored in the voids of fluvial deposits (e.g., Athy, 1930). To date, existing porosity predictors can generally be classified into two types: (1) empirical predictors; and (2) theoretical predictors. Most efforts to predict porosity have been empirically driven, to a large extent based upon median grain size D_{50} (e.g., Carling & Reader, 1982; Wu & Wang, 2006), sorting coefficient σ (e.g., Wooster et al., 2008), or a combination of different grain size characteristics (e.g., Frings et al., 2011; Desmond & Weeks, 2014). Theoretical predictors such as geometrical models (e.g., Ouchiyama & Tanaka, 1984; Suzuki & Oshima, 1985) or analytical models (e.g., Yu & Standish, 1991; Koltermann & Gorelick, 1995; Esselburn et al., 2011) relate porosity to the full grain size distribution of perfect spheres. The performance of these predictors has been investigated by comparing porosity values measured in situ with those computed by the predictors (e.g., Frings et al., 2008, 2011). Unfortunately, these predictors produced unsatisfying results in predicting fluvial sediment porosity (Frings et al., 2011), probably because such predictors mainly focused on grain size characteristics, ignoring other porosity-controlling factors such as depositional environment and grain shape.

Effects of grain shape on porosity have received less attention, due to the complexity of arbitrary shapes of natural particles. Over the past decade, the application of computer simulations for the study of granular particle packings has become more popular, supported by developments in the computer hardware industry. However, most of the computer simulations have been limited to simple analytical geometries such as cylinders (Zhang et al., 2006), disks (Desmond & Weeks, 2009), ellipsoids (Donev et al., 2007; Zhou et al., 2011) and spherocylinders (Abreu et al., 2003; Williams & Philipse, 2003; Zhao et al., 2012). The major reason is the practical difficulty of representing and handling irregular shapes using vector-based approaches. Traditional ways to construct an irregular particle require the user to place spherical elements within a meshed polyhedral body (e.g., Wang et al., 2007; Matsushima et al., 2009; Ferellec & McDowell, 2010; Fukuoka et al., 2013), which consumes high computational costs with large numbers of components (spheres) involved (Hubbard, 1996; Song et al., 2006). Although techniques using 3D polyhedral (Latham et al., 2001) or continuous superquadric functions (Williams & Pentland, 1992; Lu et al., 2012) provide a straightforward way to generate irregular particle shapes, complex contact-detection algorithms are needed,

leading to deterioration in simulation speed as particle complexity increases (Johnson et al., 2004).

In order to overcome these difficulties, a stochastic digital packing algorithm was developed (Jia & Williams, 2001). The packing algorithm is distinguished from the traditional vector-based packing models by digitization of both particles and packing space, allowing for a much easier and computationally efficient way to pack particles of irregular shapes with no more than an ordinary PC. These advantages make it attractive to create packings of complex fluvial deposits, and to study the grain shape effects on porosity. Applications of this stochastic digital packing algorithm have proven to provide relatively accurate porosity predictions for both fine powders (Jia et al., 2007) and large spheres (Caulkin et al., 2006, 2007) in the fields of material science and engineering chemistry. Nevertheless, the packing algorithm has not yet been used for generating packings of fluvial deposits. Therefore, the primary purpose of this work was to test the applicability of the stochastic digital packing algorithm in predicting fluvial sediment porosities. In this study, we focused on fluvial gravel mixtures and did so by comparing the predicted porosities with those obtained from laboratory measurements.

4.2 Materials and methods

4.2.1 Particle acquisition and analysis

The particles employed for this study came from three different sources: (1) fluvial gravels from the Rhine River (Germany), (2) fluvial gravels from the Kall River (Germany), and (3) commercial glass beads. The Rhine sediments were collected from the channel bed between the barrage of Iffezheim and the German-Dutch border between July 2008 and April 2011. Quartz is the dominant lithology. The Kall sediments were collected from the channel bed near the river mouth in June 2014. Slate is the dominant lithology.

After acquisition, the fluvial sediments were carefully cleaned by flushing with fresh water, dried in an oven at 105 °C for 48 h and sieved into seven size fractions: 2.8-4 mm, 4-5.6 mm, 5.6-8 mm, 8-11.2 mm, 11.2-16 mm, 16-22.4 mm, 22.4-31.5 mm. Subsequently, these fractions were combined into seven grain size distributions: four unimodal ones with logarithmic standard deviations (σ_φ) of 0.00, 0.32, 0.49 and 0.71, and three bimodal ones, with the finer mode, making up either $k = 30$, $k = 50$ or $k = 70$ percent of the distribution (Fig. 4.1). The glass beads with seven size fractions of 3, 4, 6, 8, 11, 16 and 22 mm were also combined into the same distributions as above.

For the fluvial sediments, nine representative particles were chosen based on visual judgments from each of the seven sieve fractions, and digitized (Fig. 4.2) using a nonmedical X-ray computed tomography (CT) scanner. Shape analysis was done according to the classic Zingg diagram (Zingg, 1935), which categorizes particle shape into sphere, disc, blade and rod categories on the basis of the elongation ratio (b/a) and

flatness ratio (c/b), where a, b and c are the long, intermediate and short orthogonal axes respectively of the smallest volume imaginary box that can contain the particle (Blott and Pye, 2008). It can be seen in Fig. 4.3 that most of the Rhine sediments locate within the sphere area while the Kall sediments are dominated by disks and blades. According to Krumbein's (1941) equation (4.1), the intercept sphericity (ψ) for each selected particle was calculated, with an average intercept sphericity of 0.74 gained for the Rhine sediments and 0.55 for the Kall sediments.

$$\psi = \sqrt[3]{\frac{b * c}{a^2}} \tag{4.1}$$

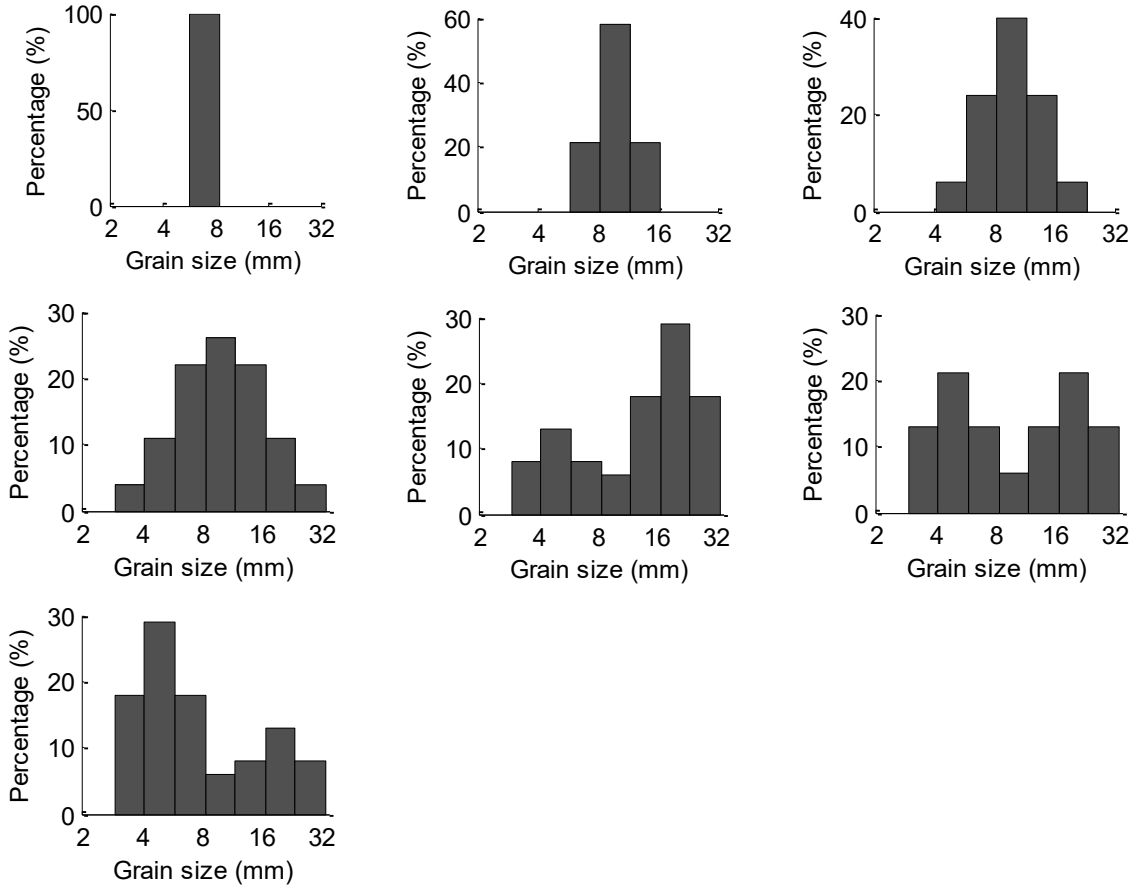

Figure 4.1. Grain size distributions used for the porosity measurements and simulations.

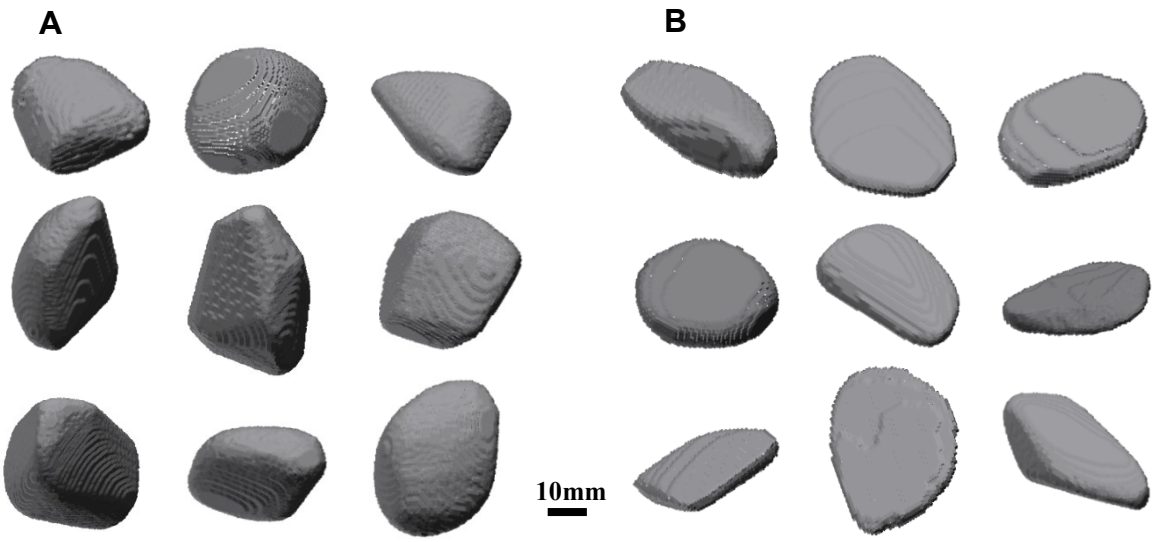

Figure 4.2. Nine representative digitized particles in the 22.4-31.5 mm fraction of (A) Rhine sediments and (B) Kall sediments represented at a resolution of 0.5 mm/voxel.

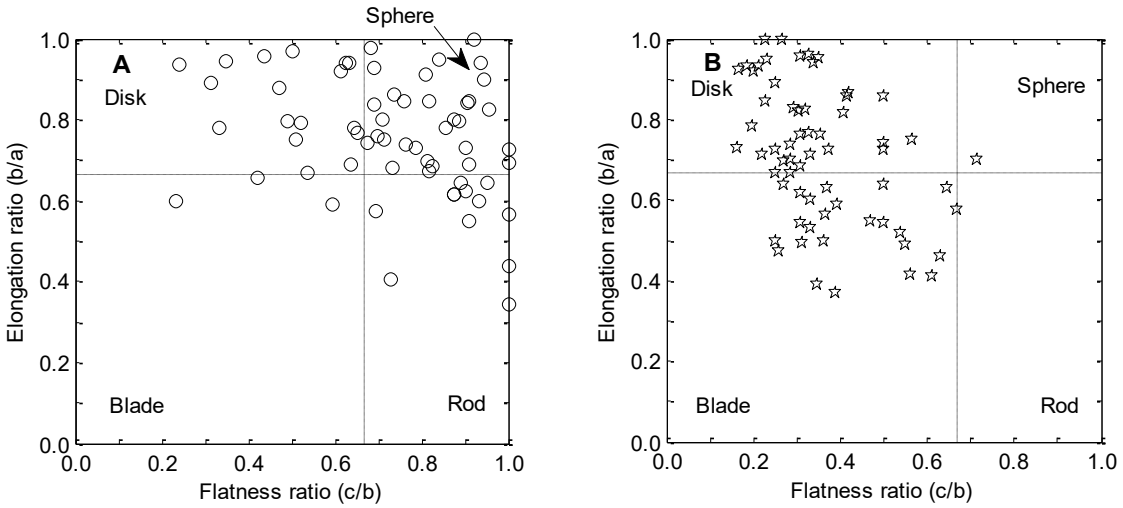

Figure 4.3. Shape properties of (A) Rhine sediments and (B) Kall sediments in the Zingg classification.

4.2.2 Laboratory porosity measurements

The water displacement method (Bear, 1972) was used for porosity measurements. The experimental procedure was as follows: firstly, a plastic cylinder with an inner diameter of 104 mm was partially filled with a known volume of water V_w larger than the expected pore volume of the particles to be added. Then, particles of 3 kg mass were added into the cylinder in small well-mixed portions, together with gently tapping the side of the cylinder in order to dislodge trapped air bubbles and obtain a stable, dense packing. The

final water level was visually read to obtain the whole accumulated volume V_a ($V_a = V_w + V_s$, where V_s is the volume of the solid fraction). The jagged surface of the particle packing caused by the wide range of sizes and shapes was then smoothed by hand and the total volume of the particle packing V_t (including pores) was obtained through reading the height of the particle packing. Eventually, the porosity was computed as $n = V_p/V_t$, where V_p ($= V_t - (V_a - V_w)$) is the pore volume of the particle packing.

In total, 42 laboratory porosity experiments were performed as a basis for the validation of the stochastic digital packing algorithm: 14 experiments with the sub-spherical Rhine sediments (7 distributions, each two times), 14 experiments with low-sphericity Kall sediments (again 7×2) and 14 experiments with the spherical glass beads (again 7×2).

4.2.3 Porosity simulation

The stochastic digital packing algorithm of Jia and Williams (2001) is designed to pack particles of arbitrary sizes and shapes in a confined space of arbitrary geometry. In this packing algorithm, every element is digitized: each particle as a coherent collection of voxels, the packing space (in a container) as a lattice grid, and the movements take place in units of grid cells. During the simulation, the movements of particles, both translational and rotational, are random. In 3D, there are 26 possible translational directions: 6 orthogonal and 20 diagonals. The diagonal moves are treated as a combination of two orthogonal moves. To ensure particles settle while still make use of every available space, a rebounding probability is used. An upward movement (which may be an orthogonal move or part of a diagonal move) is only realized with this probability. After translation, a trial rotation follows, and it is accepted if the rotation does not result in overlaps. Compared with vector-based approaches and for complex shapes, this digital approach is advantageous in several respects. First, there is no conversion or parameterization required, since objects digitized by modern imaging devices, such as X-ray tomography (e.g., Richard et al., 2003) or nuclear magnetic resonance imaging (e.g., Kleinhans et al., 2008), are already in the digital volumetric format required by the packing algorithm. Secondly, collision and overlap detection (normally the most computationally expensive part of packing simulations) is much easier to implement as computer code, and usually faster to execute for complex shapes. Thirdly, the number of voxels used to represent objects, and hence to a large extent the simulation runtime, does not necessarily increase with shape complexity. The reverse is also true: it does not necessarily reduce with shape simplification either. Further details on the stochastic digital packing algorithm can be found elsewhere (Jia & Williams, 2001; Caulkin et al., 2006, 2007).

In order to produce porosity results comparable to those aforementioned measurements, simulation conditions need to be set up to resemble the laboratory experiments, with respect to the packing space, the particle mixtures and the packing process. The digital objects (i.e., packing space and particles) were prepared with

DigiUtility, which is a bundled tool for viewing, manipulating and preparing digital files for this packing algorithm. In DigiUtility, a cylinder (packing space) with solid boundary was built with the size of 104 mm in diameter, and 300 mm in height, which is slightly higher than the largest real packing heights (about 250 mm) to ensure all the particles would drop into it. The particle mixtures (i.e., number of particles in each of the fractions) employed in these simulations were derived on a weight-to-weight basis. For glass beads, the numbers of particles in each fraction were determined as the ratio of the real mass of each fraction to the single particle mass (density of 2500 kg/m^3 used for glass beads). The regular spherical shapes with different sizes were directly created in digital formats using DigiUtility. In the case of the fluvial sediments, we used nine digitized typical particles to represent each fraction and repeated them as many times as needed to make up the feedstock according to the required grain size distributions. The density of fluvial gravels was set to 2650 kg/m^3. Resolution of 0.5 mm/voxel for the digital objects was assigned as it offers relatively precise representation of the real particles in both dimension and shape, and also limits the computational cost to a feasible amount.

Table 4.1. Set-up conditions applied in simulations.

Parameters	**Values**
Resolution	0.5 mm/voxel
Container diameter	104 mm
Dropping height	300 mm
Sediment density	2650 kg/m^3
Glass density	2500 kg/m^3
Adding source	Rain-dropping mode
Rotation	Complete random
Rebounding probability	0.35
Addition rate	1 particle/every 50 timesteps
Windup timesteps	2000

Having the digital objects created, a range of options and parameters was set to mimic the packing process. The source was set to “rain-dropping” mode to let the particles randomly drop from a circular area above the cylinder. In addition to the translational movements, particles were also allowed to rotate randomly during the simulation. Optimized values of the parameters (rebounding probability, addition rate and number of time steps) that control the generated packing structures were chosen such as to create the densest possible packings. By doing so, simulation conditions (Table 4.1) matched the experimental setups as close as possible. Finally, the porosity of the digital packings was determined as the ratio of the number of empty voxels to the total number of voxels within the corresponding packing space. Porosity was calculated for the lower 90% of the mixture to exclude effects of surface irregularities. Each simulation was also done twice and 42 simulations were achieved in total.

4.3 Results

4.3.1 Measured porosity

The porosity measured in the laboratory experiments is shown in Fig. 4.4. For the unimodal particle mixtures, porosity decreases with increasing logarithmic standard deviations, while the bimodal particle mixtures generally have lower porosity than the unimodal mixtures. This variation in porosity reflects the mixing effect between small and large particles.

Porosity comparisons between the three different particle sources show the low-spherical Kall sediments and the spherical glass beads produced higher porosity than the sub-spherical Rhine sediments, which confirms that there is a decrease and then increase in porosity as particle shape varies from spherical to platy (Tickell & Hiatt, 1938; Zou & Yu, 1996). On the other hand, in the case of the bimodal particle mixtures, different tendencies toward the porosity are appreciable (Fig. 4.4B), suggesting grain shape exerts a quite complicated influence on porosity, not merely in variation of amount but in variation of trend.

It should be noted that the dense sediment deposits packed by hand in the laboratory experiments are not fully representative of natural situations where grain arrangement is determined by depositional conditions, such as flow impact (with near-bed turbulence playing an important role) and burial depth (compaction mechanism). This topic is beyond the current effort. Nonetheless, based on the comparisons between field measurements of porosity in the River Rhine (28 measurements on the channel bed and 18 measurements on the river banks, focusing on subsurface sediments) and measurements in the laboratory (Frings et al., 2011), it was found that in most cases (59%), the difference between is less than 0.03 (Fig. 4.5), with an average porosity of 0.24 obtained ex situ and 0.22 in situ.

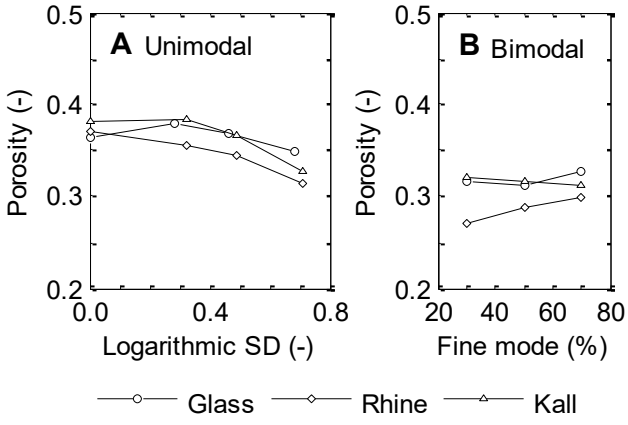

Figure 4.4. Measured porosity for the Rhine sediments, Kall sediments and glass beads over the four unimodal distributions represented by logarithmic standard deviation (A) and three bimodal distributions represented by percentage of fine mode (B).

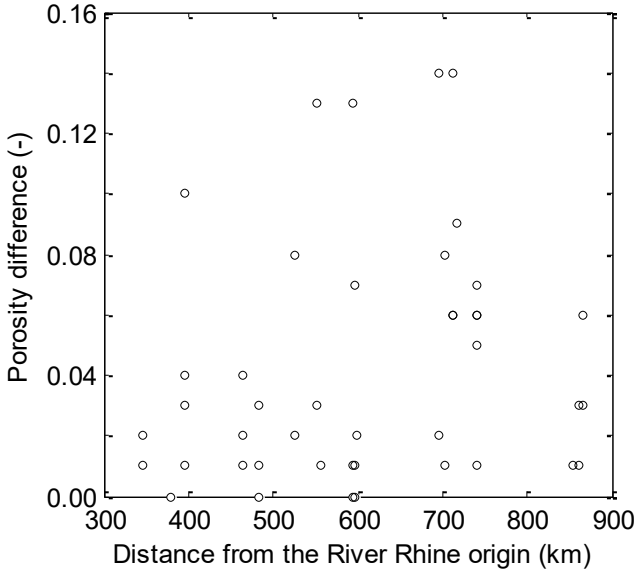

Figure 4.5. Porosity difference between field measurements and laboratory measurements, based on the porosity data set provided by Frings et al. (2011). The study area was the 520 km long river reach between the barrage of Iffezheim (Rhine kilometer 334) and the German-Dutch border (Rhine kilometer 865).

4.3.2 Algorithm behavior

The behavior of the stochastic digital packing algorithm is presented in Fig. 4.6. In order to validate the packing algorithm, comparisons were made between the measured and simulated porosity outcomes. Fig. 4.7 clearly shows that the packing algorithm successfully captures the measured variation in porosity due to grain size distributions for each particle source. While the packing algorithm also seems to be able to mimic the measured variation due to grain shape for a given grain size distribution, providing that the glass beads (spheres) are not taken into account (Fig. 4.8).

However, nearly all simulated porosities were systematically overestimated compared to the experimental measurements. To easily recognize these discrepancies, relative errors between the measured and simulated porosities were calculated (Table 4.2). The average relative error is 29.4% for the Rhine sediments, 21.7% for the Kall sediments and 6.6% for the glass beads, indicating that the packing algorithm predicted relatively higher porosities when it comes to fluvial sediments with irregular shapes. Fig. 4.9 shows the comparison between these discrepancies over the seven grain size distributions. For the unimodal particle mixtures, the discrepancies are growing as logarithmic standard deviation increases (Fig. 4.9A). For the bimodal particle mixtures, with the finer mode increasing from 30% to 70%, the discrepancies for fluvial sediments decrease while the discrepancies for glass beads increase (Fig. 4.9B).

Figure 4.6. Generated digital packings for (A) Rhine sediments, (B) Kall sediments, and (C) glass beads. From left to right, the packings represent the four unimodal distributions (1, 3, 5, 7 fractions), and three bimodal distributions (30%, 50%, 70% proportion of fine mode).

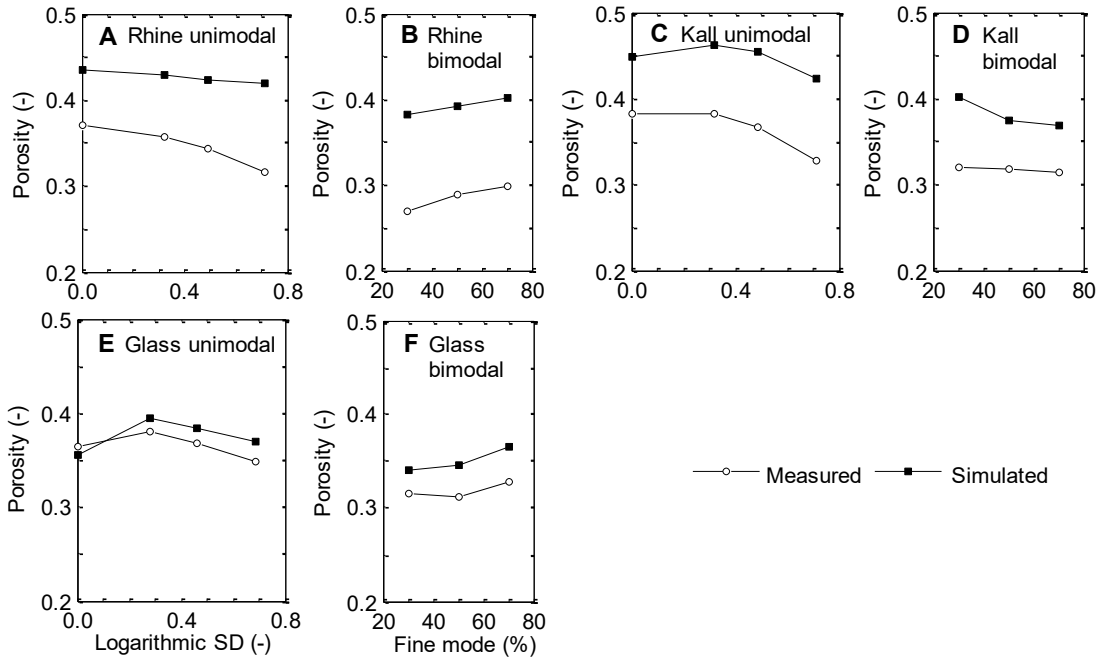

Figure 4.7. Measured versus simulated porosities for the Rhine sediments, Kall sediments and Glass beads over the four unimodal distributions represented by logarithmic standard deviation and three bimodal distributions represented by percentage of fine mode.

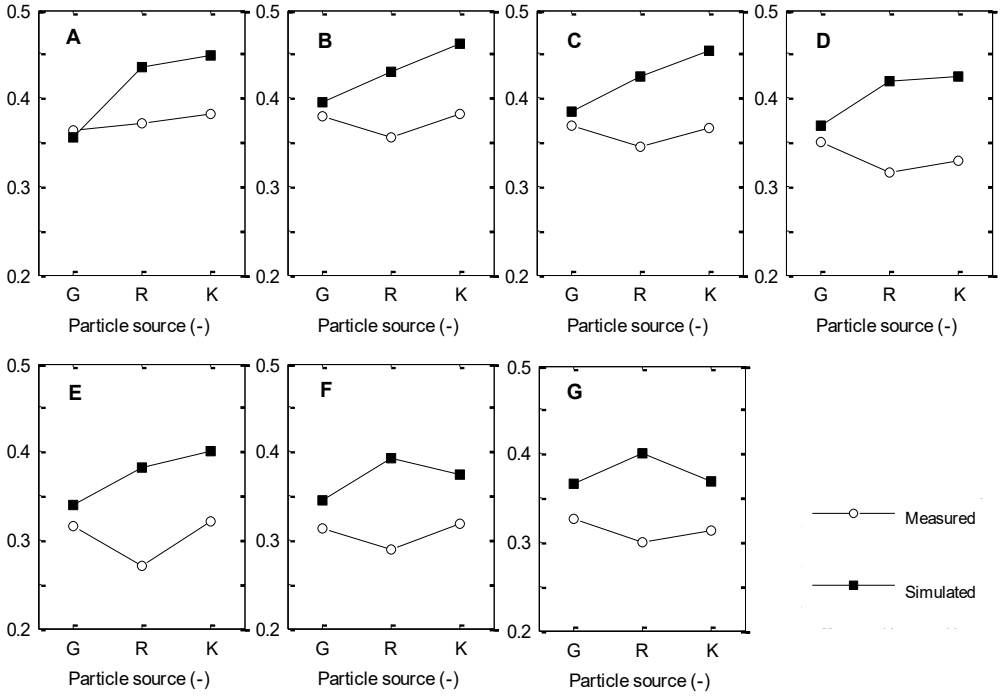

Figure 4.8. Comparison of model predictions with experimental data between the three different particle sources (i.e., the spherical glass beads, the sub-spherical Rhine sediments and the low-spherical Kall sediments) for a given grain size distribution. A to G represents the four unimodal distributions (1, 3, 5, 7 fractions), and three bimodal distributions (30%, 50%, 70% percentage of fine mode).

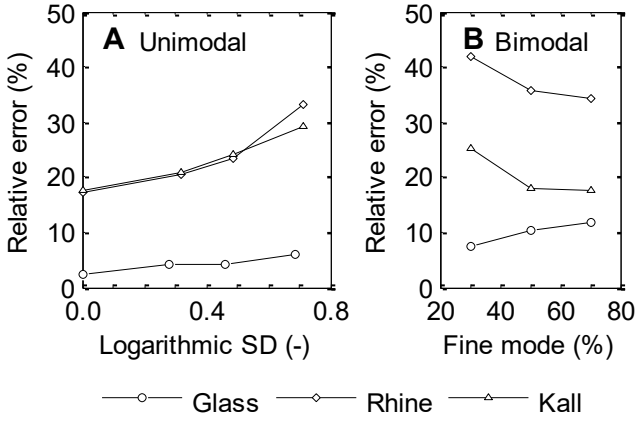

Figure 4.9. Comparisons between relative errors over the four unimodal distributions (A), and three bimodal distributions (B).

Table 4.2. Porosity outcomes attained from laboratory measurements and simulations.

ID	Description of grain size distribution			Laboratory Measurements				Simulations				Relative errors (%)
				1#	2#	Mean	SD[a]	1#	2#	Mean	SD[a]	
1	Rhine sediments	Unimodal distributions	1 Fraction	0.370	0.372	0.371	0.001	0.435	0.434	0.434	0.000	17.1
2			3 Fractions	0.359	0.353	0.356	0.003	0.431	0.428	0.429	0.002	20.5
3			5 Fractions	0.346	0.342	0.344	0.002	0.424	0.425	0.424	0.001	23.4
4			7 Fractions	0.317	0.313	0.315	0.002	0.416	0.424	0.420	0.004	33.3
5		Bimodal distributions	30%[b]	0.272	0.267	0.270	0.003	0.384	0.380	0.382	0.002	41.7
6			50%[b]	0.284	0.294	0.289	0.005	0.392	0.393	0.392	0.000	35.8
7			70%[b]	0.300	0.297	0.299	0.002	0.400	0.402	0.401	0.001	34.3
8	Kall sediments	Unimodal distributions	1 Fraction	0.383	0.380	0.382	0.002	0.447	0.448	0.448	0.001	17.4
9			3 Fractions	0.385	0.380	0.383	0.003	0.464	0.460	0.462	0.002	20.8
10			5 Fractions	0.368	0.364	0.366	0.002	0.453	0.456	0.454	0.002	24.1
11			7 Fractions	0.331	0.324	0.328	0.004	0.427	0.420	0.424	0.004	29.3
12		Bimodal distributions	30%[b]	0.325	0.315	0.320	0.005	0.401	0.400	0.401	0.001	25.2
13			50%[b]	0.316	0.317	0.317	0.001	0.371	0.376	0.374	0.003	18.0
14			70%[b]	0.314	0.312	0.313	0.001	0.370	0.365	0.368	0.003	17.4
15	Glass beads	Unimodal distributions	1 Fraction	0.365	0.362	0.364	0.002	0.357	0.353	0.355	0.002	2.3
16			3 Fractions	0.383	0.377	0.380	0.003	0.395	0.395	0.395	0.000	4.0
17			5 Fractions	0.368	0.368	0.368	0.000	0.383	0.384	0.384	0.000	4.3
18			7 Fractions	0.353	0.344	0.349	0.005	0.369	0.370	0.369	0.000	6.0
19		Bimodal distributions	30%[b]	0.317	0.314	0.316	0.002	0.339	0.340	0.340	0.001	7.6
20			50%[b]	0.314	0.310	0.312	0.002	0.344	0.345	0.345	0.001	10.4
21			70%[b]	0.330	0.324	0.327	0.003	0.364	0.366	0.365	0.001	11.7

a, standard deviation; b, percentage of fine mode.

4.4 Discussion

The purpose of determining the porosities of the samples was twofold: first, to point out that apart from grain size, grain shape also has a clear impact on porosity (shown in section 4.3.1), and second, to serve as a basis of comparison for the porosities predicted from the stochastic digital packing algorithm. It is shown in section 4.3.2 that although the packing algorithm is able to follow the experimental trend, systematic overestimation of the porosity is noticeable, especially for the fluvial sediments. The remarkable discrepancies between can be caused by (1) measurement inaccuracies, and/or (2) simulation inaccuracies.

4.4.1 Measurement inaccuracies

For the laboratory measurements, the reading errors related to the water levels and packing heights dominate the accuracy of outputs. The water levels were visually read to obtain the whole accumulated volumes V_a with a deviation of about 1 mm, and readings of the packing heights for gaining the total volume of particle packing V_t (including pores) were achieved with an accuracy of ~3 mm. These inevitable reading errors can lead to the absolute error of the porosity to be ~0.01 for the measurements. However, measured inaccuracies are small compared to the apparent differences between the measured and simulated porosities, particularly for fluvial sediments.

4.4.2 Simulation inaccuracies

4.4.2.1 Digitization inaccuracy

As can be seen in Fig. 4.10, the arrangements of particles leave unexpected pore spaces. One reason for this may be the digitization errors of digital objects represented at a resolution of 0.5 mm/voxel. The effect can be supported by the fact that the porosity of 0.355 simulated for glass beads is less than the limit of 0.36 in a random dense packing of spheres (Scott, 1960; Allen, 1985; Yu & Standish, 1991; Weltje & Alberts, 2011). This is probably because the spherical shape of glass beads is not perfectly described at such a resolution (0.9% digitization error), causing a reduction of porosity. Korte and Brouwers (2013) also observed the same effects in the simulation of packing 3D digitalized spheres under different resolutions. For this reason, a test for the ID 5 case (see Table 4.2) was carried out with a higher resolution of 0.25 mm/voxel to decrease the digitized errors, especially for smaller particles. This gave a slightly lower porosity of 0.37 instead of 0.38 at 0.5 mm/voxel resolution, indicating that effects of digitization errors are not too significant when compared to the discrepancies between measured and simulated porosities.

Another error arises from the strict non-overlap requirement in the algorithm. Imagine two large objects side by side. If for any reason, there is a voxel protruded from either of

the objects, this single voxel can stop the two objects from coming closer, thus leaving a large gap. In reality or in DigiDEM simulations, where forces instead of probabilities are used to determine in which direction and by how much each object moves in the next time step, this would not have happened.

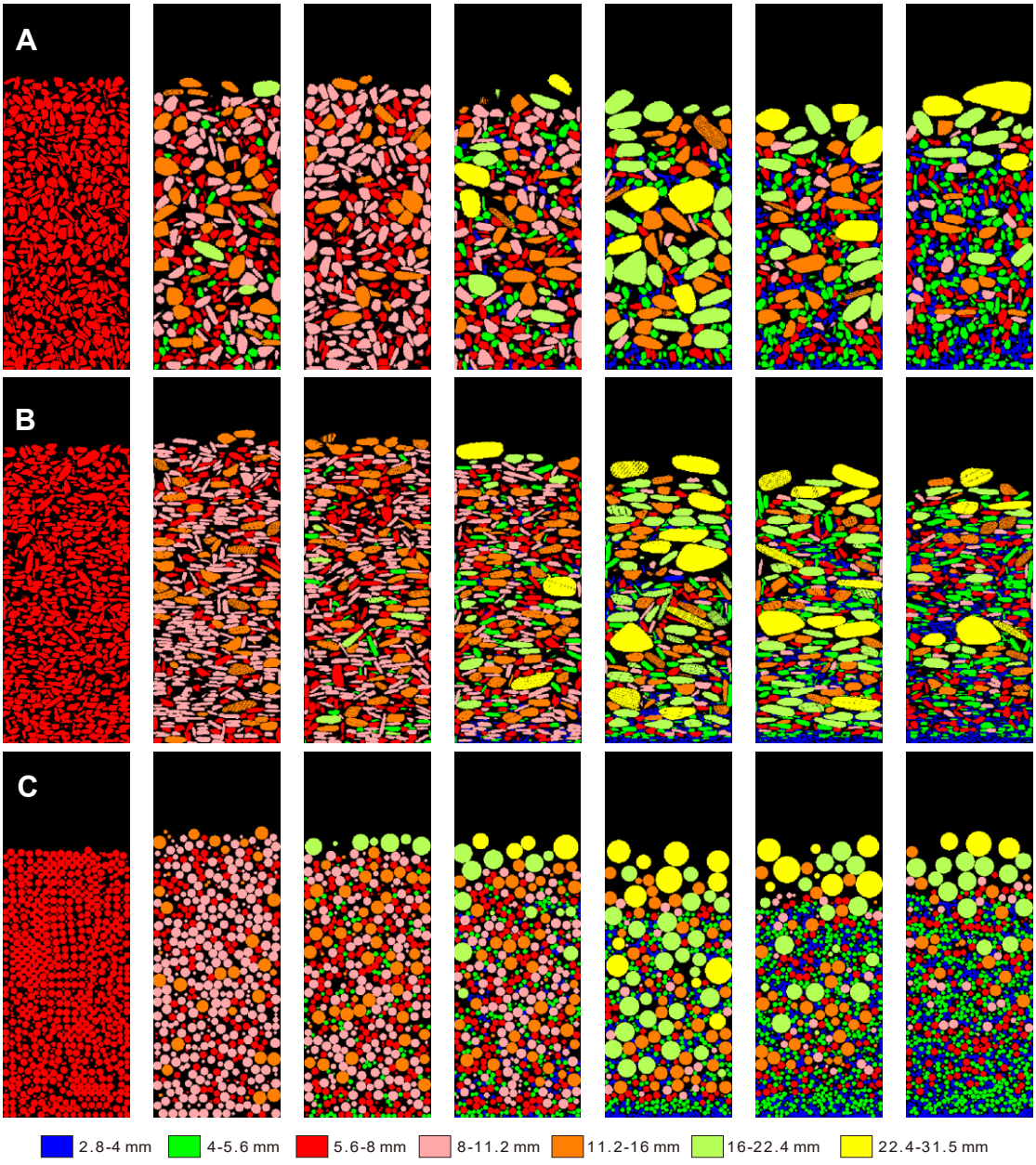

Figure 4.10. Cross section images of the generated digital packings for (A) Rhine sediments, (B) Kall sediments, and (C) glass beads. From left to right, the packings represent the four unimodal distributions (1, 3, 5, 7 fractions), and three bimodal distributions (30%, 50%, 70% percentage of fine mode).

4.4.2.2 Process control parameters

Another cause of simulation inaccuracy is the settings of process control parameters that affect the simulated packing structures, which are rebounding probability, addition rate and number of time steps. We did a sensitivity analysis to define the effects of these parameters on porosity. This was done by running a number of simulations in which one of the parameters was varied while keeping the others constant. To perform these simulations, 750 spherical particles (6.4 mm in diameter) and a cylinder (64mm in both diameter and height) were used. Resolution was set to 0.4 mm/voxel, giving a slight difference (<1% digitization error) between the digital volumes and real volumes.

Rebounding probability, designed to allow particles to move upwards, provides a non-physical way to generate vertical vibrations. The original intention of having a rebounding probability is to make it possible for particles to escape from their cramped places and continue to explore more suitable space to fit in, thereby simulating sediment compaction. The rebounding probability can be set between 0 and 1. A value of 0 means no rebounding and hence no vertical vibration applied. A value of 1 means particles having the same probability to move up or down, and hence kept suspended. To investigate its effects on porosity, seven rebounding probabilities varying from 0.1 to 0.7 were tested, while the addition rate and number of time steps remained the same (Table 4.3). The sensitivity analysis shows that bulk porosities vary parabolically as a function of the rebounding probability (Fig. 4.11A). The lowest porosity values appear at rebounding probabilities of 0.3-0.5, while lower and higher rebounding probabilities give higher porosities.

Addition rate controls the speed of introduction of particles into the packing space. Simulations with seven fixed addition rates were performed with the same sets of rebounding probability, and number of time steps (Table 4.4). Slower addition rates tend to generate denser packing structures, with bulk porosities decreasing from 0.46 to 0.42 (Fig. 4.11B). This effect is because with slower addition rates, particles have more time to find a better fitting position before being locked-in by new additions, resulting in denser packing structures.

In the packing algorithm, three types of time steps are defined: normal time steps, extra time steps and wind up time steps. Normal time steps are those during which particles drop into the packing space. They are closely related to the addition rate. For example, if the addition rate is chosen such that one particle drops down every 10 time steps, 1000 normal time steps are needed to introduce 100 particles into the packing space. In the case that a previously introduced particle still remains on top of the container, the next particle might be prevented from being introduced. In this instance, the next particle has to “wait” and extra time steps are needed to finish the packing. Wind up time steps are time steps at the end of a simulation during which no more particles are added and the rebounding probability is set to zero. These time steps enable the whole packing structure to consolidate. During the sensitivity analysis, only the effect of wind up time steps on porosity was assessed, since the effect of normal and extra time steps is directly related

to the addition rate. The number of wind up time steps was varied between 0 and 32000 (Table 4.5), and shows no systematic effect on porosity (Fig. 4.11C).

The sensitivity analysis confirms that the settings we chose for the validation of the stochastic digital packing algorithm (Table 4.1) result in the densest possible packings. This shows that the overestimation of porosity by this packing algorithm cannot be solved by choosing different settings for the simulations.

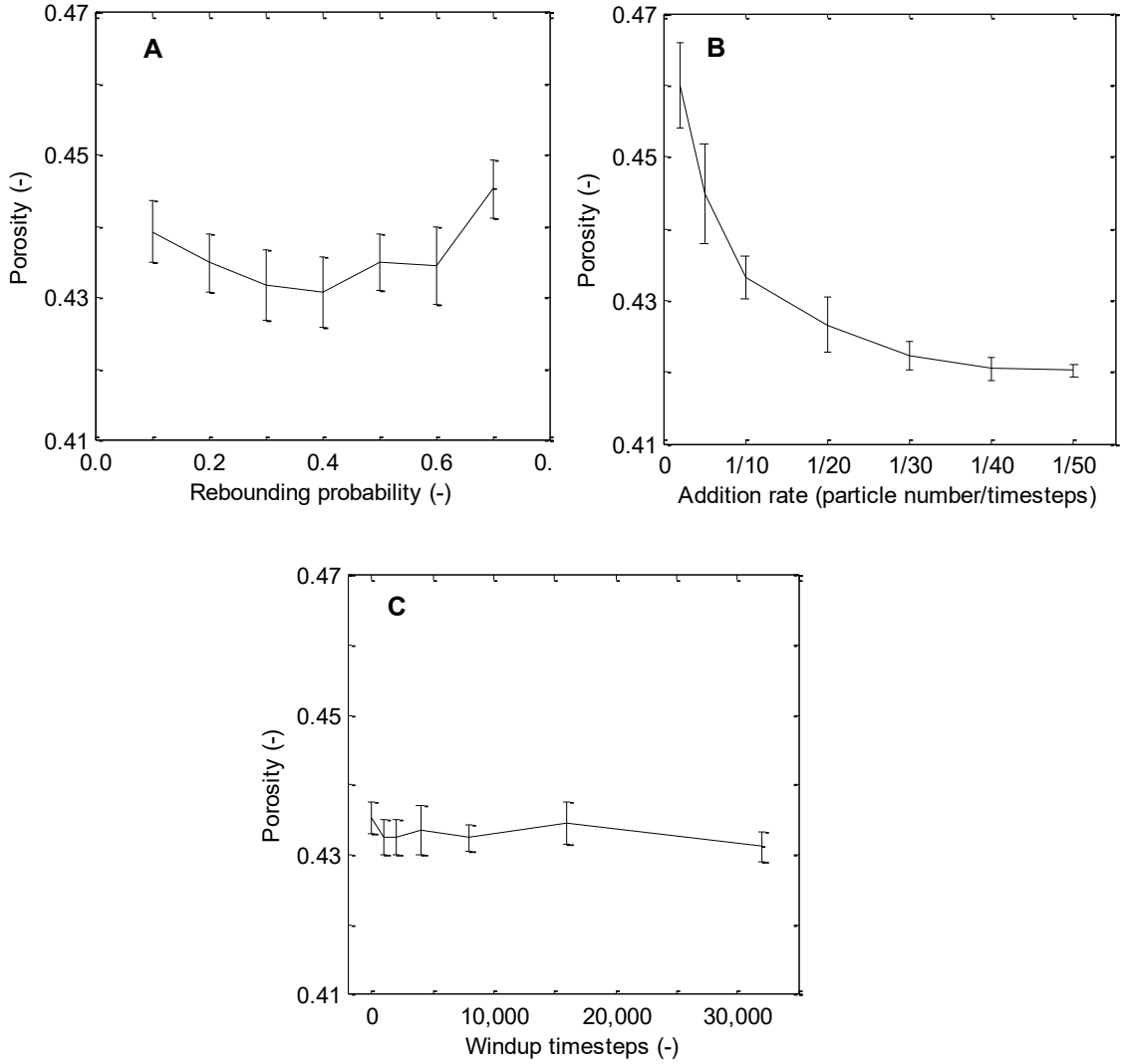

Figure 4.11. Sensitivity analysis of process control parameters on porosity, including (A) Rebounding probability, (B) Addition rate and (C) Windup timesteps. Each simulation was conducted three times and the error bar shows 95% confidence interval for the simulated porosities.

Table 4.3. Simulated porosity with varied rebounding probabilities (a, standard deviation)

ID	Rebounding Probability	Addition Rate			Extra Timesteps	Windup Timesteps	Simulated porosity				
		Amount	Every Timesteps	Normal Timesteps			1#	2#	3#	Mean	SD[a]
1	0.1	1	10	7500	0	500	0.437	0.440	0.441	0.439	0.002
2	0.2	1	10	7500	0	500	0.433	0.436	0.436	0.435	0.002
3	0.3	1	10	7500	0	500	0.434	0.429	0.432	0.432	0.002
4	0.4	1	10	7500	0	500	0.434	0.429	0.430	0.431	0.002
5	0.5	1	10	7500	0	500	0.434	0.438	0.434	0.435	0.002
6	0.6	1	10	7500	0	500	0.433	0.433	0.438	0.435	0.002
7	0.7	1	10	7500	0	500	0.446	0.447	0.443	0.445	0.002

Table 4.4. Simulated porosity with varied addition rates (a, standard deviation)

ID	Rebounding Probability	Addition Rate			Extra Timesteps	Windup Timesteps	Simulated porosity				
		Amount	Every Timesteps	Normal Timesteps			1#	2#	3#	Mean	SD[a]
1	0.25	1	2	1500	0	500	0.460	0.463	0.457	0.460	0.002
2	0.25	1	5	3750	0	500	0.446	0.448	0.441	0.445	0.003
3	0.25	1	10	7500	0	500	0.434	0.432	0.434	0.433	0.001
4	0.25	1	20	15000	0	500	0.424	0.427	0.428	0.427	0.002
5	0.25	1	30	22500	0	500	0.423	0.421	0.422	0.422	0.001
6	0.25	1	40	30000	0	500	0.421	0.421	0.420	0.421	0.001
7	0.25	1	50	37500	0	500	0.420	0.420	0.421	0.420	0.000

Table 4.5. Simulated porosity with varied windup timesteps (a, standard deviation)

ID	Rebounding Probability	Addition Rate			Extra Timesteps	Windup Timesteps	Simulated porosity				
		Amount	Every Timesteps	Normal Timesteps			1#	2#	3#	Mean	SD[a]
1	0.25	1	10	7500	500	0	0.434	0.435	0.437	0.435	0.001
2	0.25	1	10	7500	500	1000	0.432	0.432	0.434	0.433	0.001
3	0.25	1	10	7500	500	2000	0.434	0.431	0.433	0.433	0.001
4	0.25	1	10	7500	500	4000	0.435	0.432	0.435	0.434	0.002
5	0.25	1	10	7500	500	8000	0.432	0.434	0.432	0.432	0.001
6	0.25	1	10	7500	500	16000	0.434	0.433	0.436	0.435	0.001
7	0.25	1	10	7500	500	32000	0.431	0.432	0.430	0.431	0.001

4.4.2.3 Random walk-based algorithm

The reasons why the simulations failed to yield random dense packing structures can be explored in the random walk-based packing algorithm, by which the translational and rotational movements of particles during the simulation are completely random. Looking at the cross sections of the digital packings (Fig. 4.10) closely, the mixing of the particles is not uniform as smaller particles are more likely to concentrate at the bottom layer, particularly for the bimodal distributions with percentage of small particles increasing from 30% up to 70%. The phenomenon can be interpreted by kinematic sorting (i.e., segregation) effects. This is because particles kept moving randomly throughout the simulation, thus giving more chances for smaller particles to move through the pore spaces between larger particles and reach the bottom layer. Observations from Fig. 4.10 also suggest that shape effects strongly affect the simulated packing structures of fluvial sediments compared to the packings of glass beads. Because of random rotational motions during the simulation, the arrangements of particles with irregular shapes lead to create larger voids, especially between larger particles. For the simulations of glass beads, shape effects are inconsequential because the rotation of a sphere has no impact on particle packing. Therefore, kinematic sorting can fully explain the growing discrepancy trend for glass beads over the seven grain size distributions, while shape effects are the dominant reason that causes the porosity to be significantly overestimated for fluvial sediments (Fig. 4.9).

4.5 Conclusions

The applicability of a stochastic digital packing algorithm in predicting porosity of fluvial gravel deposits was validated. The conclusions are summarized as follows: (1) Apart from grain size, grain shape has a clear impact on porosity. (2) The packing algorithm provides an innovative way to simulate fluvial sediment mixtures with arbitrary shapes. (3) The packing algorithm correctly reflects the mixing effect on porosity for unimodal particle mixtures and also reproduces the differences in porosity for bimodal particle mixtures. However, in all cases, the packing algorithm systematically overestimates porosity mainly due to the unwanted kinematic sorting effects as well as shape effects introduced by the random motion of particles. (4) The packing algorithm is useful for trend analysis of packing porosity; but for a quantitative match a more rigorous model such as Discrete Element Method (DEM) where particle motion is physics-based may be needed.

References

Abreu, C.R.A., Tavares, F.W., Castier, M. (2003). Influence of particle shape on the packing and on the segregation of spherocylinders via Monte Carlo simulations. Powder Technology 134, 167-180.

Allen, J.R.L. (1985). Principles of Physical Sedimentology. Allen and Unwin, London.

Athy, L.F. (1930). Density, porosity, and compaction of sedimentary rocks. AAPG Bulletin 14, 1-24.

Bear, J. (1972). Dynamics of Fluids in Porous Media. Dover Publications, New York.

Blott, S.J., Pye, K., 2008. Particle Shape: a review and new methods of characterization and classification. Sedimentology 55, 31-63.

Boulton, A.J., Findlay, S., Marmonier, P., Stanley, E.H., Valett, H.M. (1998). The functional significance of the hyporheic zone in streams and rivers. Annual Review of Ecology, Evolution, and Systematics 29, 59-81.

Carling, P.A., Reader, N.A. (1982). Structure, composition and bulk properties of upland stream gravels. Earth Surface Processes and Landforms 7, 349-365.

Caulkin, R., Fairweather, M., Jia, X., Gopinathan, N., Williams, R.A. (2006). An investigation of packed columns using a digital packing algorithm. Computers and Chemical Engineering 30, 1178-1188.

Caulkin, R., Ahmad, A., Fairweather, M., Jia, X., Williams, R.A. (2007). An investigation of sphere packed shell-side columns using a digital packing algorithm. Computers and Chemical Engineering 31, 1715-1724.

Desmond, K.W., Weeks, E.R. (2009). Random close packing of disks andspheres in confined geometries. Physical Review E 80, 051305.

Desmond, K.W., Weeks, E.R. (2014). Influence of particle size distribution on random close packing of spheres. Physical Review E 90, 022204.

Donev, A., Connelly, R., Stillinger, F.H., Torquato, S. (2007). Underconstrained jammed packings of nonspherical hard particles: Ellipses and ellipsoids. Physical Review E 75, 051304.

Esselburn, J.D., Robert, W.R.J., Dominic, D.F. (2011). Porosity and permeability in ternary sediment mixtures. Ground Water 49, 393-402.

Ferellec, J., McDowell, G. (2010). Modeling realistic shape and particle inertia in DEM. Géotechnique 60, 227-232.

Frings, R.M., Kleinhans, M.G., Vollmer, S. (2008). Discriminating between pore-filling load and bed-structure load: a new porosity-based method, exemplified for the river Rhine. Sedimentology 55, 1571-1593.

Frings, R.M., Schüttrumpf, H., Vollmer, S. (2011). Verification of porosity predictors for fluvial sand-gravel deposits. Water Resources Research 47, 7525.

Fukuoka, S., Nakagawa, H., Sumi, T., Zhang, H. (2013). Advances in River Sediment Research, Taylor and Francis Group, London, 323-332.

Hubbard, P.M. (1996). Approximating polyhedra with spheres for time-critical collision detection. ACM Transactions on Graphics 15, 179-210.

Jia, X., Williams, R.A. (2001). A packing algorithm for particles of arbitrary shapes. Powder Technology 120, 175-186.

Jia, X., Gan, M., Williams, R.A., Rhodes, D. (2007). Validation of a digital packing algorithm in predicting powder packing densities. Powder Technology 174, 10-13.

Johnson, S., Williams, J.R., Cook, B. (2004). Contact resolution algorithm for an ellipsoid approximation for discrete element modeling. Engineering Computations 21, 215-234.

Kleinhans, M.G., Jeukens, C.R.L.P.N., Bakker, C.J.G., Frings, R.M. (2008). Magnetic Resonance Imaging of coarse sediment. Sedimentary Geology 208, 69-78.

Koltermann, C.E., Gorelick, S.M. (1995). Fractional packing model for hydraulic conductivity derived from sediment mixtures. Water Resources Research 31, 3283-3297.

Korte, A.C.J.de, Brouwers, H.J.H. (2013). Random packing of digitized particles. Powder Technology 233, 319-324.

Krumbein, W.C. (1941). Measurement and geological significance of shape and roundness of sedimentary particles. Journal of Sedimentary Research 11, 64-72.

Latham, J.P., Lu, Y., Munjiza, A. (2001). A random method for simulating loose packs of angular particles using tetrahedra. Géotechnique 51, 871-879.

Lu, G., Third, J.R., Müller, C.R. (2012). Critical assessment of two approaches for evaluating contacts between super-quadric shaped particles in DEM simulations. Chemical Engineering Science 78, 226-235.

Matsushima, T., Katagiri, J., Uesugi, K., Tsuchiyama, A., Nakano, T. (2009). 3D shape characterization and image-based DEM simulation of the lunar soil simulant FJS-1. Journal of Aerospace Engineering 22, 15-23.

Ouchiyama, N., Tanaka, T. (1984). Porosity estimation for random packings of spherical particles. Industrial and Engineering Chemistry Fundamentals 23, 490-493.

Richard, P., Philippe, P., Barbe, F., Bourlès, S., Thibault, X., Bideau, D. (2003). Analysis by X-ray microtomography of a granular packing undergoing compaction. Physical Review E 68, 020301.

Scott, G.D. (1960). Packing of spheres: packing of equal spheres. Nature 188, 908-909.

Song, Y.X., Turton, R., Kayihan, F. (2006). Contact detection algorithms for DEM simulations of tablet-shaped particles. Powder Technology 161, 32-40.

Suzuki, M., Oshima, T. (1985) Verification of a model for estimating the void fraction in a three-component randomly packed bed. Powder Technology 43. 147-153.

Tickell, F.G., Hiatt, W.N. (1938). Effect of angularity of grain on porosity and permeability of unconsolidated sands. The American Association of Petroleum Geologists 22, 1272-1274.

Vollmer, S., Kleinhans, M.G. (2007). Predicting incipient motion, including the effect of turbulent pressure fluctuations in the bed. Water Resources Research 43, 5410.

Wang, L.B., Park, J.Y., Fu, Y.R. (2007). Representation of real particles for DEM simulation using X-ray tomography. Construction and Building Materials 21, 338-346.

Weltje, G.J., Alberts, L.J.H. (2011). Packing states of ideal reservoir sands: Insights from simulation of porosity reduction by grain rearrangement. Sedimentary Geology 242, 52-64.

Wilcock, P.R. (1998). Two-fraction model of initial sediment motion in gravel-bed rivers. Science 280, 410-412.

Williams, J.R., Pentland, A.P. (1992). Superquadrics and modal dynamics for discrete elements in interactive design. Engineering Computations 9, 115-127.

Williams, S.R., Philipse, A.P. (2003). Random packings of spheres and spherocylinders simulated by mechanical contraction. Physical Review E 67, 051301.

Wooster, J.K., Dusterhoff, S.R., Cui, Y.T., Sklar, L.S., Dietrich, W.E., Malko, M. (2008). Sediment supply and relative size distribution effects on fine sediment infiltration into immobile gravels. Water Resources Research 44, 3424.

Wu, W., Wang, S.S.Y. (2006). Formulas for sediment porosity and settling velocity. Journal of Hydraulic Engineering 132, 858-862.

Yu, A.B., Standish, N. (1991). Estimation of the porosity of particle mixtures by a linear-mixture packing model. Industrial and Engineering Chemistry Research 30, 1372-1385.

Zhang, W.L., Thompson, K.E., Reed, A.H., Beenken L. (2006). Relationship between packing structure and porosity in fixed beds of equilateral cylindrical particles. Chemical Engineering Science 61, 8060-8074.

Zhao, J., Li, S.X., Zou, R.P., Yu, A.B. (2012). Dense random packings of spherocylinders. Soft Matter 8, 1003-1009.

Zhou, Z.Y., Zou, R.P., Pinson, D., Yu, A.B. (2011). Dynamic simulation of the packing of ellipsoidal particles. Industrial and Engineering Chemistry Research 50, 9787-9798.

Zingg, T. (1935). Beitrag zur Schotteranalyse. Schweizerische Mineralogische und Petrographische Mitteilungen 15, 39-140.

Zou, R.P., Yu, A.B. (1996). Evaluation of the packing characteristics of mono-sized non-spherical particles. Powder Technology 88, 71-79.

5

Grain Shape Approximation of Fluvial Sediments

Grain shape is a fundamental property of fluvial sediments and vital for various sediment processes. However, investigating the intricate role of grain shape in these processes remains difficult, due to the challenges associated with shape measurement, characterization, and control for the complex fluvial sediments. This study aimed to address these shape-related challenges by introducing an idealized regular shape that could approximate the overall form of fluvial sediments. To achieve this, we initially performed a comprehensive shape analysis of 241 digitized fluvial sediments, including 104 bulky Rhine sediments (Germany) and 137 platy Kall sediments (Germany). Subsequently, we selected four potential candidate shapes: cuboid, elliptic disk, truncated octahedron, and ellipsoid. The objective was to determine which candidate shape offered the closest approximation of sediment shape in terms of surface area, volume, and sphericity. In our investigation, we found that cuboid and elliptic disk shapes drastically overestimated the particle surface area and volume relative to the authentic shapes of the Rhine and Kall sediments, and thus were discarded. On the other hand, the truncated octahedron and ellipsoid shapes were able to provide reasonable estimates of particle surface area, volume, and sphericity, with mean ratios closely approaching unity. However, considering the prevalence of partially rounded forms in fluvial sediments as well as other factors such as the range of sphericity and numerical efficiency, we proposed the adoption of the ellipsoid shape as the idealized regular shape for approximating fluvial sediments. Furthermore, we conducted tests to assess the packing behavior when using ellipsoids as surrogates for fluvial sediments. The result revealed that ellipsoids, with sphericity values below 0.97, closely replicated the packing behavior of actual sediments in terms of both trend and accuracy.

5.1 Introduction

Grain shape, a fundamental property of fluvial sediment particles, has been demonstrated to influence packing porosity and permeability (Fraser, 1935; Frings et al., 2011; Liang et al., 2015; Rettinger et al., 2022; Rezaei et al., 2021), impact settling velocity (Komar and Reimers, 1978; Trunk et al., 2021), modify sediment transport rates and channel stability (Cassel et al., 2021; Deal et al., 2023; Jain et al., 2021; Komar & Li, 1986) amongst a host of others. The particle shape produced by physical processes, such as abrasion, selective transport, can also provide insights into the transport and depositional history and provenance of sediment grains (Bodek & Jerolmack, 2021; Novák-Szabó et al., 2018). Grain shape can be described by various parameters, among which three shape parameters, namely roughness, roundness (or angularity), and form (or sphericity), are considered to be of particular importance (Barrett, 1980; Clayton et al., 2009; Ulusoy, 2023; Yingst et al., 2008). The term roughness refers to the amount of surface irregularities or bumps on a grain surface. Roundness relates to the degree of curvature of the grain edges and corners. Sphericity, on the other hand, measures how closely a particle approximates a sphere in shape. Sphericity is dependent on roundness, as a perfect sphere indicates a constant radius of curvature (Blott & Pye, 2008). In this study, our focus is on the large-scale of form factor, i.e., sphericity.

Although it plays a prominent role in those aforementioned sediment processes, the effect of grain form has rarely been investigated systematically due to several challenges. The first challenge lies in the quantification of the sphericity for complex sediment shapes. By definition, sphericity is the ratio of the surface area of a sphere having the same volume as the grain to the surface area of the grain itself (Wadell, 1935). Such measures require information on both grain volume and surface area, which are difficult to obtain. While 3D scanning techniques such as scanning electron microscopy (SEM) (Bagheri et al., 2015), computed tomographic (CT) scanning (Voepel et al., 2019), and laser scanning (LS) (Anochie-Boateng et al., 2013) can provide detailed information about grain shape, they are cost-intensive and thus not feasible to large scale analysis. The second challenge is the confusion in charactering the form of grain shapes. Due to the difficulty in directly measuring sphericity, researchers have attempted to estimate it using simpler form terms that are practical to measure (e.g., Aschenbrenner, 1956; Blott & Pye, 2008; Corey, 1949; Folk, 1955; Janke, 1966; Krumbein, 1941; Wentworth, 1923). These terms describe grain form by combining the three size dimensions (length, breadth, and thickness) in various mathematical ways. However, each proposed shape index results in different values for the same object, leading to the confusion about which form term should be used for which type of investigation. The third challenge is the task of ensuring the reliability and reproducibility of results in shape-focused sediment studies. Natural sediment grains take on diverse shapes, due to various mechanical properties of their source rocks and transport conditions. Conventional experiments with actual sediments struggle to obtain a

sufficient number of identical-sized grains with uniform shapes (Fraser, 1935). Nonetheless, with the advent of digital scanning techniques, modern numerical simulations can now use replicated digital sediments to conduct shape-focused investigations (e.g., Coetzee, 2016; Liang et al., 2015; Rettinger et al., 2022; Wang et al., 2022; Zhao et al., 2020). However, the grain shape effect derived from a limited selection of digital sediments may not be universally representative, given the inherent variations in natural grain shapes. Thus, the validity of using a few instances of digital sediments to study the effect of sediment grain shapes remains a subject of question.

In this context, the objective of this paper was to approximate or substitute the intricate shape of fluvial sediments with an idealized regular shape. This approach can potentially overcome the challenges of shape measurement, characterization, and control, and facilitate a systematic comprehension of how grain shape impacts a range of sediment-related processes. To address this issue, we collected and analyzed two typical shape types of fluvial sediments, bulky and platy, using advanced scanning technologies. Subsequently, we selected four representative regular shapes to assess which shape renders the best approximation of the sediment particles, in terms of particle surface area, volume, and sphericity, as compared to those obtained through scanning.

5.2 Samples and Method

5.2.1 Samples

Two typical fluvial sediment samples were collected: (1) bulky sediments from the Rhine River (Germany), (2) platy sediments from the Kall River (Germany). The Rhine sediments were collected from the channel bed between the barrage of Iffezheim and the German-Dutch border. Quartz is the dominant lithology. The Kall sediments were collected from the channel bed between Simonskall and Zerkall. Slate is the dominant lithology.

The sampled sediments were then carefully cleaned, dried in an oven at 105°C for 48h and sieved with a width of 0.5 phi at the Krumbein scale: Rhine sediments (sieved from 1.4 to 31.5 mm) and Kall sediments (sieved from 0.25 to 63 mm). From each sieve fraction, 10~15 particles were randomly picked, leading to a total selection of 104 bulky Rhine sediments and 137 platy Kall sediments. These selected particles were later scanned via a nonmedical X-ray computed tomographic (CT) scanner. The scanning resolution was adjusted based on the size of particles being scanned. Specifically, resolutions of 0.0421~0.1478 mm/pixel were used for the Rhine sediments and 0.0025~0.2 mm/pixel were used for the Kall sediments. Such resolutions enabled high quality of the scanned 3D particles with examples shown in Fig. 5.1.

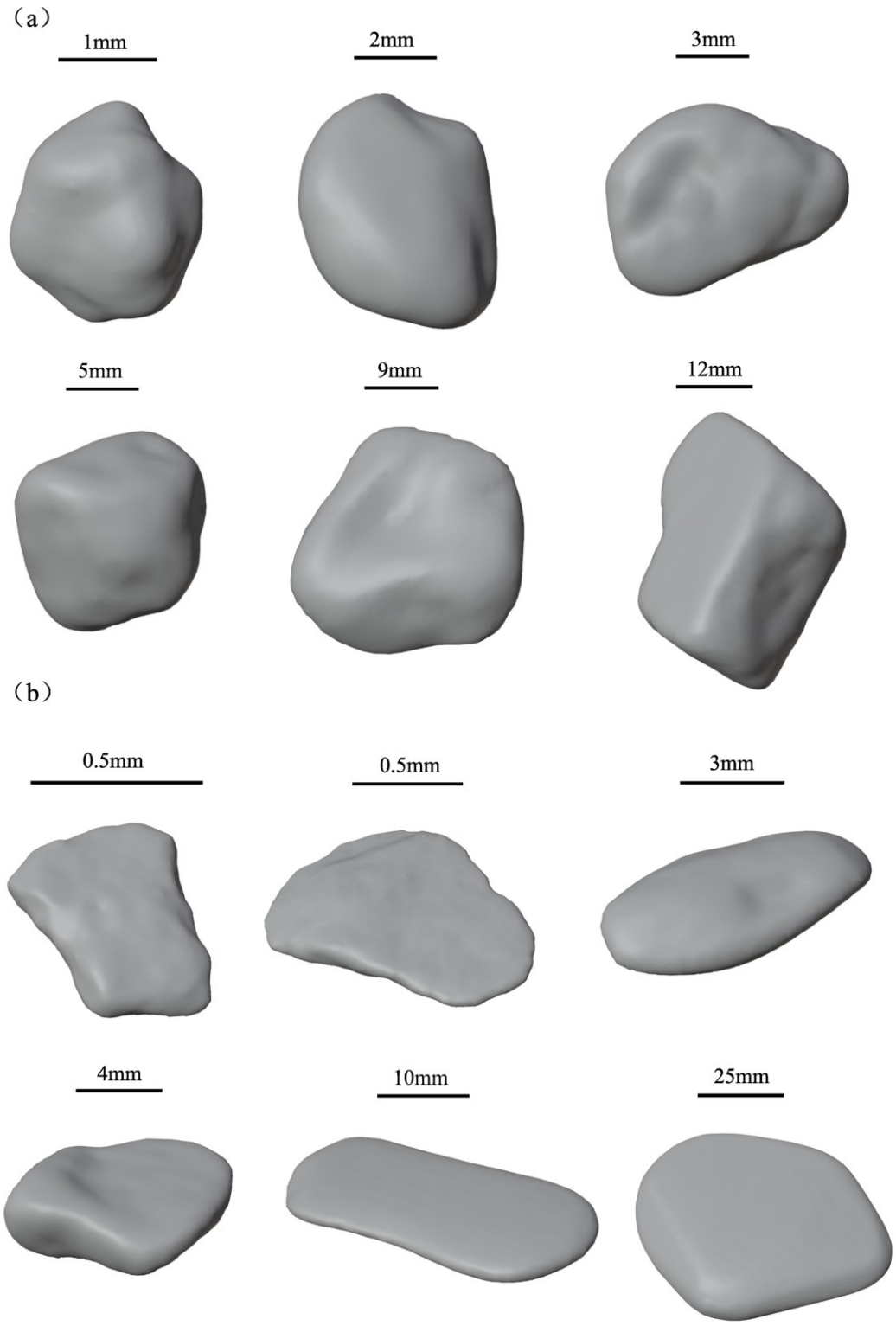

Figure 5.1. Examples of the scanned (a) bulky Rhine sediments and (b) platy Kall sediments, using the nonmedical X-ray computed tomographic (CT) technique. Noting that the scanned particles are shown in the surface-smoothed version described in section 5.2.2.2.

5.2.2 Shape Approximation

To obtain the idealized regular shape in analogue of arbitrary fluvial sediment shapes, four regular shapes were introduced as candidates, and each was compared to the scanned fluvial particles to determine the closest shape approximation in terms of particle surface area, volume, and sphericity.

5.2.2.1 Candidate Shapes

Four regular candidate shapes were chosen based on their shape similarities commonly found in natural sedimentary grains. These shapes include cuboids reminiscent of blocky fragments birthed from the intersection of fracture planes, elliptic disks dictating platy grains originating from layered or foliated rock formations, truncated octahedrons implying grains with faceted mineral surfaces, and ellipsoids representing partially rounded grains. The four candidate shapes are shown in Fig. 5.2. In geometry, both cuboid and truncated octahedron shapes are representations of convex polyhedrons, in which a cuboid is composed of three pairs of equal and opposite quadrilateral faces, while a truncated octahedron is bounded by three pairs of equal and opposite quadrilateral faces, and four pairs of equal and opposite hexagonal faces. The truncated octahedron is constructed from a regular octahedron by removing six right square pyramids. An elliptic disk resembles a solid disk but with an elliptical base instead of a circular one. It is formed by extending an ellipse along a straight line perpendicular to its plane. An ellipsoid is a quadric surface and can be derived from a sphere by deforming it by means of directional scalings.

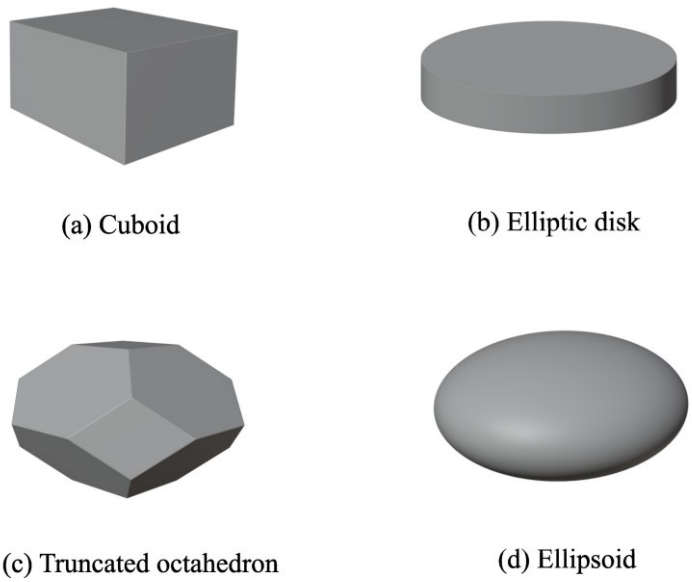

Figure 5.2. Four candidate shapes used to mimic the shape of fluvial sediments.

Calculations regarding the surface area, volume, and sphericity of the four candidate shapes are summarized below, in which L, I, S represent the long, intermediate, and short dimensions, measured along three orthogonal axes respectively.

For a cuboid

Surface area:

$$A_c = 2(LI + IS + LS) \tag{5.1a}$$

Volume:

$$V_c = LIS \tag{5.1b}$$

For an elliptic disk

Surface area:

$$A_d = BS + \frac{\pi}{2}LI \tag{5.2a}$$

where B is the circumference of an ellipse calculated using Ramanujan's approximation:

$$B \approx \frac{\pi}{2}(L + I)\left(1 + \frac{3\lambda^2}{10 + \sqrt{4 - 3\lambda^2}}\right) \tag{5.2b}$$

where $\lambda = \frac{(L-I)}{(L+I)}$, the error is on the order of λ to the 10th power, i.e., $O(\lambda^{10})$.

Volume:

$$V_d = \frac{\pi}{4}LIS \tag{5.2c}$$

For a truncated octahedron

Surface area:

$$A_t = \frac{1}{4}(LI + IS + LS) + \frac{3}{2}\sqrt{(LI)^2 + (IS)^2 + (LS)^2} \tag{5.3a}$$

Volume:

$$V_t = \frac{1}{2}LIS \tag{5.3b}$$

For an ellipsoid

Surface area:

$$A_e \approx \pi \left[\frac{(LI)^p + (LS)^p + (IS)^p}{3} \right]^{1/p} \tag{5.4a}$$

with $p \approx 1.6075$ yielding a relative error of at most $\pm 1.061\%$.

Volume:

$$V_e = \frac{\pi}{6} LIS \tag{5.4b}$$

For all the candidate shapes, the term sphericity is calculated as the ratio of the surface area of a sphere that has the same volume as the given shape to the surface area of that shape (Wadell, 1935), expressed as:

$$\Psi = \frac{A_s}{A_p} = \frac{\pi^{\frac{1}{3}} (6V_p)^{\frac{2}{3}}}{A_p} \tag{5.5}$$

where A_S is the surface area of the sphere of the same volume as the given particle. A_p and V_p denote the surface area and the volume of that given particle separately.

5.2.2.2 Shape Analysis

To compare with fluvial sediment shapes, shape analysis was performed on each scanned particle, with a focus on the characterization of 1D variables, i.e., form dimensions: L, I, S, respectively the length of long, intermediate, and short orthogonal axes, and 3D variables, i.e., particle surface area A_p, solid volume V_p, and sphericity Ψ.

With respect to the measurement of 1D variables, we applied the protocol of Blott and Pye (2008), which defines the L, I, and S dimensions being equivalent to the side lengths of the smallest imaginary box enclosing the particle, so-called the Minimal Bounding Box (MBB) here calculated using the MATLAB toolbox of Korsawe (2023) (Fig. 5.3).

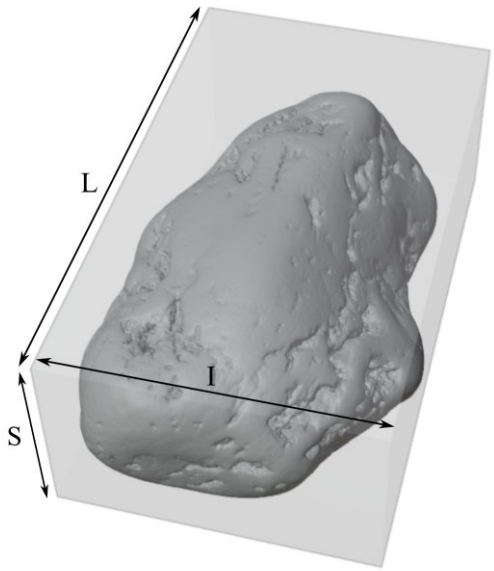

Figure 5.3. Schematic illustration of the protocol of the Minimal Bounding Box (MBB) used to measure form dimensions.

In order to focus solely on the overall form of the grain shape when measuring 3D variables, we initially applied a surface smoothing treatment to the original scanned particles. To achieve this, we introduced the Remesh method, which involves generating a new manifold mesh for the current geometry. By carefully tuning the resolution of this new mesh, we were able to smooth out the small-scale surface irregularities (roughness) while minimizing the impact on the large form of irregular shapes (Fig. 5.4). In doing so, we simplified the complexity of the particle surface by transforming it into a smooth solid that could be more easily approximated.

To obtain the surface area and volume of the smoothed grains, we utilized the 3D Print Toolbox, an add-on bundled with Blender, and subsequently calculated the sphericity of the grains based on Eq. (5.5). It is noteworthy that all of these operations were carried out in Blender (v. 3.3), a free and open-source software known for its versatility and capabilities in the field of 3D modeling and rendering.

Figure 5.4. Comparison of the original grain geometry to the smoothed version (shown in shade smooth mode) after applying the Remesh modifier in Blender. In this specific case, the surface area decreased by approximately 18.25% after smoothing, while the volume only reduced by about 1.23%. However, for most cases with less extreme surface irregularities, the surface area decreased within 10%, and the volume decreased by less than 1%.

5.3 Results

5.3.1 Measured Characteristics of Fluvial Sediments

The relationship between the measured I_ϕ, intermediate size in phi unit, transformed using the expression $I_\phi = -log_2 I$, where I in millimeters, and the surface area, volume and sphericity of Rhine and Kall grains is shown in Fig. 5.5. The scanned fluvial sediments are characterized by a large size range from 0.29 mm up to 54.3 mm (-5.76-1.77 in phi scale), thus from medium sand to very coarse gravel. In general, as the intermediate size of fluvial sediment increases, the surface area and volume also tend to increase, exhibiting an exponential growth trend formulated as follows (Fig. 5.5a&b):

$$A_p = ae^{bI_\phi} \tag{5.6a}$$

$$V_p = ce^{dI_\phi} \tag{5.6b}$$

where coefficients a = 2.87, b = -1.38, c = 0.33 and d = -2.04, yielding the mean absolute percentage error (MAPE) of around 21% and 49% for the estimation of particle surface area and volume respectively.

While the general trend suggests that an increase in intermediate size corresponds to an increase in surface area and volume, variations can occur due to the fact that the surface area or volume for fluvial sediments could be influenced by numerous factors, such as the sediment source, hydraulic conditions, and transport processes. This explains the relatively high MAPE estimated by Eq. (5.6).

However, no relationship between intermediate size I_ϕ and sphericity Ψ was found, suggesting that the sphericity of a fluvial grain can vary independently of the grain's intermediate size (Fig. 5.5c). This is in accord with the observation of Gale that there is no evidence of any variation in Ψ as a function of size (Gale, 2021). And this study suggests that values of Ψ for sands and gravels from fluvial environments lies in the range of 0.46 ~ 0.96, with the mean Ψ of 0.86 for the bulky Rhine sediments and 0.71 for the platy Kall sediments.

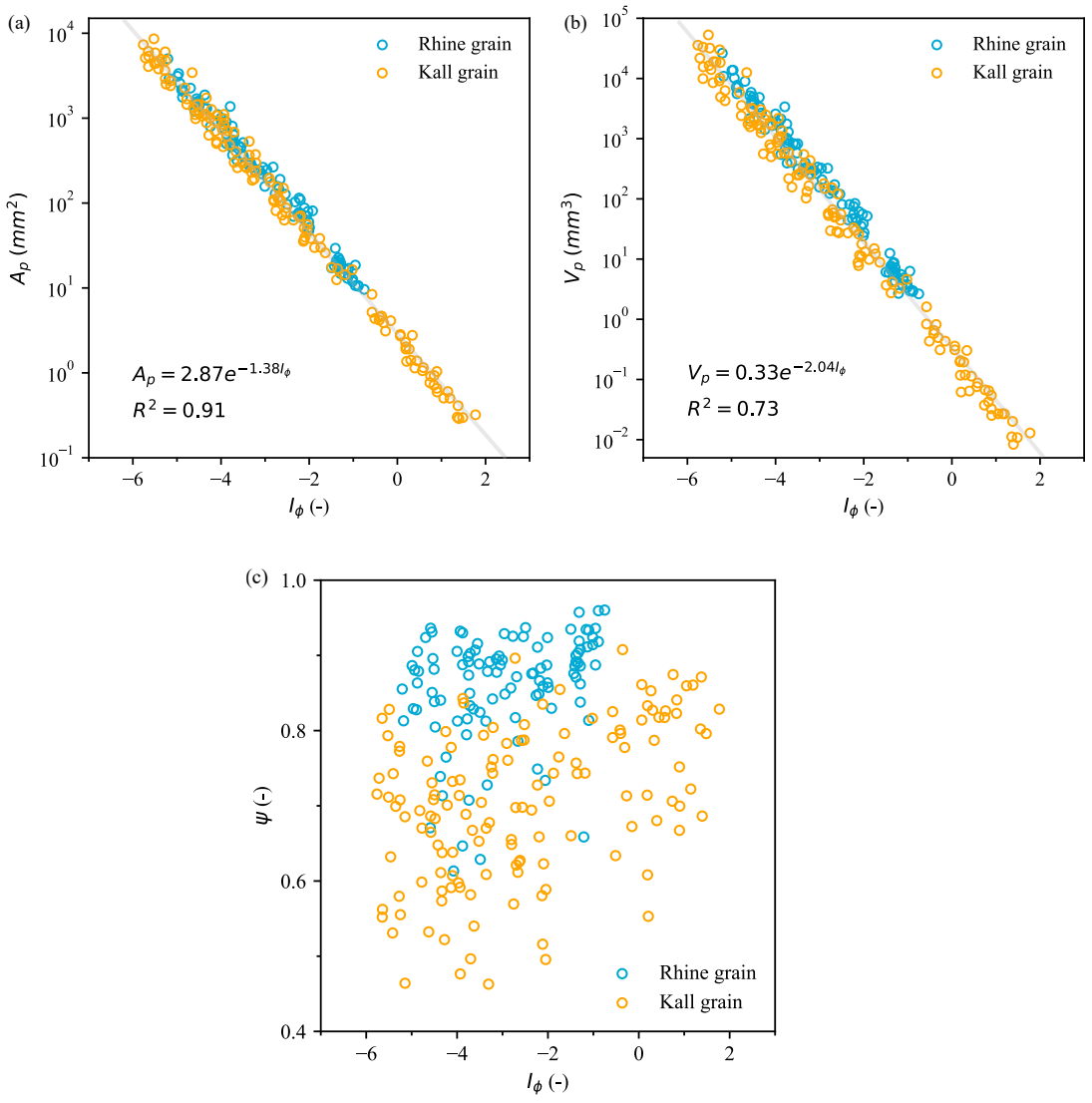

Figure 5.5. Relationship between the intermediate size I_ϕ (phi unit) and the (a) surface area A_p, (b) volume V_p, (c) sphericity Ψ of fluvial sediments. As noted, the exponential growth trend is actually displayed in linear forms under the logarithmic scale of A_p and V_p (shown in gray line).

5.3.2 Approximation of Fluvial Sediments

To compare and determine which regular shape best approximates fluvial sediments, we calculated ratios of the surface area, volume, and sphericity between the four candidate shapes and the smoothed sediments illustrated in Fig. 5.6. Each boxplot provides a comprehensive overview of the distribution of data through their quartiles. The actual box itself represents the first and third quartiles, while the band inside represents the second quartile (the median). The whiskers extend to the lowest and highest data points that are still within 1.5 times interquartile range of the lower and upper quartiles, respectively. Any outliers that fall outside the whiskers are featured as circles, and the mean of each distribution is also displayed.

As shown in Fig. 5.6, the cuboid and elliptic disk shapes exhibit significantly larger ratios (measuring 1.45~2.21 times greater, on average) in terms of surface area and volume when compared to the authentic shapes of Rhine and Kall sediments, suggesting that they are not qualified for approximating fluvial sediments. In contrast, both truncated octahedron and ellipsoid shapes manifest ratios that are substantially closer to unit and display a narrower degree of dispersion. Specifically, for fluvial sediments, the ellipsoid offers a superior estimation of particle surface area (mean ratio of 1.04) compared to the truncated octahedron (mean ratio of 1.12), while the truncated octahedron is more adept at particle volume estimation (mean ratio of 1.11) than the ellipsoid (mean ratio of 1.16). As a result, according to Eq. (5.5), the ellipsoid yields a slightly higher ratio of particle sphericity (mean ratio of 1.06) than the truncated octahedron (mean ratio of 0.95).

While both truncated octahedron and ellipsoid shapes provide reasonable representations for fluvial sediments in terms of surface area, volume and sphericity, the ellipsoid shape might be a more suitable choice to mimic the shape of fluvial sediments. In general, fluvial sediments are often rounded or semi-rounded, and the ellipsoid shape can closely mimic this feature. Moreover, an ellipsoid can represent the full range of particle sphericity from 0 to 1, providing a wider range of applicability compared to a truncated octahedron, which can only represent the particle sphericity up to 0.91 when the three orthogonal dimensions are set equal. In addition, an ellipsoid might be more numerically efficient than a truncated octahedron. This is because the equations that describe an ellipsoid are simpler and more symmetrical, which can make computations involving the shape faster and less prone to numerical errors. Conversely, a truncated octahedron, with its more complex shape and less symmetry, might require more complex and time-consuming computations.

In sum, while ellipsoids may not be capable of capturing the full complexity of real-world sediment particles, they still offer advantages in approximating fluvial sediments. Ellipsoids can serve as an idealized, tractable model-input solid body for better understanding the crucial role of grain shape in sediment-related physical processes and properties.

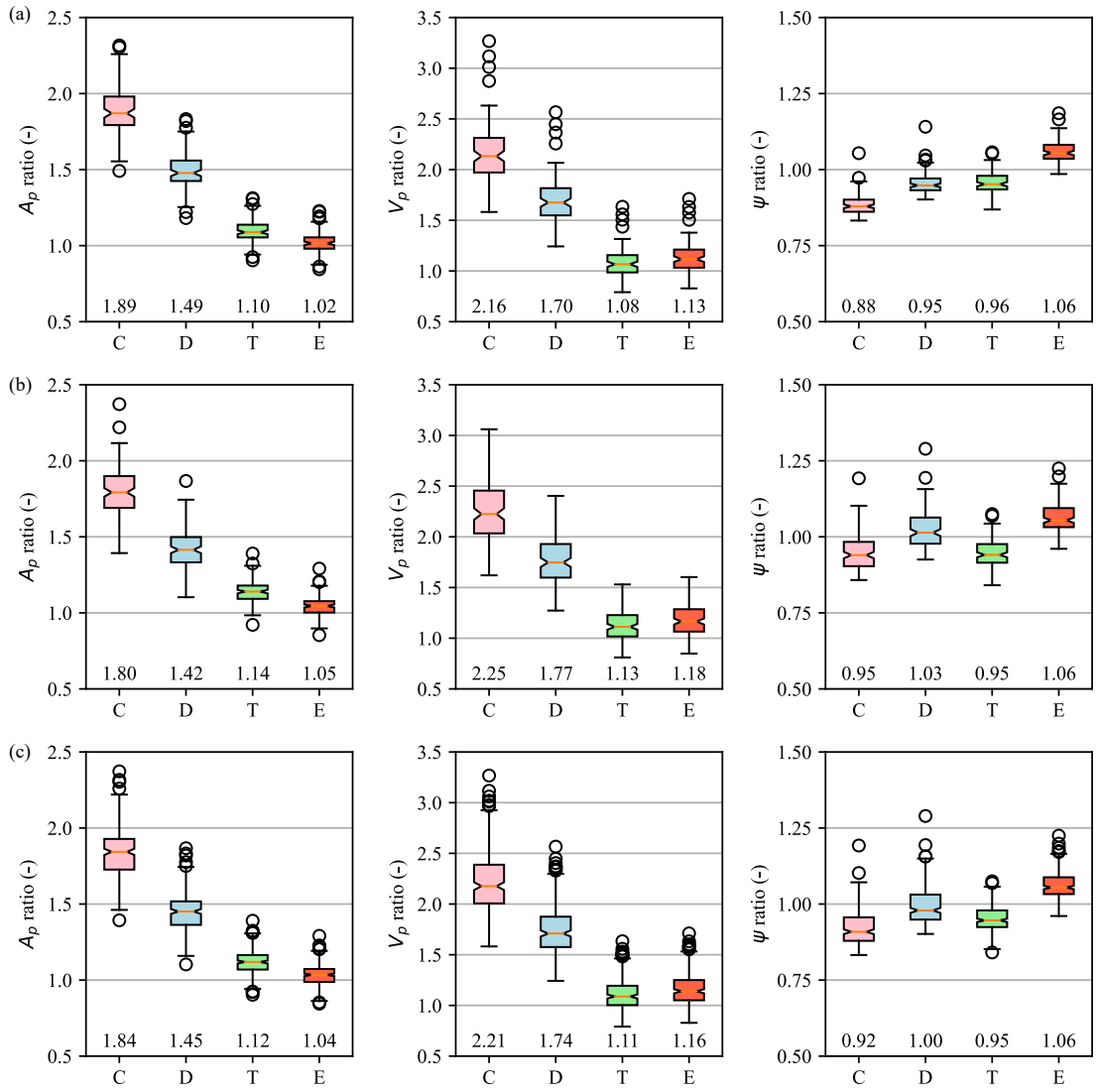

Figure 5.6. Box plot representing the ratios of surface area, volume, and sphericity between the four candidate shapes and the smoothed (a) Rhine sediments ($N = 104$), (b) Kall sediments ($N = 137$), and (c) Rhine and Kall sediments ($N = 241$). Labels C, D, T and E represent cuboid, elliptic disk, truncated octahedron, and ellipsoid shapes separately.

5.4 Discussion

5.4.1 New Definition of Sphericity

Sphericity is a concept introduced by Wadell (1935) to describe the degree to which a particle approaches a perfect sphere in shape. According to Wadell's definition, sphericity is the ratio of the surface area of a sphere having the same volume as the particle to the surface area of the particle itself. However, we argue that a more appropriate definition of sphericity should be based on the smoothed surface area of the particle, rather than the

actual surface area. This is due to the fact that small-scale surface irregularities do not have a significant impact on the overall form of a particle.

Consider, for example, a nearly perfect sphere with extreme surface irregularities, such as blocky surfaces (Fig. 5.7). According to the general geometry of the shape, this particle should have a sphericity close to 1. However, the result shows that such a particle actually has a sphericity of only about 0.66 based on the definition of Wadell, resulting in a 33% decrease in the true sphericity value. While such extreme deviations in sphericity may not be common in reality, our findings suggest that sphericity deviations for fluvial sediments can be up to 18%, which is still unacceptable.

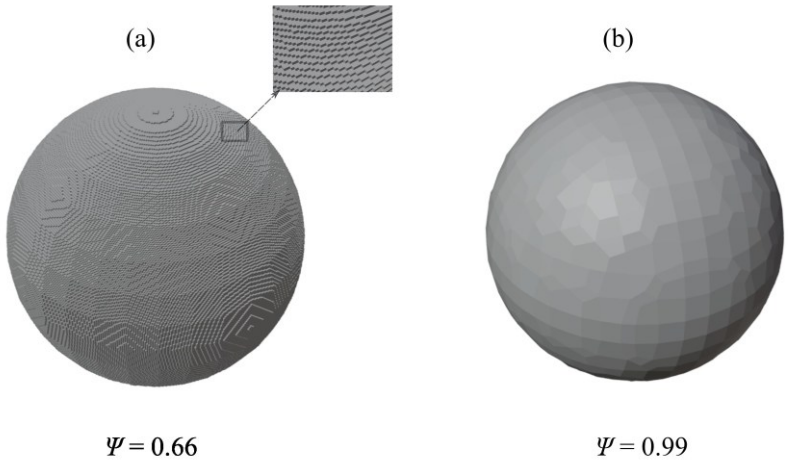

Figure 5.7. General form comparison between (a) a sphere with extreme surface roughness and (b) the same sphere after applying a surface smoothing treatment.

To address this issue, we propose the actual surface area as in the Wadell's definition of sphericity should be replaced by the smoothed surface area of the particle. With this new definition, more accurate and reliable measurements of sphericity can be derived, especially for particles with complex surface morphology.

5.4.2 Behavior of Using Ellipsoids on Behalf of Fluvial Sediments

While ellipsoids have been posited as an idealized shape to approximate fluvial sediments, the intricacies of their behaviors necessitate thorough testing prior to any sediment-related applications. Here, we demonstrate, as an example, the packing behavior of fluvial sediments approximated by ellipsoids, based on the pioneering work of Rettinger et al. (2022).

In the work, 63 digitized grains, sourced from the Rhine River, were utilized to generate random dense packings with the discrete element method. Each simulation featured only one single grain. The size of each single grain was rescaled to match the desired sizes for three grain size distributions used for the simulations (Table 5.1), while retaining the general form of the original grains. Afterwards, 63 form-equivalent ellipsoids were also conducted for the same set of simulations. This resulted in a total of

189 simulations for both digital sediments and their corresponding ellipsoids, with 63 simulations done for each of the three grain size distributions.

Table 5.1. Mass-based grain size distributions used for the simulation studies.

Case	2.8-4 mm	4-5.6 mm	5.6-8 mm	8-11.2 mm	11.2-16 mm	16-22.4 mm	22.4-31.5 mm
U1	.0	.0	1.	.0	.0	.0	.0
U7	.04	.11	.22	.26	.22	.11	.04
B50	.13	.21	.13	.06	.13	.21	.13

U1, U7 represent unimodal distributions, with the numeral denoting the number of size fractions, while B50 represents the bimodal distribution, with the numerical indicating the mass percentage of finer grains.

We use the comparison of generated porosity as a metric for assessing the packing behavior of using ellipsoids as a surrogate for fluvial sediments (Fig. 5.8). Our findings point to the general similarity between the ellipsoid shape and the actual sediment shape, with a root-mean-square difference of around 0.008 across all three distributions. However, we observe a marked deviation when the ellipsoid shape approaches a sphere, as indicated by sphericity values exceeding approximately 0.97. Specifically, the ellipsoids evince a minimum porosity followed by an abrupt increase, a trend that stands in stark contrast to the further decrease of porosity exhibited by actual sediments. This intriguing behavior is particularly pronounced in the case of unimodal distributions, whilst being comparatively less marked in the bimodal distribution.

Such abrupt turning behavior of ellipsoids was also observed in other studies, which likewise obtained a comparably shaped curve featuring a minimum porosity located at aspect ratios of approximately 1.5 (prolate) or 0.67 (oblate), corresponding to the sphericity value of approximately 0.97 (see Delaney and Cleary, 2010; Donev et al., 2004; Zhou et al., 2011). The reason for this distinct behavior in this region is likely due to the heightened sensitivity of particle arrangement to the irregularities or blockiness of the actual geometry as it approaches a spherical form (Rettinger et al., 2022).

To sum up, in most cases, ellipsoids with sphericity values less than 0.97 are capable of closely approximating the packing behavior of actual sediments in both trend and accuracy. However, for ellipsoids that exhibit a sphere-like form, with sphericity values exceeding 0.97, the packing behavior is strikingly altered, implying the potential for similar effects to occur in other sediment-related processes. This example serves to highlight the efficiency of ellipsoids as a reliable approximation shape, but meanwhile emphasizes the critical importance of validating their behavior prior to utilizing them.

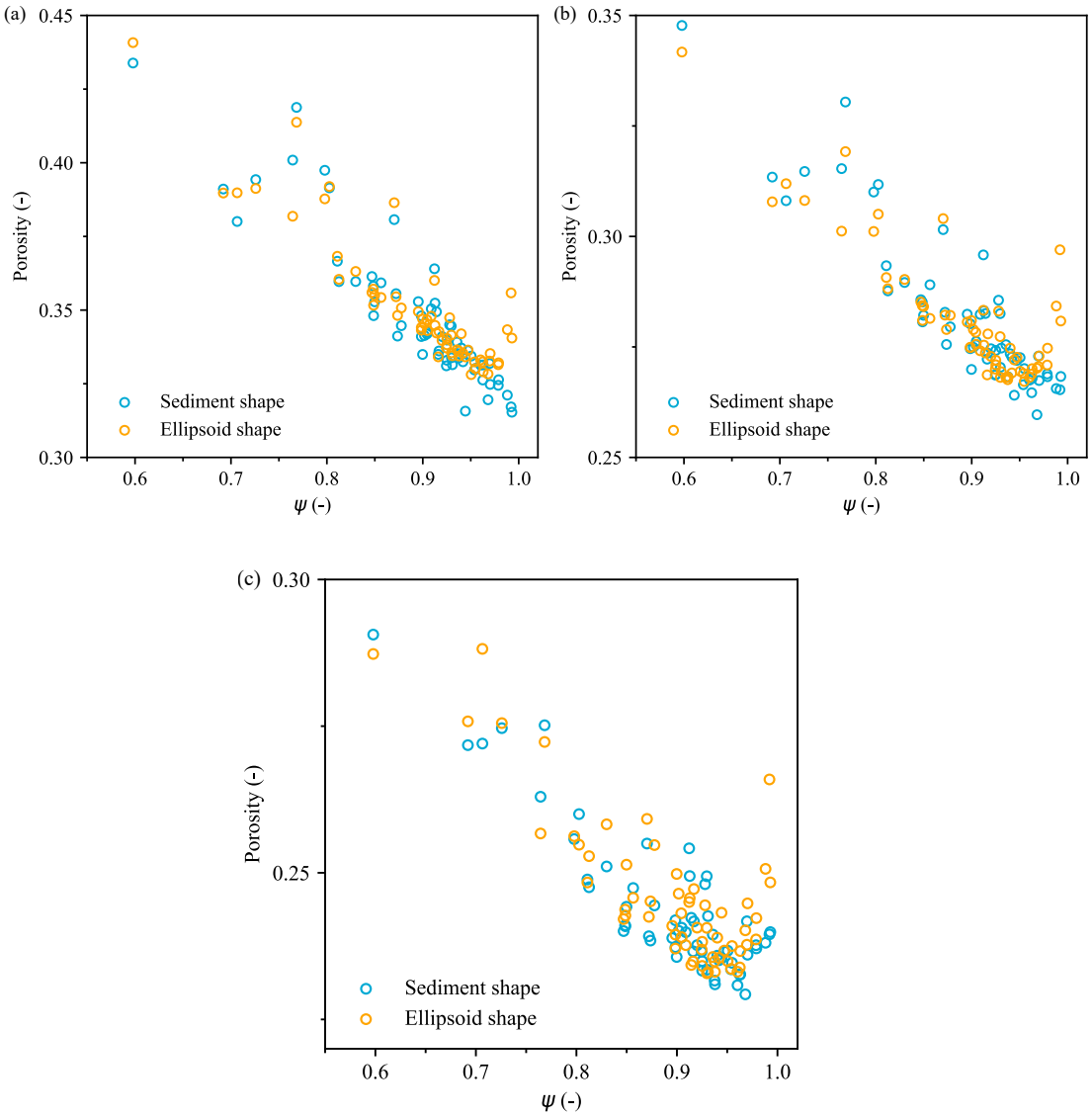

Figure 5.8. Comparing the packing behavior of fluvial sediments and equivalent ellipsoids using simulated porosity values as a function of sphericity, for (a) U1 distribution, (b) U7 distribution, (c) B50 distribution. Note that the sphericity values shown here are calculated based on the equivalent ellipsoids.

5.5 Conclusions

In this study, we explored the possibility of employing regular shapes to approximate the intricate shapes of fluvial sediments. Four potential candidate shapes were chosen, namely the cuboid, elliptic disk, truncated octahedron, and ellipsoid, to approximate the surface area, volume, and sphericity of fluvial sediment shapes. The result reveals that both the truncated octahedron and ellipsoid shapes are able to deliver reasonable accuracies. Nevertheless, taking into account the typical partially round forms that fluvial sediments often exhibit, as well as other factors such as the range of sphericity and numerical efficiency, we recommend the ellipsoid shape as a better option for

approximating fluvial sediments. The general similarity of the packing behavior between ellipsoids and actual sediments demonstrates the reliability of using the ellipsoid approximation. However, it must be emphasized that validating the behavior of ellipsoids is critical prior to any sediment-related applications.

References

Anochie-Boateng, J.K., Komba, J.J., Mvelase, G.M. (2013). Three-dimensional laser scanning technique to quantify aggregate and ballast shape properties. Construction and Building Materials, 43, 389-398.

Aschenbrenner, B.C. (1956). A new method of expressing particle sphericity. Journal of Sedimentary Research, 26, 15-31.

Bagheri, G.H., Bonadonna, C., Manzella, I., Vonlanthen, P. (2015). On the characterization of size and shape of irregular particles. Powder Technology, 270, 141-153.

Barrett, P.J. (1980). The shape of rock particles, a critical review. Sedimentology, 27, 291-303.

Blott, S.J., Pye, K. (2008). Particle shape: a review and new methods of characterization and classification. Sedimentology, 55, 31-63.

Bodek, S., Jerolmack, D.J. (2021). Breaking down chipping and fragmentation in sediment transport: The control of material strength. Earth Surface Dynamics, 9, 1531-1543.

Cassel, M., Lavé, J., Recking, A., Malavoi, J.R., Piégay, H. (2021). Bedload transport in rivers, size matters but so does shape. Scientific Reports, 11, 508.

Clayton, C.R.I., Abbireddy, C.O.R., Schiebel, R. (2009). A method of estimating the form of coarse particulates. Géotechnique, 59, 493-501.

Coetzee, C.J. (2016). Calibration of the discrete element method and the effect of particle shape. Powder Technology, 297, 50-70.

Corey, A.T. (1949). Influence of shape on the fall velocity of sand grains. MSc Thesis.

Deal, E., Venditti, J.G., Benavides, S.J., Bradley, R., Zhang, Q., Kamrin, K., Perron, J.T. (2023). Grain shape effects in bed load sediment transport. Nature, 613, 298-302.

Delaney, G.W., Cleary, P.W. (2010). The packing properties of superellipsoids. Europhysics Letters Association, 89, 34002.

Donev, A., Cisse, I., Sachs, D., Variano, E.A., Stillinger, F.H., Connelly, R., Torquato, S., Chaikin, P.M. (2004). Improving the Density of Jammed Disordered Packings Using Ellipsoids. Science, 303, 990-993.

Folk, R.L. (1955). Student operator error in determination of roundness, sphericity, and grain size. Journal of Sedimentary Research, 25, 297-301.

Fraser, H.J. (1935). Experimental Study of the Porosity and Permeability of Clastic Sediments. The Journal of Geology, 43, 910-1010.

Frings, R.M., Schüttrumpf, H., Vollmer, S. (2011). Verification of porosity predictors for fluvial sand-gravel deposits. Water Resources Research, 47, 7525.

Gale, S.J. (2021). The Shape of Fluvial Gravels: Insights from Fiji's Sabeto River. Geosciences, 11, 161.

Jain, R., Tschisgale, S., Fröhlich, J. (2021). Impact of shape: DNS of sediment transport with non-spherical particles. Journal of Fluid Mechanics, 916.

Janke, N.C. (1966). Effect of shape upon the settling velocity of regular convex geometric particles. Journal of Sedimentary Research, 36, 370-376.

Komar, P.D., Li, Z. (1986). Pivoting analyses of the selective entrainment of sediments by shape and size with application to gravel threshold. Sedimentology, 33, 425-436.

Komar, P.D., Reimers, C.E. (1978). Grain Shape Effects on Settling Rates. The Journal of Geology, 86, 193-209.

Krumbein, W.C. (1941). Measurement and geological significance of shape and roundness of sedimentary particles. Journal of Sedimentary Research, 11, 64-72.

Liang, R., Schruff, T., Jia, X., Schüttrumpf, H., Frings, R.M. (2015). Validation of a stochastic digital packing algorithm for porosity prediction in fluvial gravel deposits. Sedimentary Geology, 329, 18-27.

Korsawe Johannes, (2023). Minimal Bounding Box. https://www.mathworks.com/matlabcentral/fileexchange/18264-minimal-bounding-box.

Novák-Szabó, T., Sipos, A.Á., Shaw, S., Bertoni, D., Pozzebon, A., Grottoli, E., Sarti, G., Ciavola, P., Domokos, G., Jerolmack, D.J. (2018). Universal characteristics of particle shape evolution by bed-load chipping. Science Advances, 4(3), 4946.

Rettinger, C., Rüde, U., Vollmer, S., Frings, R.M. (2022). Effect of sediment form and form distribution on porosity: a simulation study based on the discrete element method. Granular Matter, 24, 1-23.

Rezaei, E., Zeinalzadeh, K., Ghanbarian, B. (2021). Effects of particle shape and size distribution on hydraulic properties of grain packs: An experimental study. Journal of Contaminant Hydrology, 243, 103918.

Trunk, R., Bretl, C., Thäter, G., Nirschl, H., Dorn, M., Krause, M.J. (2021). A Study on Shape-Dependent Settling of Single Particles with Equal Volume Using Surface Resolved Simulations. Computation, 9, 40.

Ulusoy, U. (2023). A Review of Particle Shape Effects on Material Properties for Various Engineering Applications: From Macro to Nanoscale. Minerals, 13, 91.

Voepel, H., Leyland, J., Hodge, R.A., Ahmed, S., Sear, D. (2019). Development of a vector-based 3D grain entrainment model with application to X-ray computed tomography scanned riverbed sediment. Earth Surface Processes and Landforms, 44, 3057-3077.

Wadell, H. (1935). Volume, Shape, and Roundness of Quartz Particles. The Journal of Geology, 43, 250-280.

Wang, X., Yin, Z.Y., Su, D., Wu, X., Zhao, J. (2022). A novel approach of random packing generation of complex-shaped 3D particles with controllable sizes and shapes. Acta Geotechnica, 17, 355-376.

Wentworth, C.K. (1923). The shapes of beach pebbles. Professional Paper, 131, 75-83.

Yingst, R.A., Crumpler, L., Farrand, W.H., Li, R., Cabrol, N.A., Neakrase, L.D. (2008). Particle Shape Quantities and Measurement Tecniques - A review. Electronic Journal of Geotechnical Engineering, 113.

Zhao, L., Zhang, S., Huang, D., Wang, X., Zhang, Y. (2020). 3D shape quantification and random packing simulation of rock aggregates using photogrammetry-based reconstruction and discrete element method. Construction and Building Materials, 262.

Zhou, Z.Y., Zou, R.P., Pinson, D., Yu, A.B. (2011). Dynamic Simulation of the Packing of Ellipsoidal Particles. Industrial & Engineering Chemistry Research, 50, 9787-9798.

6

Characterization of Ellipsoids and The Porosity-Shape Relation

The packing of ellipsoids has been extensively investigated to elucidate the grain shape effect on properties of non-spherical packing systems, such as porosity or packing fraction. However, most studies have engaged spheroids, as their research subjects, thus overlooking the majority of ellipsoidal geometries. This likely stems from the convenient characterization of spheroids by a single shape factor, the aspect ratio (α), whereas no comparable general metric exists to describe the varied shapes of general ellipsoids. In this study, the shape of general ellipsoids was characterized based on two well-defined parameters, Wadell's sphericity (Ψ_e) and Zingg's intercept ratio (F), which can be directly computed from semi-axis lengths. Sphericity (Ψ_e) quantifies the extent to which an ellipsoid approximates a spherical form, while the intercept ratio (F), a more advanced version of aspect ratio (α), captures the combined effects of flatness and elongation. Next, we employed the non-linear programming algorithm (NLP) to simulate random dense packings across 63 distinct ellipsoid geometries. The resultant porosity was related as a function of Ψ_e and F, yielding three distinct relationships. Initially, as ψ_e reduced from 1 to 0.97, a parabolic decrease of porosity to a minimum occurred, with F exerting negligible influence (relation 1). As Ψ_e further decreased from 0.97 to 0, porosity sharply ascended towards 1, where the influence of F became significant. In this region, for a given Ψ_e, porosity initially declined to a minimum (relation 2) and subsequently went up with increasing F (relation 3), with the transition occurring at $F = 0.33$, distinguishing the two separate relations. A piecewise formula illustrating these relations was developed and verified, demonstrating good agreement in both trends and values.

6.1 Introduction

Particle packing system is vital and widely encountered in nature and industries. For instance, the porosity of fluvial sediment packings serves as a critical input for calculating bed level (Frings et al., 2008; Núñez-González et al., 2016) and provides spaces for retention of water, nutrients, and oxygen needed by aquatic organisms (Boulton et al., 1998; Noack et al., 2017; Sawyer & Cardenas, 2009). Many attempts have been made to predict the properties of particle packing systems, such as porosity or packing fraction, on spherical particles (An et al., 2009; Bernal & Mason, 1960; de Ryck, 2023; Li et al., 2011; Schruff et al., 2018; Wang et al., 2021; Weitz, 2004). However, actual particles found in nature and industries are normally aspherical, such as fluvial sediments with arbitrary shapes. Ignoring the grain shape effect can cause significant deviations in the prediction of properties for non-spherical particle packing systems.

Integrating the grain shape effect into particle packing systems is hard, particularly when dealing with particles that possess irregular shapes. This is mainly due to the difficulties in describing the shape of irregular particles (Szabó & Domokos, 2010). As a result, studies investigating the grain shape effect have primarily focused on analytical regular shapes, such as cubes (Fraige et al., 2008; Xie et al., 2019), cylinders (Gan & Yu, 2020a; Qian et al., 2018; Yu et al., 2023), disks (Yoshida et al., 2021; Zou & Yu, 1996), ellipsoids (Chen et al., 2021; Li et al., 2021), and other regularly shaped particles (Zhang et al., 2019; B. Zhao et al., 2017). Among these shapes, the ellipsoid has gained significant attention due to its ability to represent a wide range of different shapes, from very platy to highly elongated. Owing to this unique feature, ellipsoids have been often utilized as a surrogate to resemble irregularly shaped particles (Džiugys et al., 2001; Hu et al., 2023; Jain et al., 2021; Lu et al., 2023; Rettinger et al., 2022; Rothenburg & Bathurst, 1991).

The packing of ellipsoids has been extensively studied in material science and engineering chemistry (e.g., Gan & Yu, 2020b; Gan et al., 2016; Li et al., 2020; Mori & Sakai, 2022). A major focus of these studies involves examining the dependence of packing fraction (= 1-porosity) on the shape of ellipsoids. For example, Donev et al. (2004) utilized the so-called Lubachevsky-Stillinger (LS) simulation approach to analyze the packing of mono-sized ellipsoids and discovered a distinct “M-type” relationship between packing fraction and aspect ratio (α). Similar trends have also been observed from other researchers employing alternative simulation techniques (Sherwood, 1997; Zhao et al., 2017; Zhou et al., 2011). However, the majority of these studies have exclusively utilized spheroids, either oblate or prolate, as the feedstock in simulations, neglecting most ellipsoidal geometries. This is likely because spheroids can be readily characterized by a single shape factor, the aspect ratio (α), whereas no analogous general metric is available to describe the diverse shapes of general ellipsoids.

In this context, the objective of this study was to characterize the shape of general ellipsoids and establish a comprehensive quantitative relationship between porosity and

ellipsoidal geometry. In the following sections, first, we present a novel ellipsoid diagram capable of representing all possible ellipsoidal shapes. Next, we introduce a nonlinear programming algorithm for generating random dense packings of ellipsoids. Finally, we show how to establish the relationship between porosity and the full range of ellipsoid shapes describable within the proposed diagram.

6.2 Characterization of General Ellipsoids

An ellipsoid is a quadric surface that can be defined by three mutually orthogonal principal axes of differing lengths, the major axis ($2a$), intermediate axis ($2b$), and minor axis ($2c$). An ellipsoid in its simplest form becomes a sphere when the three principal axes are of equivalent length ($a = b = c$). Through directional scalings via an affine transformation, a sphere can be deformed into spheroidal shapes, specifically prolate spheroids ($a > b = c$) and oblate spheroids ($a = b > c$). Further transformations can generate the most general triaxial ellipsoids ($a > b > c$). While the volume of an ellipsoid (V_e) can be readily calculated with the semi-axes a, b and c through the formula:

$$V_e = \frac{4}{3}\pi abc \tag{6.1}$$

Calculating the surface area of an ellipsoid (A_e) is rather complex. Instead, an approximate formula is usually used to estimate:

$$A_e \approx 4\pi \left[\frac{(ab)^z + (bc)^z + (ac)^z}{3}\right]^{1/z} \tag{6.2}$$

with $z \approx 1.6075$ producing a relative error of at most 1.061%.

In order to characterize the shape of ellipsoids, two geometric shape factors were commonly used in previous studies, namely the aspect ratio (α) and sphericity (Ψ_e). However, the term aspect ratio (α) is of limitation in describing arbitrary ellipsoids, as it represents only certain ellipsoidal sub-types. Specifically, the aspect ratio delineates prolate spheroids ($\alpha = a/(b\ or\ c) > 1$) and oblate spheroids ($\alpha = c/(a\ or\ b) < 1$), along with a narrow subset of triaxial ellipsoids defined by semi-axes $a = \alpha^{-1}$, $b = 1$, and $c = \alpha$. Here, α measures the asphericity as elucidated by Donev et al. (2004).

The term sphericity indicates how closely a non-spherical particle approaches a perfect sphere, based on the ratio of the surface area of a sphere that has the same volume as the given particle to the surface area of that particle (Wadell, 1935). For ellipsoids, the term sphericity (Ψ_e) can be expressed as:

$$\Psi_e = \frac{A_s}{A_e} \tag{6.3}$$

where A_s is the surface area of the sphere of the same volume as the given ellipsoid.

However, ellipsoids expressed by sphericity is not unique, as Krumbein (1941) first noted that particles of different flatness and elongation can also have the same sphericity. Thus, characterizing the full range of ellipsoids requires incorporation of an additional shape factor to capture aspects of both elongation and flatness. To achieve this, we introduce the shape factor, so-called the intercept ratio (F) proposed by Zingg (1935). Following Zingg's terminology, the intercept ratio (F) can be expressed as the ratio between short to intermediate length (c/b) and intermediate to long length (b/a):

$$F = \frac{c/b}{b/a} = \frac{p}{q} = \frac{ac}{b^2} \tag{6.4}$$

where p and q are the measures of the flatness and elongation of an ellipsoid respectively.

Using Eqs. (6.1-6.3) and substituting p and q for c/b and b/a, we can express the sphericity of an ellipsoid (Ψ_e) as (see Appendix):

$$\Psi_e = (p^2 q)^{1/3} \left[\frac{3}{\left(1 + p^z(1 + q^z)\right)}\right]^{1/z} \tag{6.5}$$

In view of the concept of the intercept ratio $F\ (= ac/b^2)$, i.e., the measure of flatness and elongation combined, it actually can be considered as an extended version of the aspect ratio metric. The intercept ratio F can naturally transform into $\alpha = a/(b\ or\ c)$, when $a > b = c$ to express prolate spheroids, or $\alpha = c/(a\ or\ b)$ to express oblate spheroids, when $a = b > c$. Moreover, using α as a measure of fully aspherical ellipsoids with axes $a = \alpha^{-1}$, $b = 1$, and $c = \alpha$, however, turns out to be just a sub-type of general ellipsoids with $F = \alpha^{-1}\alpha/1^2 = 1$.

By combining the two geometric shape factors, sphericity (Ψ_e) and intercept ratio (F), a novel characterization diagram can be constructed for visualizing the full spectrum of ellipsoids (Fig. 6.1). This two-parameter representation spans the full range of Ψ_e from 0 to 1 and F from 0 to $+\infty$, delineating a one-to-one mapping between shape metrics and ellipsoidal geometries. The upper and right boundaries of the diagram correspond to the oblate and prolate spheroid subclasses respectively, with the point on the top-right corner denoting the simplest form of ellipsoids, the sphere. In between, the diagram illustrates the vast majority of triaxial ellipsoids.

Overall, the novel characterization diagram developed here provides a complete description of general ellipsoids in terms of Wadell's sphericity (Ψ_e) and Zingg's intercept ratio (F) that can be directly calculated from the semi-axes of a, b and c.

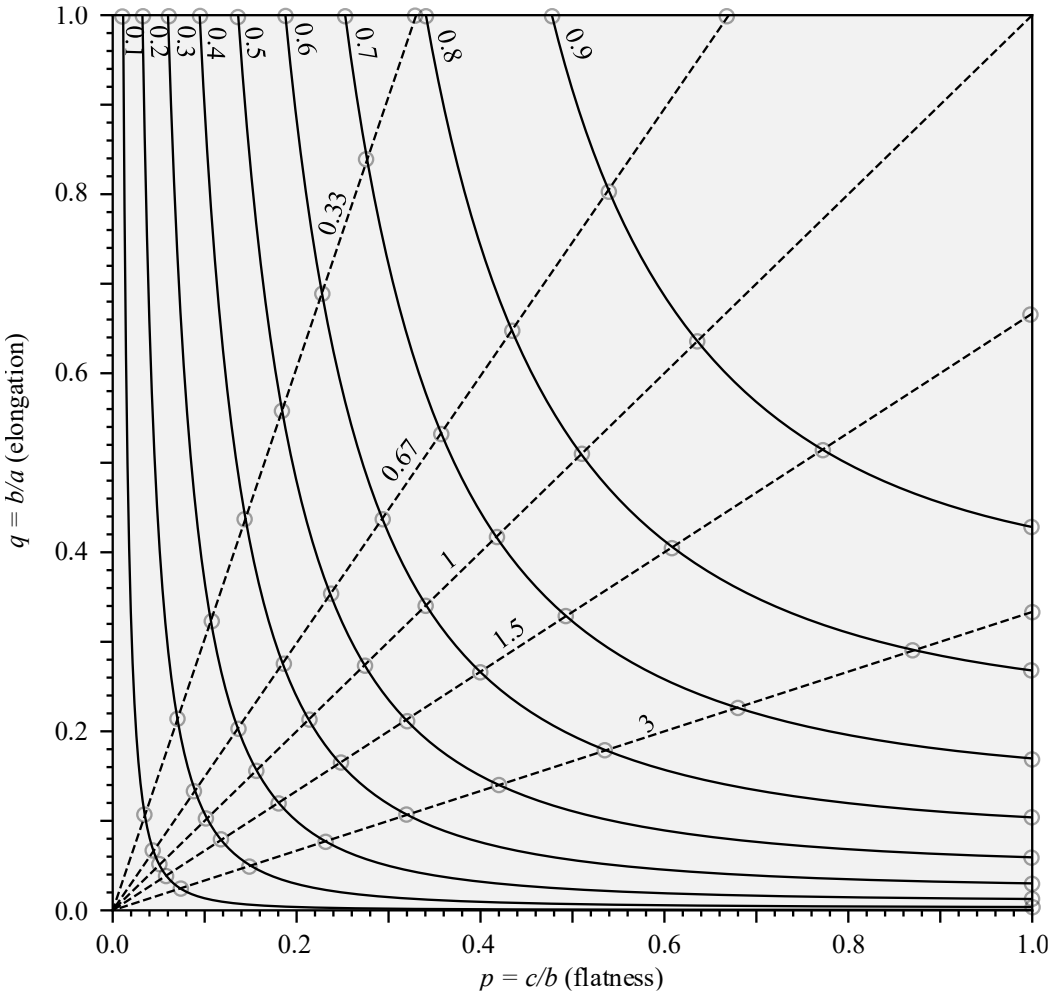

Figure 6.1. A novel ellipsoid diagram characterizing the full range of ellipsoids in terms of sphericity (Ψ_e) and intercept ratio (F), in which ψ_e values of 0.1-0.9 (- line) and F values of 0.33-3 (-- line) are drawn. The intersection points marked in gray circles are the selected ellipsoidal shapes for this study ($N = 63$).

6.3 The Non-linear Programming Algorithm

In the past decades, numerical techniques have become more popular in the study of particle packing systems, advanced by robust computational algorithms and developments in the computer hardware industry. In particular, with respect to the problem of packing ellipsoids, several simulation techniques have emerged, such as the random sequential addition algorithm (RSA) (Sherwood, 1997), the stochastic digital packing algorithm (SDP) (Jia & Williams, 2001), the Lubachevsky-Stillinger algorithm (LS) (Donev et al., 2004), and the discrete element method (DEM) (Zhou et al., 2011), each linked to a different packing mechanism. In this work, we introduced the non-linear programming algorithm (NLP) (Birgin et al., 2016; Birgin & Lobato, 2019) to simulate packings of ellipsoids and explored their shape relationship with porosity. Below, we

present a brief summary of the features of the numerical method, and direct the reader to the original work for a more detailed and mathematical description of the NLP algorithm.

The NLP algorithm implements two strategies to generate random dense packings of ellipsoids. The first aims to maximize the number of non-overlapping ellipsoids packed within a defined container. Three constraints are imposed: (1) ellipsoids must have specified semi-axis lengths (with major semi-axis normalized to unity); (2) ellipsoids must not intersect; and (3) ellipsoids must be enclosed by the container. The packing process proceeds iteratively. In each iteration, one ellipsoid is positioned within the container. The ellipsoid's location is restricted to an isolation box, with randomly selected (x, y) center coordinates, encouraging uniform spatial distribution. The ellipsoid's center and rotation are adjusted until no overlap occurs with existing ellipsoids (satisfying the non-intersection constraint), while its z-coordinate is minimized to maximize packing density. Once positioned, the ellipsoid's parameters are fixed. Packing terminates when the algorithm cannot place an additional ellipsoid after a set number of attempts. Overlap detection utilizes a linear transformation that, for every pair of ellipsoids, converts one of the ellipsoids into a unit sphere. An ellipsoid with its center outside the transformed sphere, separated by at least one radius, guarantees no intersection. The non-intersection constraints localize overlap detection between the new and nearby existing ellipsoids. This decomposition into low-dimensional subproblems enables large-scale packing of thousands or millions of ellipsoids.

The second strategy aims to minimize container volume for packing a specified set of ellipsoids. Unlike the first approach which maximizes ellipsoid count for a fixed container, this strategy seeks the minimum bounding container to enclose a predefined number of ellipsoids. The process comprises constructing initial solutions then iteratively optimizing them. An initial packing can be imported from solutions generated by the first strategy. An optimization subproblem then iteratively minimizes the container volume, subject to keeping all ellipsoids inside and non-intersecting. The optimized subproblem solution becomes a candidate for the overall minimum-volume packing problem. This candidate is randomly perturbed and re-optimized until reaching either a maximum iteration count or time limit. As before, detecting overlap relies on the linear transformation technique. Since the subproblem optimizes the full packing at each iteration, with variables and constraints growing linearly with ellipsoid count, computational complexity escalates rapidly. Consequently, this approach is limited to packing hundreds, rather than thousands or millions, of ellipsoids.

6.4 Sensitivity Analysis

Prior to implementing the NLP algorithm, we performed a sensitivity analysis to assess the behavior of involved parameters on porosity for two representative ellipsoid shapes. The first was a more spherical ellipsoid with semi-axis lengths of 1, 0.75, and 0.5 ($\Psi_e = 0.94$, $F = 0.89$). The second was a more elongated ellipsoid with semi-axis lengths of 1,

0.11, and 0.03 ($\Psi_e = 0.4$, $F = 3$). Simulations were conducted using cubic containers with side lengths (L) of 30 and 5 for the near-spherical and elongated cases, respectively. Note that all data is given in relevant units.

For the first packing strategy, three parameters were identified as potentially exerting influence on the packing process and thus porosity, i.e., the number of attempts, the side length of the isolation box in the x and y directions, and the height of the isolation box in the z direction. The number of attempts (τ) tells how many attempts must be made to pack the next ellipsoid. If the next ellipsoid cannot be packed after τ attempts, the method terminates. The side length and the height of the isolation box are given by the side length factor (η) and the height factor (γ) multiplied by the length of the major semi-axis of the current ellipsoid (which is normalized to unity). The greater the values of these parameters, the harder the subproblem becomes and it is expected that the solution quality improves (i.e., leading to a denser packing). However, if these values are given too great, the subproblem may become too hard to solve, returning bad quality solutions instead.

To test the effect of these parameters on porosity, we performed a number of simulations in which one of the parameters was varied while keeping the others constant. The packing porosity (n) is computed according to:

$$n = 1 - \left[\frac{N(4/3)\pi abc}{L^3}\right] \tag{6.6}$$

where N is the total number of the ellipsoids being packed.

Fig. 6.2 reveals the packing porosity (representing solution quality) to be invariant to τ beyond values of 10, for both near-spherical and elongated ellipsoidal shapes. This indicates that if the next ellipsoid cannot be packed within 10 attempts, adding more extra attempts appears not helpful. Regarding the remaining parameters, the findings accord with a priori expectations. Packing porosity improves with increasing side length factor η for both morphologies, up to a critical value of 10, beyond which solution quality degrades. For the height factor γ, the optimum point occurs at $\gamma = 5$ for near-spherical particles and $\gamma = 2$ for elongated ones. The deterioration in solution quality due to overlarge η and γ values suggests that the associated packing subproblems exceed the solving capacity of the algorithm.

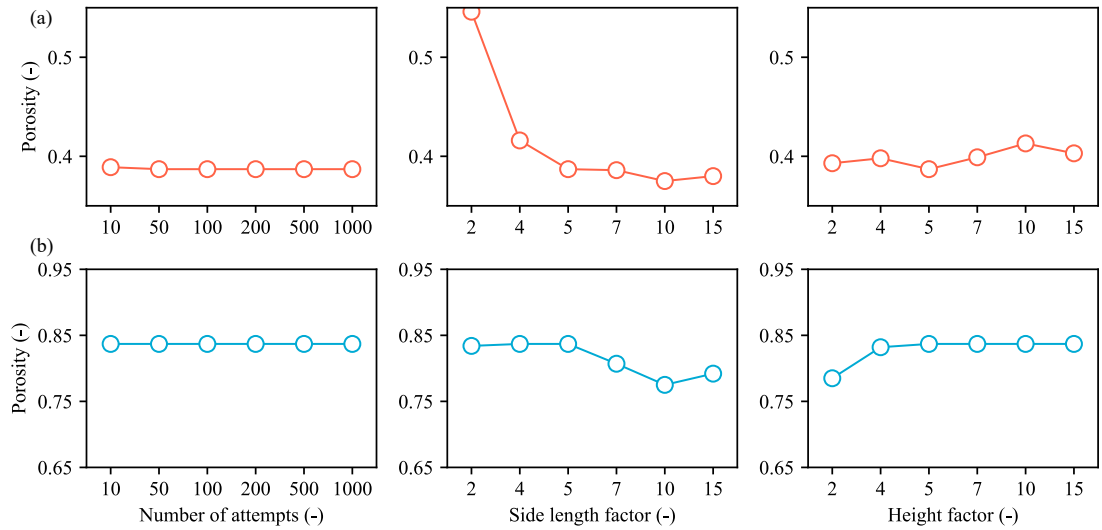

Figure 6.2. The effects of the number of attempts (τ), the side length factor (η), and the height factor (γ) on porosity for the (a) near-spherical ellipsoid, and (b) elongated ellipsoid, with the first packing strategy.

For the second packing strategy, the sole parameter governing the packing process and thus porosity is the perturbation magnitude (δ). This parameter defines the maximum degree to which the current solution is randomly altered, with a perturbation of 1% signifying that the rotation angles and centers of an ellipsoid, and container dimensions may individually be perturbed by up to 1% of their original values.

To investigate the influence of perturbation magnitude, initial packings comprising 376 near-spherical and 499 elongated ellipsoids were first generated via the first packing strategy. These configurations were then utilized to seed the perturbed packing approach, with the aforementioned container size supplying the initial bounds. Simulations were performed for a fixed duration of 72 h. The porosity was also calculated using Eq. (6.6), where L denotes the side length of the minimum bounding container. The outcome reveals that improved solutions were achievable for both ellipsoid shapes under small perturbations (Fig. 6.3).

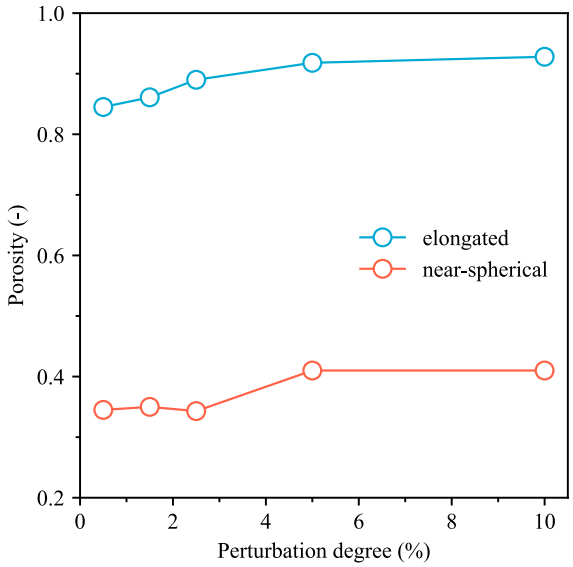

Figure 6.3. The effect of the degree of perturbation (δ) on porosity for both near-spherical and elongated ellipsoids, with the second packing strategy.

6.5 The Porosity-Shape Relationship

To elucidate the relationship between ellipsoid shape and packing porosity, 63 distinct ellipsoid geometries were selected as representatives from the newly introduced diagram. These selections, denoted by gray circles in the diagram (see Fig. 6.1), comprised 42 triaxial ellipsoids, 11 oblate spheroids, and 10 prolate spheroids, representing a diverse range of shapes from very platy to highly elongated. Employing the two packing strategies of the NLP algorithm, large-scale (≈10000 particles) and medium-scale (≈400 particles) random dense configurations were generated for each shape. The algorithm parameters were chosen based on the preceding sensitivity analysis and are tabulated in Table 6.1. This comprehensive investigation aims to systematically map the influence of particle shape on packing porosity across the full spectrum of ellipsoidal geometries.

Table 6.1. Parameter values used in the NLP simulations.

Packing Strategies	Parameters	Values
1	Number of attempts (τ)	100
	Side length factor (η)	10
	Height factor (γ)	5, when $\Psi_e \geq 0.9$; 2, when $\Psi_e < 0.9$
	Fixed container size (L)	10-30
2	Perturbation (δ)	0.5 %
	Initial container size (L)	5-15
	Execution time (T)	120 h

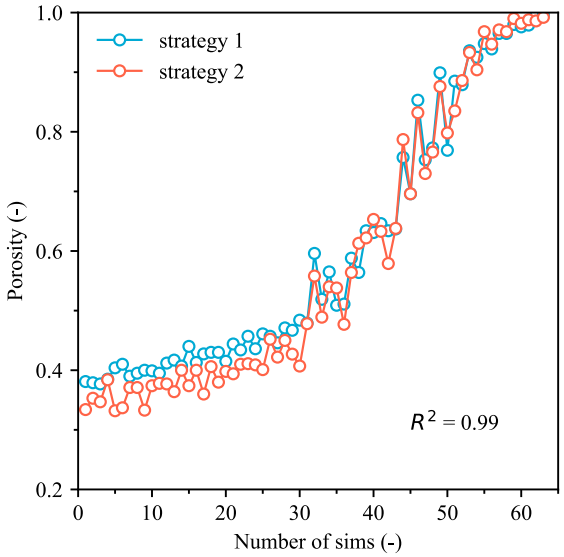

Figure 6.4. The packing porosity produced by the two strategies of the NLP algorithm for each of the 63 ellipsoidal shapes.

A comparison of the packing porosities (n) produced by the two algorithmic strategies across the 63 ellipsoid shapes is presented in Fig. 6.4. While both protocols exhibit a similar qualitative trend ($R^2 = 0.99$), strategy 2 consistently yielded denser packings than strategy 1 for most morphologies examined ($\approx$76%). This suggests that despite their common objective of generating random dense configurations, the precise packing porosities are sensitive to the procedural details intrinsic to each approach. Notably, the present implementation was not designed to guarantee maximal random dense states, unlike some past work (e.g., Donev et al., 2004; Torquato, 2018). Instead, the focus herein was to empirically depict general tendencies in packing density as a function of ellipsoid, i.e., the sphericity (Ψ_e) and intercept ratio (F). To mitigate confounding effects from packing protocol variations, only the denser configurations generated by each approach were analyzed further. Examples of the generated random dense packings of ellipsoids are exhibited in Fig. 6.5.

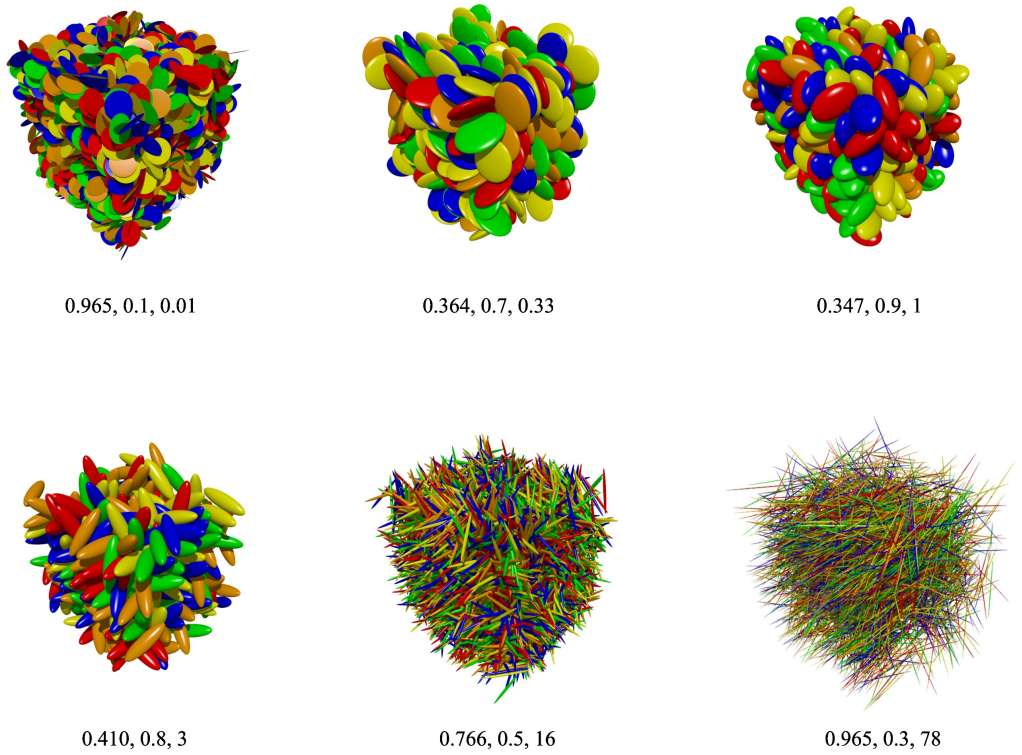

Figure 6.5. Examples of the simulated random dense packings of ellipsoids, showing ellipsoidal shapes from very platy to highly elongated. The data below each packing denotes the porosity, sphericity, and intercept ratio, separately.

The filtered packing porosities (i.e., the denser ones) are plotted as a function of sphericity (Ψ_e) and intercept ratio (F) in Fig. 6.6. Several salient correlations emerge. For fixed intercept ratio (Fig. 6.6a), the porosity exhibits a slight initial decline as sphericity is reduced to $\Psi_e \approx 0.97$, followed by a steep porosity increase as sphericity is further diminished. At fixed sphericity (Fig. 6.6b), the porosity decreases with increasing intercept ratio until $F = 0.33$, beyond which the porosity rises. Overall, the intercept ratio F exerts a marked influence on packing porosity for $0.1 \leq \Psi_e \leq 0.9$, but a negligible impact for highly stretched ($\Psi_e < 0.1$) or sub-spherical ($\Psi_e > 0.9$) particles, as evidenced by the porosity spread at a given sphericity in this regime (Fig. 6.6a).

The results further confirm that slight deviations from perfect sphericity can enable denser particle packings compared to ideal spheres. This phenomenon appears universal, being observed not only for ellipsoids but also other non-spherical shapes like cylinders and disks (Zou & Yu, 1996). Ellipsoids with $\Psi_e \geq 0.9$ produced porosities below 0.36, the theoretical minimum for random sphere packs (Song et al., 2008). A minimum ellipsoidal particle porosity of 0.33 was obtained at $\Psi_e \approx 0.97$ (corresponding to aspect ratio $\alpha = 0.67$ for oblate and 1.5 for prolate spheroids). As Ψ_e further decreases, porosity dramatically increases (Fig. 6.6a), likely because restricted particle rearrangements in packs of low-sphericity particles impede densification. An analogous effect also occurs for the intercept ratio F, with porosity increasing towards very platy

shapes at low F and highly elongated shapes at high F, yielding a relative minimum around $F = 0.33$ (Fig. 6.6b).

For the purpose of prediction, using the present data, a piecewise formula was developed below:

for $0 < \Psi_e < 0.97$:

$$n = \begin{cases} A + \dfrac{1 - A}{[1 + Q_1\, exp(F)\, exp(B\Psi_e)]^{\Psi_e}}, & 0 < F < 0.33 \quad (6.7a) \\ A + \dfrac{1 - A}{[1 + Q_2 F^{-1}\, exp(B\Psi_e)]^{\Psi_e}}, & F \geq 0.33 \quad (6.7b) \end{cases}$$

for $0.97 \leq \Psi_e \leq 1$:

$$n = A + \frac{C - A}{(1 - 0.97)^2}(\Psi_e - 0.97)^2 \quad (6.7c)$$

where A represents the minimum porosity of ellipsoids in random packings (0.33 obtained in this study), and $C = 0.36$ represents the theoretical minimum porosity of spheres in random packings, with coefficients of $Q_1 \approx 1.664$, $Q_2 \approx 0.769$, $B \approx 6.133$.

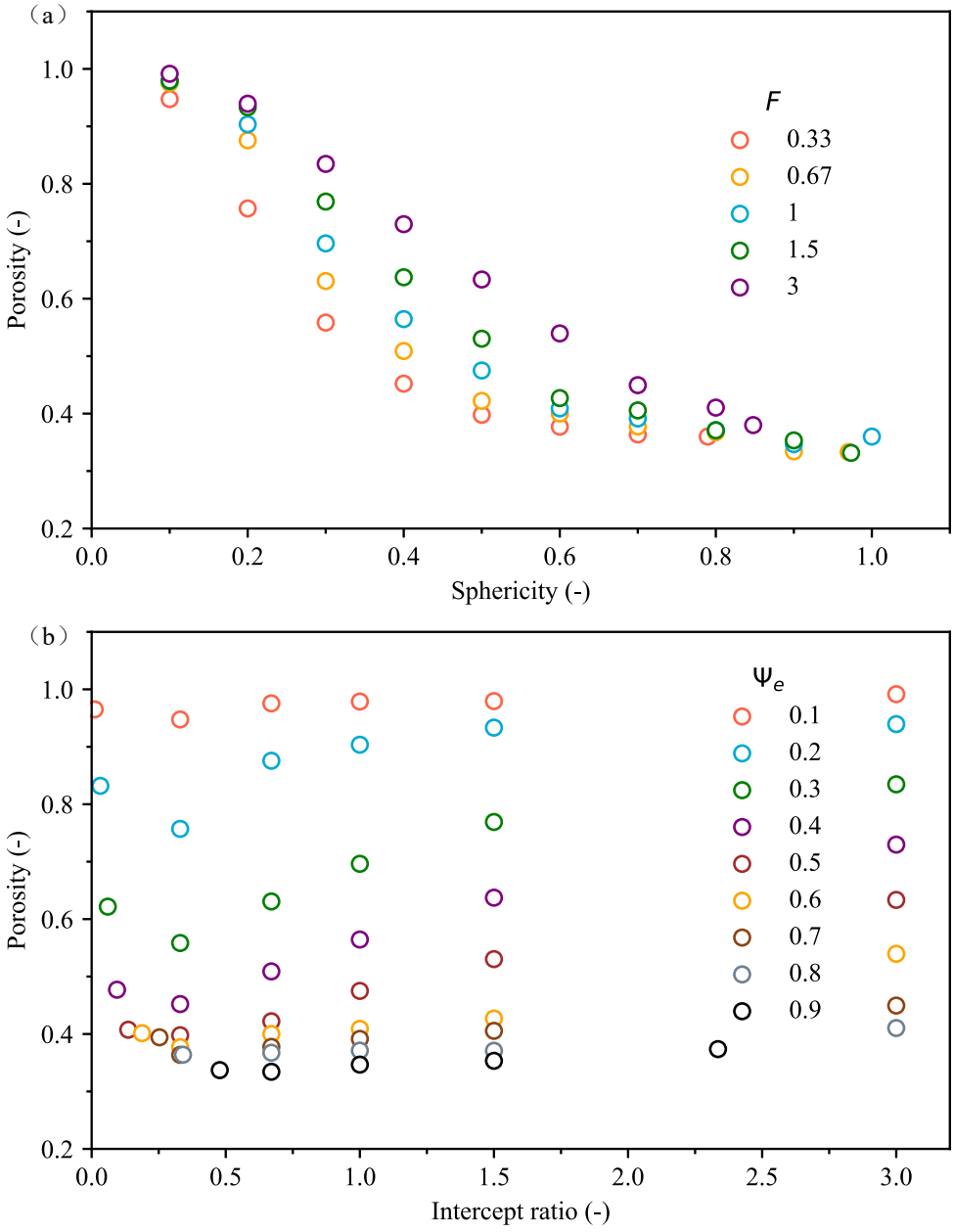

Figure 6.6. The relationship between packing porosity and ellipsoidal shape, characterized by sphericity (Ψ_e) and intercept ratio (F). Note that some of the data are not displayed herein just for clarity and concision.

The piecewise formula describes the three distinct porosity trends as a function of sphericity and intercept ratio observed in Fig. 6.6. Formula 8 describes the pure porosity increase with diminishing sphericity from $\Psi_e = 0.97$ (the minimum porosity point) down to $\Psi_e \to 0$ (Fig. 6.6a). Specifically, Formula $6.7a$ represents the decreasing porosity region for $0 < F < 0.33$, while Formula $6.7b$ describes the increasing porosity region for $F \geq 0.33$ (Fig. 6.6b). Formula $6.7c$ captures the initial porosity decline as sphericity is reduced from $\Psi_e = 1$ to 0.97, where the intercept ratio effect becomes negligible (Fig. 6.6a). To elucidate this region further, three additional shapes with identical $\Psi_e = 0.985$

but varying $F = 0.75$, 1, and 1.35 were simulated, exhibiting nearly identical porosities around 0.34 as expected. Overall, the established formula explains 98% of the total porosity variance with a root mean square error (RMSE) of approximately 0.03, representing good agreement with the data (Fig. 6.7).

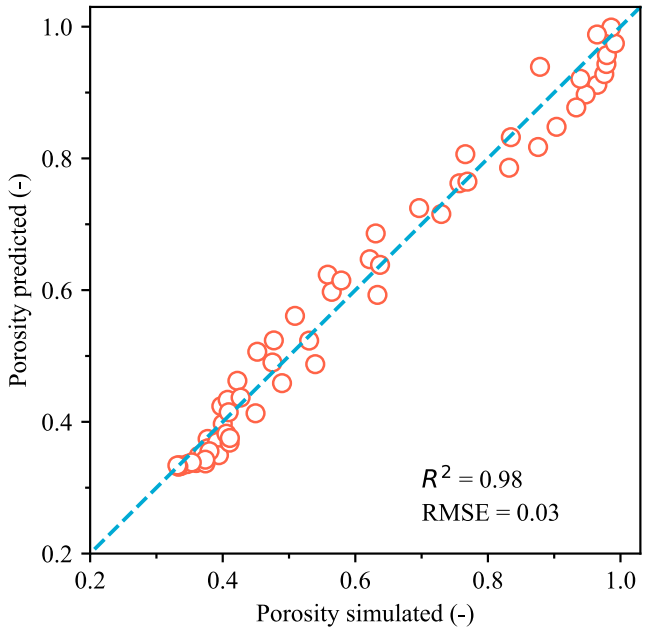

Figure 6.7. Comparison of the simulated porosity to the porosity predicted by the established piecewise formula.

It should be noted that the parameters A and C, representing the minimum porosity for ellipsoids and spheres in random packings respectively, can be treated with some flexibility as indicators of the packing state. Different packing states (e.g., loose versus dense) are known to primarily influence absolute porosity values rather than porosity trends (e.g., Liang et al., 2015; Zou & Yu, 1996), and thus such effect may be captured by modifying A and C. Specifically, increasing A and C (implying looser packs) elevates predicted porosities uniformly without altering trends, and vice versa. To demonstrate this, the formula predictions were compared with four published datasets on random ellipsoidal particle packs. As shown in Fig. 6.8, the data of Donev et al. (2004), Zhou et al. (2011), and Zhao et al. (2017) reflect relatively dense packings, while Sherwood (1997) represents loose packings, attributed to the distinct simulation techniques. Despite different absolute values, the trends are similar. Using $A = 0.30$, $C = 0.36$ for dense packs and $A = 0.59$, $C = 0.62$ for loose packs, the formula accurately captures the trends in both cases. Good agreement is observed, except for $F < 0.5$ where porosities are slightly underestimated.

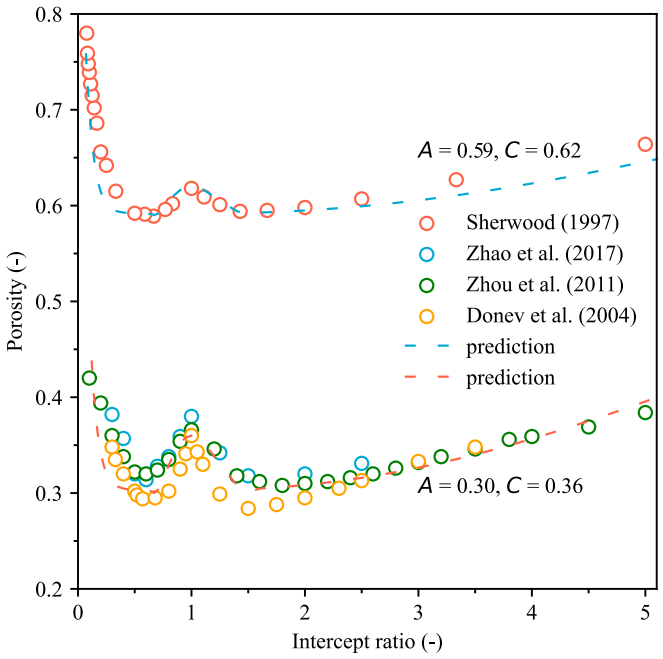

Figure 6.8. Comparison of the four porosity datasets to the porosity predicted by the established piecewise formula.

6.6 Conclusions

In this work, we characterized the shape of general ellipsoids based on Wadell's sphericity (Ψ_e) and Zingg's intercept ratio (F), which can be directly computed from the lengths of the semi-principal axes. The sphericity (Ψ_e) quantifies the degree to which an ellipsoid approaches to a spherical form, while the intercept ratio (F) expresses the combined effects of flatness and elongation. By combining the two well-defined shape factors, the ellipsoidal form can be uniquely delineated, as visualized on a constructed sphericity-intercept ratio diagram. Next, we employed the non-linear programming algorithm (NLP) to simulate random dense packings of ellipsoids and related the resulting porosity as a function of Ψ_e and F. Three distinct relationships were found. First, as Ψ_e decreased from 1 to 0.97, porosity declined parabolically, with negligible influence of F (relation 1). As Ψ_e further diminished from 0.97 to 0, porosity increased dramatically, in which the effect of F became significant. Here, at a certain Ψ_e, porosity initially decreased to a minimum (relation 2) and then increased (relation 3) with increasing F, the transition occurring at $F = 0.33$, separating the two distinct relations. A piecewise formula describing these relations was derived and verified, exhibiting good agreement in both trends and values.

Appendix

The approximation for the surface area of an ellipsoid is:

$$A_e = 4\pi\left[\frac{(ab)^z + (bc)^z + (ac)^z}{3}\right]^{1/z}$$

By definition $p = c/b$, $q = b/a$. Substituting p and q for c/b and b/a, the expression for the surface area of an ellipsoid then becomes:

$$A_e = 4\pi\left[\frac{(b^2/q)^Z + (b^2p)^Z + (b^2p/q)^Z}{3}\right]^{1/z}$$

which reduces to:

$$A_e = 4\pi(b^2/q)\left[\frac{\left(1 + p^z(1+q^z)\right)}{3}\right]^{1/z}$$

Let r be the radius of a sphere having the same volume of an ellipsoid, then:

$$\frac{4}{3}\pi abc = \frac{4}{3}\pi r^3$$

and solving for r:

$$r = (abc)^{1/3}$$

So, the surface area of a sphere of the same volume as an ellipsoid is:

$$A_s = 4\pi(abc)^{2/3}$$

Substituting p and q for c/b and b/a, the expression becomes:

$$A_s = 4\pi b^2(p/q)^{2/3}$$

Then, the sphericity of an ellipsoid is calculated by:

$$\Psi_e = \frac{A_s}{A_e}$$

$$= \frac{4\pi b^2(p/q)^{2/3}}{4\pi(b^2/q)\left[\frac{\left(1 + p^z(1+q^z)\right)}{3}\right]^{1/z}}$$

This reduces to:

$$\Psi_e = \frac{A_s}{A_e} = (p^2q)^{1/3}\left[\frac{3}{(1+p^z(1+q^z))}\right]^{1/z}$$

References

An, X.Z., Li, C.X., Yang, R.Y., Zou, R.P., Yu, A.B. (2009). Experimental study of the packing of mono-sized spheres subjected to one-dimensional vibration. Powder Technology, 196, 50-55.

Bernal, J.D., Mason, J. (1960). Packing of Spheres: Co-ordination of Randomly Packed Spheres. Nature, 188, 910-911.

Birgin, E.G., & Lobato, R.D. (2019). A matheuristic approach with nonlinear subproblems for large-scale packing of ellipsoids. European Journal of Operational Research, 272(2), 447-464.

Birgin, E.G., Lobato, R.D., Martínez, J.M. (2016). Packing ellipsoids by nonlinear optimization. Journal of Global Optimization, 65, 709-743.

Boulton, A.J., Findlay, S., Marmonier, P., Stanley, E.H., & Maurice Valett, H. (1998). The functional significance of the hyporheic zone in streams and rivers. Annual Review of Ecology and Systematics, 29, 59-81.

Chen, C., Bai, S., Huang, Y., Lam, L., Yao, Y., Keer, L.M. (2021). 3D random packing algorithm of ellipsoidal particles based on the Monte Carlo method. Magazine of Concrete Research, 73, 343-355.

de Ryck, A. (2023). A model packing based on a tree of face-to-face regular tetrahedra for monodisperse spheres. Granular Matter, 25, 1-15.

Donev, A., Cisse, I., Sachs, D., Variano, E.A., Stillinger, F.H., Connelly, R., Torquato, S., Chaikin, P.M. (2004). Improving the Density of Jammed Disordered Packings Using Ellipsoids. Science, 303, 990-993.

Džiugys, A., Peters, B., Džiugys, A., Peters, B. (2001). An approach to simulate the motion of spherical and non-spherical fuel particles in combustion chambers, Granular Matter, 3, 231-266.

Fraige, F.Y., Langston, P.A., Chen, G.Z. (2008). Distinct element modelling of cubic particle packing and flow. Powder Technology, 186, 224-240.

Frings, R.M., Kleinhans, M.G., Vollmer, S. (2008). Discriminating between pore-filling load and bed-structure load: a new porosity-based method, exemplified for the river Rhine. Sedimentology, 55, 1571-1593.

Gan, J.Q., Yu, A. (2020a). DEM simulation of the packing of cylindrical particles. Granular Matter, 22, 22.

Gan, J.Q., Yu, A. (2020b). DEM study on the packing density and randomness for packing of ellipsoids. Powder Technology, 361, 424-434.

Gan, J.Q., Yu, A.B., Zhou, Z.Y. (2016). DEM simulation on the packing of fine ellipsoids. Chemical Engineering Science, 156, 64-76.

Hu, X., Shum, C.K., Bevis, M. (2023). A triaxial reference ellipsoid for the Earth. Journal of Geodesy, 97, 29.

Jain, R., Tschisgale, S., Fröhlich, J. (2021). Impact of shape: DNS of sediment transport with non-spherical particles. Journal of Fluid Mechanics, 916.

Jia, X., Williams, R.A. (2001). A packing algorithm for particles of arbitrary shapes. Powder Technology, 120, 175-186.

Krumbein, W.C. (1941). Measurement and geological significance of shape and roundness of sedimentary particles. Journal of Sedimentary Research, 11, 64-72.

Li, C.X., An, X.Z., Yang, R.Y., Zou, R.P., Yu, A.B. (2011). Experimental study on the packing of uniform spheres under three-dimensional vibration. Powder Technology, 208, 617-622.

Li, C.X., Gan, J.Q., Pinson, D., Yu, A.B., Zhou, Z.Y. (2021). Dynamic analysis of poured packing process of ellipsoidal particles. Powder Technology, 385, 444-454.

Li, C.X., Zou, R.P., Pinson, D., Yu, A.B., Zhou, Z.Y. (2020). An experimental study of packing of ellipsoids under vibrations. Powder Technology, 361, 45-51.

Liang, R., Schruff, T., Jia, X., Schüttrumpf, H., Frings, R.M. (2015). Validation of a stochastic digital packing algorithm for porosity prediction in fluvial gravel deposits. Sedimentary Geology, 329, 18-27.

Lu, C., Gao, Z., Li, H., He, J., Wang, Q., Wei, X., Wang, X., Jiang, S., Xu, J., He, D., Li, Y. (2023). An ellipsoid modelling method for discrete element simulation of wheat seeds. Biosystems Engineering, 226, 1-15.

Mori, Y., Sakai, M. (2022). Advanced DEM simulation on powder mixing for ellipsoidal particles in an industrial mixer. Chemical Engineering Journal, 429.

Noack, M., Ortlepp, J., Wieprecht, S. (2017). An Approach to Simulate Interstitial Habitat Conditions During the Incubation Phase of Gravel-Spawning Fish. River Research and Applications, 33, 192-201.

Núñez-González, F., Martín-Vide, J.P., Kleinhans, M.G. (2016). Porosity and size gradation of saturated gravel with percolated fines. Sedimentology, 63, 1209-1232.

Qian, Q., Wang, L., An, X., Wu, Y., Wang, J., Zhao, H., Yang, X. (2018). DEM simulation on the vibrated packing densification of mono-sized equilateral cylindrical particles. Powder Technology, 325, 151-160.

Rettinger, C., Rüde, U., Vollmer, S., & Frings, R.M. (2022). Effect of sediment form and form distribution on porosity: a simulation study based on the discrete element method. Granular Matter, 24(4), 1-23.

Rothenburg, L., Bathurst, R.J. (1991). Numerical simulation of idealized granular assemblies with plane elliptical particles. Computers and Geotechnics, 11, 315-329.

Sawyer, A.H., Cardenas, M.B. (2009). Hyporheic flow and residence time distributions in heterogeneous cross-bedded sediment. Water Resources Research, 45.

Schruff, T., Liang, R., Rüde, U., Schüttrumpf, H., Frings, R.M. (2018). Generation of dense granular deposits for porosity analysis: assessment and application of large-scale non-smooth granular dynamics. Computational Particle Mechanics, 5(1), 59-70.

Sherwood, J.D. (1997). Packing of spheroids in three-dimensional space by random sequential addition. Journal of Physics A: Mathematical and General, 30, 839-843.

Song, C., Wang, P., Makse, H.A. (2008). A phase diagram for jammed matter. Nature, 453, 629-632.

Szabó, T., Domokos, G. (2010). A new classification system for pebble and crystal shapes based on static equilibrium points. Central European Geology, 53, 1-19.

Torquato, S. (2018). Perspective: Basic understanding of condensed phases of matter via packing models. Journal of Chemical Physics, 149.

Wadell, H. (1935). Volume, Shape, and Roundness of Quartz Particles. The Journal of Geology, 43, 250-280.

Wang, Z., Pereira, J.M., Gan, Y. (2021). Packing of wet monodisperse spheres. Powder Technology, 378, 60-64.

Weitz, D.A. (2004). Packing in the spheres. Science, 303, 968-969.

Xie, Z., An, X., Yang, X., Li, C., Shen, Y. (2019). Numerical realization and structure characterization on random close packings of cuboid particles with different aspect ratios. Powder Technology, 344, 514-524.

Yoshida, M., Kawabata, D., Yamada, H., Shimosaka, A., Shirakawa, Y. (2021). Experimental analysis of overtaking behavior in disks falling in a low-density particle bed. Advanced Powder Technology, 32, 3564-3573.

Yu, F., Cui, D., Zhang, Y., Zhou, G. (2023). Effect of vibration direction on the packing of sphero-cylinders. Advanced Powder Technology, 34(9), 104138.

Zhang, G., An, X., Zhao, B., Qian, Q., Zhao, H. (2019). Discrete element method dynamic simulation of icosahedral particle packing under three-dimensional mechanical vibration. Particuology, 44, 117-125.

Zhao, B., An, X., Wang, Y., Qian, Q., Yang, X., Sun, X. (2017). DEM dynamic simulation of tetrahedral particle packing under 3D mechanical vibration. Powder Technology, 317, 171-180.

Zhao, S., Zhang, N., Zhou, X., Zhang, L. (2017). Particle shape effects on fabric of granular random packing. Powder Technology, 310, 175-186.

Zhou, Z.Y., Zou, R.P., Pinson, D., Yu, A.B. (2011). Dynamic simulation of the packing of ellipsoidal particles. Industrial & Engineering Chemistry Research, 50, 9787-9798.

Zingg, T. (1935). Beitrag zur Schotteranalyse. Schweizeriscke Mineralogische und Petrologische Mitteilungen, 39-140.

Zou, R.P., Yu, A.B. (1996). Evaluation of the packing characteristics of mono-sized non-spherical particles, Powder Technology, 88, 71-79.

7

An Integrated Binary-Unit Conceptual Packing Model

Porosity prediction for fluvial sediment packings is vital in many ecological, morphological, and geological applications. The binary-unit conceptual (BUC) packing model has shown its generality and simplicity in predicting the porosity of fluvial sediments with spherical shapes (or sub-spherical), outperforming other existing models. However, the BUC model is still struggling to apply for poorly-spherical sediment packings. In this context, the objective was to enhance the BUC model by coupling the influence of non-spherical shapes, leading to the development of an integrated BUC (IBUC) packing model for universal application. We did this by introducing the concept of equivalent packing diameter, with which a non-spherical sediment mixture can be transformed into a spherical packing with an equivalent size effect on porosity that can be well handled by the established BUC model, alongside an initial porosity that embodies the isolated non-spherical shape effect at a specific packing stage. As a result, only two inputs are required in the IBUC model: the grain size distribution (GSD) of the transformed spherical packing, and the initial porosity. It turns out that the GSD of the spherical packing can be reasonably substituted with the measured GSD of the original packing. Furthermore, instead of individually measuring the initial porosity for each sample, which is often impractical, we proposed the use of a mean initial porosity for an approximate characterization of a field site. Despite this simplification, the IBUC model still yielded accurate porosity predictions with a root-mean-square error (RMSE) of 0.03 when validated against 138 porosity measurement data across four diverse rivers: the Rhine, Bès, Galabre, and Kuqa. This positions the IBUC model as an efficient tool for investigating the spatial variability in riverbed porosity.

7.1 Introduction

Riverbeds are natural packing systems composed of fluvial sediments with varying sizes and shapes. Quantifying the porosity of fluvial sediments is vital in various ecological, morphological, and geological applications related to riverbeds (Ackers & White, 1973; Boulton et al., 1998; Coleman & Nikora, 2009; Frings et al., 2008; Liang et al., 2015; Mulatu et al., 2018; Noack et al., 2017; Núñez-González et al., 2016; Rettinger, et al., 2022a; Sawyer & Cardenas, 2009; Schruff et al., 2018; Tabesh et al., 2019, 2022; Vollmer & Kleinhans, 2007). However, directly measuring porosity in situ is an arduous and costly task, which has led to the development of porosity prediction models as a more feasible alternative. Existing porosity predictors can be generally categorized into two types: regression-based models and analytical models. While simplistic, regression-based models suffer from limited applicability stemming from their localized nature (e.g., Carling & Reader, 1982; Frings et al., 2011; Wooster et al., 2008; Wu & Wang, 2006). On the other hand, analytical models, such as the linear-mixture packing model (Yu & Standish, 1991) or the compressible packing model (De Larrard, 1999), despite their general usefulness, are complex to compute and have been observed to systematically underestimate porosity due to underlying assumptions (Frings et al., 2011; Rettinger et al., 2023).

Chapter 3 addressed these problems by proposing a novel porosity predictor named the binary-unit conceptual (BUC) packing model, which combines the simplicity of regression models with the generality of analytical models. The core of this model is based on the newly proposed binary-unit concept, which states that any multi-sized spherical packing can be conceptualized into a binary-unit spherical packing, i.e., the most element packing unit that is capable of capturing the equivalent particle-particle interactions of multi-component (or continuous) mixtures of spheres. Upon this concept, the porosity of arbitrary sediment mixtures can be easily estimated by models being able to predict the porosity of spherical binary mixtures, such as the Westman equation (Westman, 1936). However, the BUC packing model focuses primarily on the effect of grain size on porosity by assuming spherical sediment shapes, disregarding the other important porosity-influencing effect of non-spherical grain shape.

The non-spherical grain shape has also a significant impact on porosity, which can be readily demonstrated by modeling mono-sized packings of regular non-spherical shapes (Gan & Yu, 2020; Qian et al., 2018; Rettinger et al., 2022b; Xie et al., 2019; Zhang et al., 2019; Zhao et al., 2017). However, the investigation of the non-spherical shape effect on sediment porosity is challenging, due to the difficulty in precisely describing the irregular shapes of sediment particles given their inherent variability. Considering this, Chapter 5 introduced an idealized regular shape to approximate the arbitrary morphologies of fluvial sediments. By comparing a large number of scanned fluvial sediments to candidate regular shapes, it was found that the ellipsoidal shape provided the closest shape similarity

to natural sediments in terms of solid volume, surface area, and sphericity. Building on this work, Chapter 6 systematically investigated the packing porosity of mono-sized fluvial sediments (with ellipsoidal geometry), deriving correlations between porosity and two shape factors, namely the Wadell's sphericity and Zingg's intercept ratio, that characterize general ellipsoid morphology.

Nevertheless, the non-spherical shape effect has not been taken into account for multi-sized sediment mixtures. Therefore, the objective of this study was to incorporate the non-spherical grain shape effect into the BUC packing model to develop an integrated BUC (IBUC) packing model for general applications. One potential approach is to conduct a series of packing experiments using various sized and shaped ellipsoids to empirically determine the combined effect of grain size and shape. However, this method appears cumbersome due to the numerous variables involved. In contrast, in this study, we introduced the concept of equivalent packing diameter proposed by Yu et al (1993a), enabling to transform a non-spherical packing system into an equivalent spherical packing system, such that the porosity can then be directly predicted using the established BUC model in Chapter 3. In section 7.2, we introduce the equivalent packing diameter concept. Then, we explain how to establish the IBUC packing model in section 7.3. Next, we validate the IBUC model against datasets obtained from four different rivers in section 7.4, followed by discussion and conclusions (sections 7.5 & 7.6).

7.2 The Concept of Equivalent Packing Diameter

The concept of equivalent packing diameter (EPD) proposed by (Yu & Standish, 1993a) aims to convert the size of a non-spherical particle into an equivalent spherical diameter that has the same size-dependent packing property as the non-spherical particle. Since the particle-particle interaction within a packing depends upon the relative but not absolute particle sizes, the evaluation of the EPD of a non-spherical particle can be directly made from the analysis of binary mixtures of the considered particle and spheres of different diameters, based on the similarity between the packing systems of spherical and non-spherical particles as explained below.

For a spherical binary packing system, it is well known that a mixture of two different sized spheres will lead to lower porosities than for mono-sized spheres, due to the particle-particle interaction. Therefore, the maximum porosity should be gained when the dimeter of the sphere equals to that of the considered spherical particle. In other words, the EPD of a spherical particle should be its own diameter producing the maximum porosity. Similarly, when this consideration is extended to a non-spherical binary packing system, the EPD of a non-spherical particle should also be identical to the diameter of a sphere giving the maximum porosity. In general, the EPD of a non-spherical particle can be determined as the diameter of a sphere which, when combined with the non-spherical particle at a given fractional solid volume, gives maximum porosity (Yu & Standish, 1993a).

By conducting packing experiments for binary mixtures of various non-spherical particles and spheres of different diameters, an empirical equation was initially established by Yu and Standish (1993a) and further improved by Zou and Yu (1996), given below:

$$d_p = \frac{d_v}{\Psi^{2.785} exp[2.946(1-\Psi)]} \tag{7.1}$$

Where d_p is the EPD of the given non-spherical particle. d_v is the equivalent volume diameter, the dimeter of the sphere having the same volume of the non-spherical particle. Ψ is the sphericity of the non-spherical particle, defined as the ratio of the surface area of a sphere having the same volume as the particle to the surface area of the particle itself (Wadell, 1935).

Since the ($d_p - d_v, \Psi$) relation is ono-to-one correspondence, the established equation to determine EPD should be generally applied for any shaped particles (Zou & Yu, 1996).

7.3 The IBUC Packing Model

Here we introduce the IBUC packing model, by coupling the non-spherical grain shape effect into the original BUC packing model. This evolution unfolds through a four-step process as follows:

(1) Turn an arbitrary sediment packing into an equivalent ellipsoidal packing.

(2) Turn the ellipsoidal packing into an equivalent spherical packing.

(3) Turn the spherical packing into an equivalent binary-unit spherical packing.

(4) Predict the porosity of the equivalent binary-unit spherical packing.

The four processes are also visualized in Fig. 7.1.

The first transformation leverages the intrinsic shape similarities between fluvial sediments and ellipsoids, as outlined in Chapter 5. Demonstrating that ellipsoids offer the closest geometrical approximation to fluvial sediments in terms of solid volume, surface area and sphericity, this transformation takes a straightforward approach. It involves mapping the three dimensions of an irregular sediment particle, long (L), intermediate (I), and short (S), directly onto the three orthogonal major axes of an approximated ellipsoid, major axis ($2a$), intermediate axis ($2b$), and minor axis ($2c$). During this conversion, the porosity of the resulting ellipsoidal packing (Fig. 7.1) remains virtually unaltered from the original sediment packing, with Chapter 5 reporting an absolute porosity deviation of less than 1%.

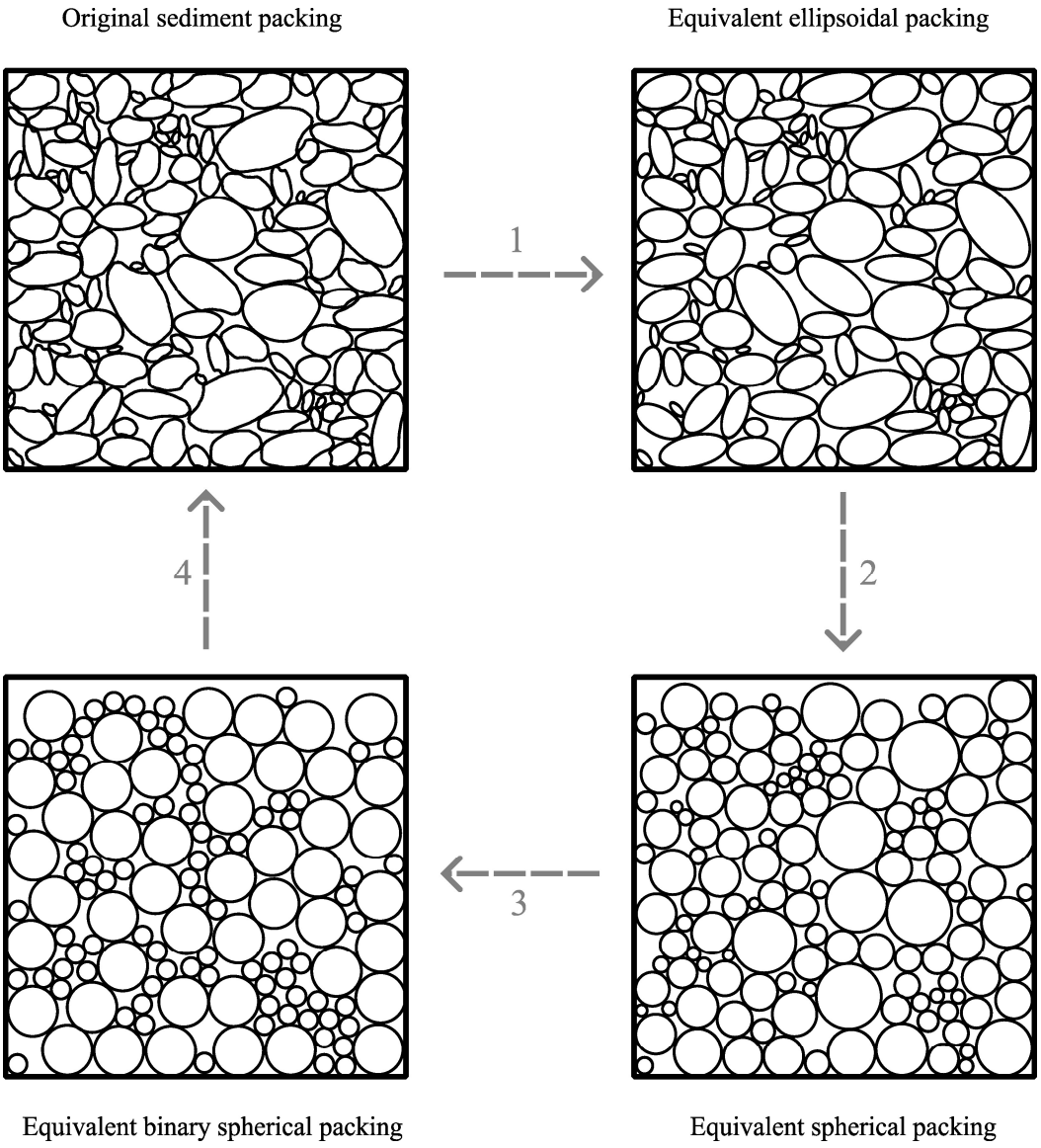

Figure 7.1. Two-dimensional illustration of the four processes applied for the establishment of the integrated BUC (IBUC) packing model.

The second transformation is based on the concept of equivalent packing diameter (EPD) introduced in section 7.2, which converts an ellipsoidal particle size into an equivalent spherical diameter preserving size-dependent packing properties using Eq. (7.1). Through this conversion, the non-spherical shape effect on porosity is isolated, resulting in a packing only subject to the particle-particle interactions between spheres. As illustrated in Fig. 7.1, the equivalent spherical packing shrinks to some degree due to the isolation of the ellipsoidal grain shape effect. To properly estimate the porosity of the equivalent spherical packing, the initial porosity range of 0.36 to 0.4, indicating whether a random packing of spheres is in a loose or dense state (Allen, 1985), must be adjusted to incorporate the isolated non-spherical shape effect. As a simple example, consider a uniform ellipsoidal packing with a known porosity of 0.5. Applying EPD yields a uniform spherical packing, whose porosity is constrained between 0.36 and 0.4 without accounting

for the isolated shape effects. Therefore, to correctly predict porosity, the initial porosity must be modified to 0.5, reflecting the isolated influence of ellipsoidal geometry under a certain packing state.

The third transformation capitalizes on the binary-unit concept, which is central to the established binary-unit conceptual (BUC) packing model in Chapter 3. The binary-unit concept refers to that any multi-sized (or continuous) spherical packing system can be conceptualized into an equivalent binary spherical packing system, through the link of identical grain size statistics of mean, standard deviation and skewness. Detailed in Chapter 3, this transition ensures the preservation of the original porosity value, as the resulting binary-unit mixture (Fig. 7.1) maintains the equivalent particle-particle interactions inherent in the original packing. Porosity estimation in the derived binary-unit packing can be done using available models that have the capability to predict the porosity of mixtures containing binary spheres (e.g., Dias et al., 2004; Koltermann & Gorelick, 1995). Here, we employ the Westman equation (Westman, 1936), a key component of the BUC packing model, for this purpose, as outlined in procedure 4.

The fourth procedure summarizes the complete explicit mathematical equations embedded in the three fundamental transformations for predicting the porosity of the equivalent binary spherical packing, which in turn refers to the porosity of the original sediment mixture.

Transformation 1

For each individual sediment particle, apply:

$$L, I, S = 2a, 2b, 2c \tag{7.2}$$

Transformation 2

First, calculate the sphericity (Ψ_e) and the equivalent volume diameter (d_v^e) of the approximated ellipsoid:

$$\Psi_e = \frac{A_s}{A_e} = \frac{\pi^{\frac{1}{3}}(6V_e)^{\frac{2}{3}}}{A_e} = \frac{4\pi(abc)^{\frac{2}{3}}}{A_e} \tag{7.3}$$

where A_S is the surface area of the sphere having the same volume as the ellipsoid. A_e and V_e denote the surface area and the volume of the ellipsoid separately, in which:

$$A_e = 4\pi\left[\frac{(ab)^p + (ac)^p + (bc)^p}{3}\right]^{1/p} \tag{7.3a}$$

with $p \approx 1.6075$ producing a relative error of at most $\pm 1.061\%$.

$$V_e = \frac{4\pi}{3}abc \tag{7.3b}$$

$$d_v^e = \left(\frac{6V_e}{\pi}\right)^{\frac{1}{3}} = 2(abc)^{\frac{1}{3}} \tag{7.4}$$

Then, the equivalent packing diameter (d_p^e) of an ellipsoid can be obtained using Eq. (7.1).

Transformation 3

Initially, compute the statistical mean (μ), standard deviation (σ) and skewness (Sk) of the equivalent multi-sized spherical packing. This can be done with the method of moments (Blott & Pye, 2001) or the Folk and Ward (1957) graphical measures. Here, we only show the former method as an example:

$$\mu_\phi = \sum f x_\phi \tag{7.5}$$

$$\sigma_\phi = \sqrt{\sum f(x_\phi - \mu_\phi)^2} \tag{7.6}$$

$$Sk_\phi = \frac{\sum f(x_\phi - \mu_\phi)^3}{{\sigma_\phi}^3} \tag{7.7}$$

Where μ_ϕ, σ_ϕ, Sk_ϕ represent the logarithmic statistical measures of mean, standard deviation and skewness. f represents the weights (%) and x_ϕ denotes the particle size in phi unit. It is worth mentioning that we employ the logarithmic statistics, a commonly used scale to characterize the size of natural sediments. Nevertheless, alternative statistical scales can be leveraged as well, including arithmetic or geometric scales.

Next, derive the equivalent binary-unit spherical packing using the same logarithmic statistics of the multi-sized spherical packing:

$$\mu_\phi = f_d d_\phi + f_D D_\phi \tag{7.8}$$

$$\sigma_\phi = \sqrt{f_d(d_\phi - \mu_\phi)^2 + f_D(D_\phi - \mu_\phi)^2} \tag{7.9}$$

$$Sk_\phi = \frac{f_d(d_\phi - \mu_\phi)^3 + f_D(D_\phi - \mu_\phi)^3}{{\sigma_\phi}^3} \tag{7.10}$$

Where d_ϕ, D_ϕ represent the size of smaller and larger spherical particle (phi unit) in the binary-unit mixture respectively, while f_d, f_D reflect the percentage of the smaller and larger components that satisfies the constraint $f_d + f_D = 1$. Note that to calculate the d_ϕ, D_ϕ, and f_d (or f_D) from the three Eqs. (7.8-7.10) is analytically possible, but not straightforward. Instead, we suggest using a numerical solver, such as the hybrid Powell and Newton method, to perform this task. To initialize the algorithm, rational initial

values should be specified for the sizes of the two components and one of their proportions, along with a termination tolerance, which is conventionally designated as $1e^{-8}$ to ensure highly accurate outcomes. The solver iteratively refines the solution until convergence based on the prescribed tolerance. Subsequently, the logarithmic sizes of the two components (d_ϕ, D_ϕ) should be converted back into the corresponding arithmetic sizes, denoted d and D, to obtain the equivalent binary spherical packing according to:

$$\begin{cases} d = 2^{-d_\phi} \\ D = 2^{-D_\phi} \end{cases} \tag{7.11}$$

Once the equivalent binary spherical packing is derived, the conic Westman equation as employed in the BUC packing model can then be utilized to predict the porosity, written as:

$$\left(\frac{V - V_D f_D}{V_d}\right)^2 + 2G\left(\frac{V - V_D f_D}{V_d}\right)\left(\frac{V - f_D - V_d f_d}{V_D - 1}\right) + \left(\frac{V - f_D - V_d f_d}{V_D - 1}\right)^2 = 1 \tag{7.12}$$

where V represents the specific volume of the binary spherical packing. V_d and V_D are the initial specific volume of the smaller and larger particles separately. The specific volume represents the reciprocal of packing density, which can be easily converted to porosity (n) by $n = 1 - 1/V$. The coefficient G was found to be dependent solely on the size ratio r ($= d/D$, in arithmetic scale) between finer and coarser particles (Yu et al., 1993b):

$$\frac{1}{G} = \begin{cases} 1.355\, r^{1.566} & (r \le 0.824) \\ 1 & (r > 0.824) \end{cases} \tag{7.13}$$

Note that the initial porosities for the two imaginary components, i.e., n_d ($= 1 - 1/V_d$) and n_D ($= 1 - 1/V_D$), are set to be equal here, denoted as n_0, by assuming that any component within the original mixture is packed at the same level, thus the two components within the equivalent binary spherical packing. As mentioned earlier, n_0 should not be appropriated from the typical range of 0.36 to 0.4 as for spherical packings. Rather, n_0 must be specified appropriately to reflect the isolated non-spherical grain shape effect subject to a specific packing state.

Finally, we can figure the porosity (n) analytically by rephrasing the Westman equation in a quadratic form with its positive square root being the solution:

$$V = \frac{-B + \sqrt{B^2 - 4AC}}{2A} \tag{7.14}$$

where

$$A = \left(\frac{1}{V_d}\right)^2 + \frac{2G}{V_d(V_D-1)} + \frac{1}{(V_D-1)^2} \tag{7.14a}$$

$$B = -\frac{2V_D f_D}{(V_d)^2} + \frac{2G}{V_d(V_D-1)}(V_d f_D - V_d - f_D - V_D f_D) + \frac{2(V_d f_D - V_d - f_D)}{(V_D-1)^2} \tag{7.14b}$$

$$C = \left(\frac{V_D f_D}{V_d}\right)^2 - \frac{2G}{V_d(V_D-1)} V_D f_D (V_d f_D - V_d - f_D) + \left(\frac{(V_d f_D - V_d - f_D)^2}{(V_D-1)^2}\right) - 1 \tag{7.14c}$$

Overall, the development of the integrated binary-unit conceptual (IBUC) packing model consists of three theoretical transformations delineated through Eqs. (7.1-7.14). Evidently, the prior two transformations pose practical implementation challenges, since measuring the three dimensions of each individual sediment particle is infeasible. To overcome such limitation, we directly utilize the measured grain size distribution (GSD) of the original sediment mixture as a reasonable approximation for the GSD of the equivalent spherical packings (discussed in section 7.5). In doing so, the calculation procedure is simplified as:

(1) Input measured GSD of the fluvial sediment packing.

(2) Calculate μ, σ and Sk of the GSD for the equivalent spherical packing.

(3) Derive d, D, and f_d (or f_D) of the equivalent binary-unit spherical packing.

(4) Predict n based on d, D, f_d (or f_D) and n_0.

Upon simplification, the IBUC packing model narrows its input requirements to solely the grain size distribution (GSD) and the initial porosity (n_0) of a fluvial sediment mixture. Although the GSD of a sediment mixture can be easily measured via sieve analysis, the measurement of n_0 is less straightforward, as it serves as a comprehensive indication of the averaged or collective impact of non-spherical grain shapes within a specific packing state. The determination of n_0 is a critical aspect that requires careful consideration, which is extensively discussed in sections 7.4 and 7.5.

7.4 Validation of the IBUC Packing Model

7.4.1 Porosity Datasets Obtained from Literature

Through the search of literatures, we have identified three laboratory datasets that exhibit suitability to validate the IBUC packing model. The first dataset is from Frings et al. (2011), who conducted 46 porosity measurements for the Rhine River in Germany. Sediment samples were collected from sub-layers of the channel bed and river bank along a 520 km stretch of the river between the Iffezheim barrage and the German-Dutch border. To emulate the original packing conditions in the laboratory, random mixing and compaction procedures were employed, followed by porosity determination with the water displacement method (Bear, 1972).

The second dataset, created by Tabesh et al. (2021), comprises 35 porosity measurements for the Bès River and 16 porosity measurements for the Galabre River within the Rhône-Alpes region of France. After the removal of the armor layer, sediment samples were taken at three distinct sites along the Bès River and one site along the Galabre River, featuring varying sediment characteristics. The laboratory procedure for porosity determination remained consistent with the aforementioned Rhine sediments.

Lastly, Yan et al. (2019) presents the third dataset, encompassing 41 porosity measurements undertaken in the Kuqa River of western China. Sediment samples were obtained from the surface layer of a braided channel and mid-channel bars at an upstream location of the Kuqa River. Instead of using the water displacement method, their porosity was analyzed in the laboratory by gas pycnometer, which utilizes Boyle's law (Bonnar, 1956) to determine the volume of a sample by measuring the pressure change of a gas (usually helium or nitrogen) displaced by the sample.

The grain size distributions within the sampled sediments exhibited a wide range, extending from 0.02 mm to 200 mm for the Rhine, Bès and Galabre sediments, and approximately 0.09 mm to 11.2 mm for the Kuqa sediments. These distributions displayed a mix of unimodal and multi-modal patterns, contributing to the complexity of the sediment compositions. Morphologically, the Rhine sediments showcased a predominantly sub-spherical grain shape, while the Kuqa sediments exhibited a poorly-spherical morphology. Unfortunately, no details regarding the shape characteristics of the Bès and Galabre sediments were provided. In terms of packing states, the Rhine, Bès and Galabre samples were subject to random dense packing states, while the Kuqa sediments were subject to a random loose packing state, based on the corresponding measurement strategies adopted.

7.4.2 Validation against Porosity Datasets

As mentioned in section 7.3, the IBUC packing model requires two parameters for the porosity prediction of a fluvial sediment mixture, i.e., the grain size distribution (GSD) and the initial porosity (n_0). The available grain size distributions of the three porosity datasets (Rhine, Bès and Galabre, Kuqa) were directly used as inputs for calculating the grain size statistics of mean, standard deviation and skewness of the corresponding equivalent spherical packings, upon which the equivalent binary spherical packings were obtained.

In contrast to the grain size distributions, the initial porosities, however, remained unknown. In its essence, the initial porosity of a sediment packing embodies the averaged grain shape effects subject to a certain packing state. Although a direct laboratory method for measuring the initial porosity is possible (elucidated in section 7.5), individually measuring each sediment sample would be a very laborious undertaking. Therefore, a good estimation of the mean initial porosity, serving as an optimized surrogate for a sampling region, is necessary. In fact, by taking a certain number of measurements, an

informed approximation of the mean initial porosity can be derived, enabling a general characterization of a specific site (detailed in section 7.5).

In this validation study, as no information regarding the initial porosity for the three porosity datasets exists; to address this limitation, we fed the measured porosity values as inputs into the model. Through the utilization of the numerical hybrid Powell and Newton method, we performed a reverse calculation to obtain the individual initial porosity value. Next, the mean initial porosity was computed as a comprehensive indicator, reflecting the combined effects of grain shape and packing state across the four distinct sediment groups obtained from the rivers Rhine ($n_0 = 0.38$), Bès ($n_0 = 0.44$), Galabre ($n_0 = 0.47$), and Kuqa ($n_0 = 0.49$). These calculated mean values were then used to evaluate the behavior of the IBUC packing model.

We quantify the model's prediction accuracy with two skill metrics: the coefficient of determination (R^2) and the root mean square error (*RMSE*). The comparison in Fig. 7.2 shows that the IBUC packing model achieves a remarkable performance in porosity estimation of the fluvial sediments, explaining 79% (R^2) of the total variance in porosity and the prediction error (*RMSE*) is only 0.03.

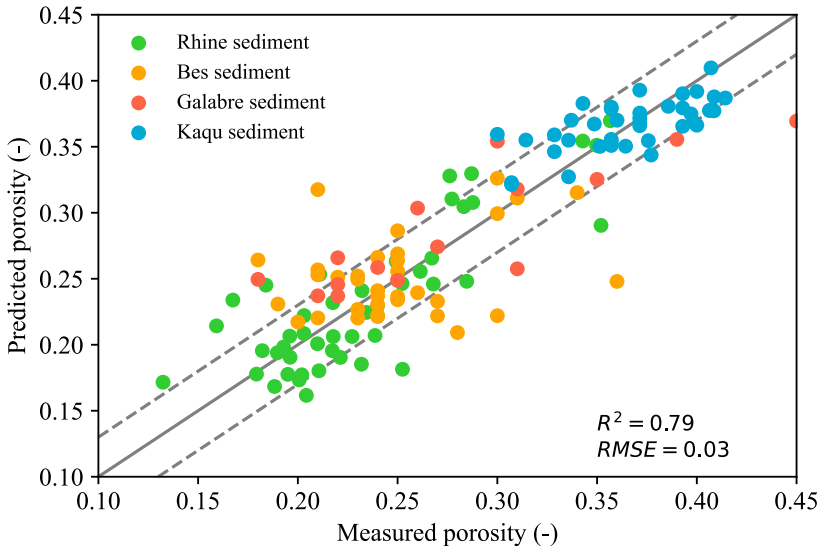

Figure 7.2. Comparison of the measured porosity (Rhine, Bès, Galabre, and Kuqa sediments) to the porosity predicted by the IBUC packing model. The grey line indicates a perfect fit, while the dotted grey lines represent a deviation of 0.03 from the perfect correlation.

While certain predicted points exhibit deviations from the true values far beyond 0.03 (with a maximum absolute error of up to 0.11), these discrepancies are inevitable due to the inherent limitations of employing mean initial porosity, which may not adequately capture extreme cases (discussed in section 7.5). Nevertheless, the IBUC model outperforms the original BUC model developed in Chapter 3, with a significant

improvement around 167% in *RMSE* skill score (i.e., the normalized *RMSE* difference between model *A* (the original model) and model *B* (the integrated model) defined as ($RMSE_A$ - $RMSE_B$)/$RMSE_B$). The original BUC model yields a R^2 score of 0.63 and a *RMSE* score of 0.08 when provided with an initial porosity input of 0.36 for the Rhine, Bès, and Galabre sediment groups, and 0.4 for the Kuqa sediment group, according to their respective packing state mentioned earlier.

7.5 Discussion

In this section, we investigate the uncertainties associated with the IBUC packing model. In general, three main uncertainty sources were identified that cause errors in porosity prediction: (1) approximation of the equivalent spherical packing, (2) the Westman equation, and (3) the use of mean initial porosity.

7.5.1 Approximation of the Equivalent Spherical Packing

Converting into an equivalent spherical mixture during the first two transformations presents a challenge since measuring the three dimensions of each sediment particle becomes impractical. To overcome this hurdle, an alternative approach was adopted. It involves utilizing the standard sieve-measured grain size, which represents the geometric mean size between two adjacent sieve meshes, as a direct representation of the corresponding equivalent spherical diameter. This substitution, however, introduces some uncertainties when estimating porosity.

In order to assess the degree of uncertainties caused by such proxy, a comparison analysis was made between the standard sieve-measured grain size and the calculated equivalent spherical diameter, based on a dataset containing a total of 241 high-resolution scanned sediments sampled from the rivers Rhine and Kall (from Chapter 5). These scanned sediments spanned from 0.29 mm to 54.3 mm, thus from medium sand to coarse gravel, representing a good portion of fluvial sediments.

In undertaking this comparison, we combined the scanned particles into seven distinct size fractions, ranging from 0.25-0.5 mm to 16-32 mm, each with a width of 1 phi on the Krumbein scale. This ensures that each fraction contains a sufficient number of particles (around 30 grains) for a good estimate of the mean equivalent spherical diameter. Noteworthy is the exclusion of particles exceeding 32 mm in size from the analysis. This deliberate choice was necessitated due to the absence of sizes larger than 54.3 mm, essential for maintaining the integrity of the size interval of 32-64 mm. Employing the measured three dimensions of the scanned sediments, we computed the equivalent spherical diameter for each individual particle, using Eqs. (7.1-7.4). The subsequent step involved deriving the mean value for each of the seven size intervals. The results, as illustrated in Fig. 7.3, demonstrate a commendable consistency, with the deviation between the standard measured grain size and the corresponding equivalent spherical diameter maintained at levels generally below 10%.

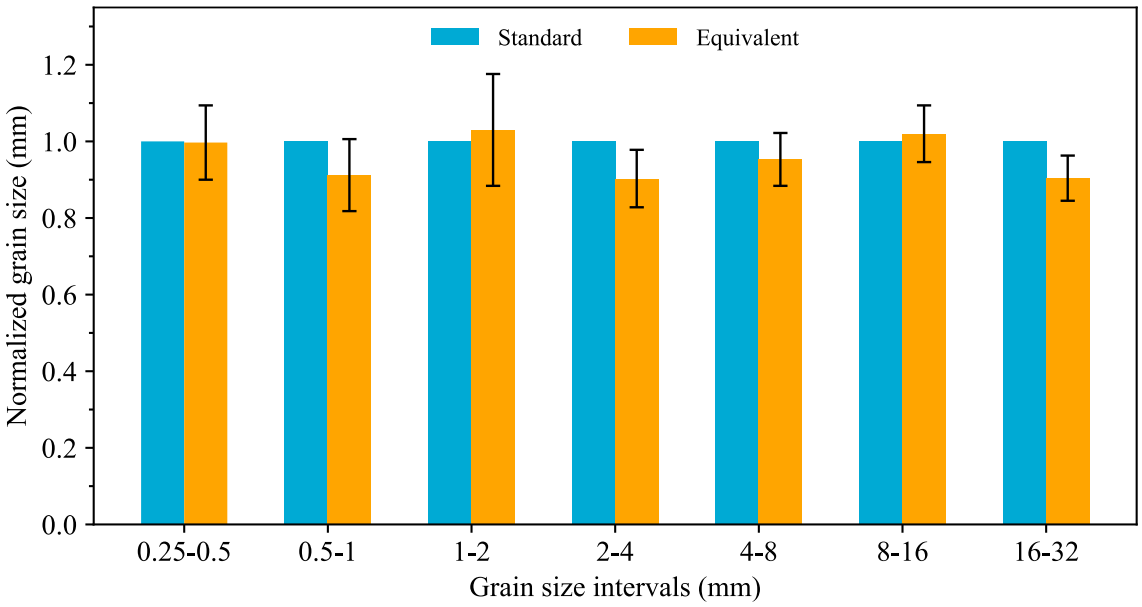

Figure 7.3. Comparison between the standard sieve-measured grain size and corresponding equivalent spherical diameter based on a dataset provided by Chapter 5. All grain size values are normalized with respect to the standard measurement. Error bars represent bootstrapped 95% confidence intervals for the mean equivalent spherical diameter of each size interval.

To quantify the error of porosity estimation, we conducted a sensitivity analysis. This involved systematically adjusting each grain size by 10% to gauge its impact on the porosity values. To streamline the complexities inherent in multi-component spherical packings, we opted for equivalent binary spherical packings as the analytical framework.

In our exploration, we tested seven size ratios ($r = d/D$) spanning from 0.01 to 0.9. Each ratio underwent eight unique uncertainty scenarios, as outlined in Table 7.1. To amplify the grain size effect, we allocated equal percentages for each component ($f_d = f_D = 50\%$). The initial porosity was set to 0.5.

The results, summarized in Table 7.1, reveal that in the majority of cases (90%), the absolute porosity error remains below 1%. Negligible porosity estimation errors are observed with size ratio either minuscule (below 0.05) or approached unity (exceeding 0.9). The most substantial influences manifest within the intermediate size ratios (0.3-0.7), in which the particle-particle interactions exhibit heightened intensity.

Table 7.1. Porosity estimation error using approximation of the equivalent spherical packing.

ID	Uncertainty scenarios		Absolute porosity error at different size ratios r (d/D)						
	d	D	0.01	0.05	0.10	0.30	0.50	0.70	0.90
1	↑	↑	0.000	0.000	0.000	0.000	0.000	0.000	0.000
2	↓	↓	0.000	0.000	0.000	0.000	0.000	0.000	0.000
3	↑	–	0.000	0.001	0.003	0.008	0.008	0.007	0.000
4	↓	–	0.000	0.001	0.003	0.008	0.009	0.008	0.000
5	–	↑	0.000	0.001	0.003	0.007	0.008	0.007	0.000
6	–	↓	0.000	0.002	0.004	0.008	0.008	0.007	0.000
7	↑	↓	0.000	0.003	0.008	0.016	0.016	0.014	0.000
8	↓	↑	0.000	0.002	0.006	0.015	0.016	0.015	0.000

"↑, ↓" denote a 10% increase or decrease of the grain size, respectively, while "–" represents the grain size keeps unchanged.

7.5.2 The Westman Equation

The other potential porosity prediction error lies in the application of the Westman equation for estimating the porosity of equivalent binary-unit spherical packings. To evaluate the accuracy of the Westman equation, a total of 189 experimental measurements on spherical binary packings were gathered (data from Dias et al., 2004; Mcgeary, 1961; Mota et al., 2001; Westman & Hugill, 1930; Yerazunis et al., 1965; Yu et al., 1992). These binary packings encompassed a broad spectrum of size ratios, featured diverse materials, and spanned packing stages from loosely to densely packed.

The porosity comparison results shown in Fig. 7.4 confirm the reliability of the Westman equation in predicting the porosity of binary packings of spherical particles. The evaluation yielded a remarkable R^2 score of 0.95 and a low *RMSE* score of 0.01.

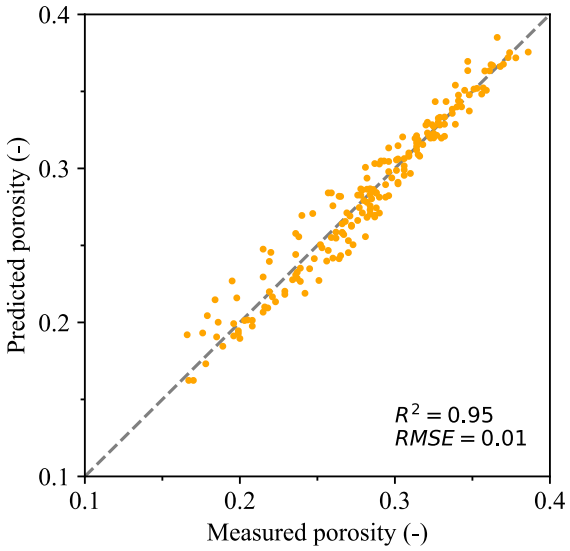

Figure 7.4. Comparison of the measured porosity to the porosity predicted by the Westman equation, for 189 spherical binary packings.

7.5.3 The Use of Mean Initial Porosity

In light of the relatively low porosity estimation errors (~1% deviation) arising from the previously discussed sources, the use of mean initial porosity in the IBUC packing model must account for the atypically high prediction errors shown in Fig. 7.2. Specifically, the degree of the model error associated with mean initial porosity heavily depends on the spatial variability of initial porosity within a given environment.

The initial porosity distribution across the four sampled environments is depicted in Fig. 7.5. Notably, the standard deviation of the initial porosity varies across these environments, standing at 0.04 for both the Rhine and Bès sites, 0.05 for the Galabre site, and 0.02 for the Kuqa site. The overall standard deviation across all four environments stands at 0.04. These standard deviation values serve as indicators of the spatial variability in the initial porosity, with higher values suggesting a broader dispersion relative to the mean initial porosity. This dispersion, especially in extreme cases, contributes to elevated model errors.

Despite the spatial variability, relying on mean initial porosity proves to be a viable strategy, yielding reasonable porosity estimates within ± 0.03 for the majority of cases (79% in this study). The result aligns with expectations, given that the sediment characteristics (size and shape) and depositional conditions (packing state) typically cluster around the population mean for a given local environment with a shared sediment transport history (Deal et al., 2023; Novák-Szabó et al., 2018). Such concentration effect is evident in Fig. 7.5 (a, b&d) for the Rhine, Bès, and Kuqa sites, but less obvious for the Galabre site (Fig. 7.5c), likely attributable to the smaller sample size ($N = 16$) collected for this area.

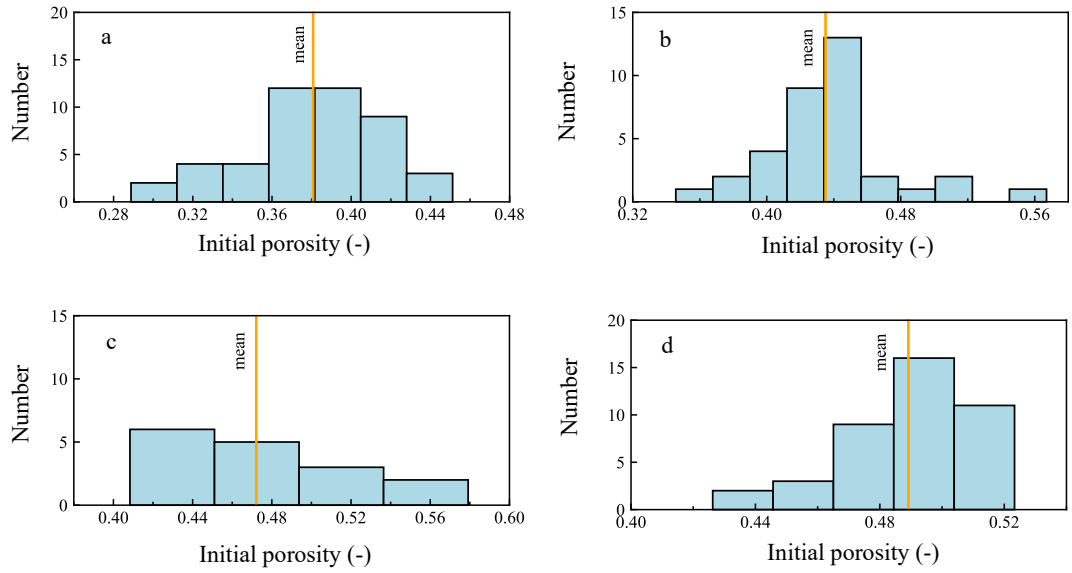

Figure 7.5. Distribution of the initial porosity for the sampled (a) Rhine sediment, (b) Bès sediment, (c) Galabre sediment, and (d) Kuqa sediment. The width of the bins was

selected based on the interquartile range and the number of samples at each environment following the Freeman-Diaconis rule.

Therefore, a good estimate of the mean initial porosity is vital in determining the model's predictive capacity. It becomes apparent that the accuracy of a mean initial porosity is dependent on the spatial variability of initial porosity in an environment (i.e., the standard deviation of the initial porosity σ) as well as the number of samples (N), which can be effectively assessed by calculating the standard error of the mean (SEM) using the following expression:

$$SEM = \frac{\sigma}{\sqrt{N}} \tag{7.15}$$

In this context, the SEM measures the standard deviation of the mean initial porosity for a given sample size. A lower SEM value indicates higher accuracy in estimating the mean initial porosity. However, achieving a low SEM necessitates a large number of sampling points for a given environment. Considering practical constraints, a SEM value of 0.01 is suggested. This value strikes a balance between maintaining a good estimate of the mean initial porosity and keeping the sample size within feasible limits. For instance, taking into account the average standard deviation of the initial porosity observed in this study ($\sigma = 0.04$), obtaining an accuracy level of 0.01 for the mean initial porosity would require only 16 samples. However, pursuing uncertainty levels below 0.01 triggers a rapid increase in sampling effort. For estimates with an uncertainty as low as 0.005, at least 64 samples would be required, which may pose practical challenges in the context of river management studies.

The laboratory procedure for measuring the initial porosity closely resembles the method for porosity measurement in sediment samples. The key difference lies in the need to divide the sediment sample into multiple uniform size classes where the size effect on porosity is considered negligible. Averaging the porosity measured for each uniform sediment at a predefined packing state gives the initial porosity for that specific sample.

However, obtaining the mean initial porosity through this procedure is still cumbersome. For instance, if 16 samples are collected from a local environment, and each sample contains 10 identical uniform size classes, a total of 160 measurements would be required to determine the mean initial porosity, which is still infeasible. To fix this, a more refined method is to merge identical uniform size factions present in all samples and subsequently measure the porosity for this well-mixed uniform size fraction. This approach provides an equivalent but more effective way to determine the mean initial porosity. With this strategy, only 10 measurements would be necessary instead of the previously required 160.

An illustrative example can be found in Frings et al. (2011). In addition to contributing the first dataset for this study, the researchers also conducted porosity

measurements for uniform sediment packings derived from the same samples from the Rhine River. They obtained 18 well-mixed uniform classes, each with a width of 0.5 phi and spanning from 0.09 mm to 45 mm, based on the general range of grain sizes present in those sediment samples. The porosity of each uniform class was measured at a dense packing state using the water replacement method. Such measurements align precisely with the proposed principle for measuring the mean initial porosity. The computed mean porosity of the 18 classes was 0.37, remarkably matching the mean initial porosity of 0.38 calculated for the Rhine sediments.

In regions without any measurements about the mean initial porosity, the values obtained from this study can be considered as a first recommendation. Specifically, for environments akin to the Rhine characterized by sub-spherical shapes and densely packed conditions, a recommended range of 0.37-0.39 is proposed for the mean initial porosity, taking into account a bootstrapped 95% confidence interval. Conversely, for environments resembling the Kuqa, marked by poorly-spherical shapes and loosely packed conditions, a range of 0.48-0.50 for the mean initial porosity is advised. Notably, as porosity generally increases with the departure from spherical grain shapes as elucidated in Chapter 6, these two environments could be perceived as representing extreme cases. Consequently, a comprehensive mean initial porosity range spanning from 0.37 to 0.50 is recommended to encompass all possible situations in diverse environments, including the Bès ($n_0 = 0.44 \pm 0.01$) and Galabre ($n_0 = 0.47 \pm 0.02$) locales.

7.6 Conclusions

The present work has provided a general framework for the development of an integrated binary-unit conceptual (IBUC) packing model that considers key porosity-controlling factors including grain size, grain shape, and packing state. The IBUC model operates by conceptualizing an arbitrary sediment packing as a fusion of two distinct components: an equivalent spherical packing that holds crucial size-dependent information, and an initial porosity that conveys valuable insights into the effect of shape and packing state. The grain size distribution (GSD) of the equivalent spherical packing can be reasonably approximated by the measured GSD of the original packing. Due to the infeasibility of measuring the initial porosity for each sediment packing, the use of a mean initial porosity as an approximate representation for a local sampling region is suggested. The mean initial porosity can be simply obtained through the averaging of measured porosity values across well-mixed uniform size classes present within sampled sediments. A minimum of 16 samples (equivalent to 16 GSDs) is recommended to obtain a reliable estimate of the mean initial porosity with an accuracy of 0.01. Despite the use of mean initial porosity, the IBUC model is still able to generate accurate porosity predictions with a root-mean-square error (RMSE) of 0.03 on 138 validation targets due to the concentration effect. Given the ubiquitous availability of grain size distribution data, the IBUC model emerges as a user-friendly tool for quantifying the spatial variability in riverbed porosity.

References

Ackers, P., & White, W.R. (1973). Sediment transport: new approach and analysis. Journal of the Hydraulics Division, 99, 2041-2060.

Allen, J.R.L. (1985). Principles of physical sedimentology. George Allen & Unwin, London.

Bear, J. (1972). Dynamics of fluids in porous media. Elsevier, 764.

Blott, S.J., & Pye, K. (2001). Gradistat: A grain size distribution and statistics package for the analysis of unconsolidated sediments. Earth Surface Processes and Landforms, 26(11), 1237-1248.

Bonnar W.B. (1956). Boyle's Law and Gravitational Instability. Monthly Notices of the Royal Astronomical Society, 116(3), 351-359.

Boulton, A.J., Findlay, S., Marmonier, P., Stanley, E. H., & Valett, H.M. (1998). The functional significance of the hyporheic zone in streams and rivers. Annual Review of Ecology, 29, 59-81.

Carling, P.A., & Reader, N.A. (1982). Structure, composition and bulk properties of upland stream gravels. Earth Surface Processes and Landforms, 7(4), 349-365.

Coleman, S.E., & Nikora, V.I. (2009). Exner equation: A continuum approximation of a discrete granular system. Water Resources Research, 45(9), 9421.

De Larrard, F. (1999). Concrete mixture proportioning: a scientific approach. Concrete Mixture Proportioning.

Deal, E., Venditti, J.G., Benavides, S.J., Bradley, R., Zhang, Q., Kamrin, K., & Perron, J.T. (2023). Grain shape effects in bed load sediment transport. Nature, 613, 298-302.

Dias, R.P., Teixeira, J.A., Mota, M.G., & Yelshin, A.I. (2004). Particulate binary mixtures: dependence of packing porosity on particle size ratio. Industrial and Engineering Chemistry Research, 43(24), 7912-7919.

Folk, R.L., & Ward, W.C. (1957). Brazos River bar: a study in the significance of grain size parameters. Journal of Sedimentary Research, 27(1), 3-26.

Frings, R.M., Kleinhans, M.G., & Vollmer, S. (2008). Discriminating between pore-filling load and bed-structure load: a new porosity-based method, exemplified for the river Rhine. Sedimentology, 55(6), 1571-1593.

Frings, R.M., Schüttrumpf, H., & Vollmer, S. (2011). Verification of porosity predictors for fluvial sand-gravel deposits. Water Resources Research, 47(7), 7525.

Gan, J., & Yu, A. (2020). DEM study on the packing density and randomness for packing of ellipsoids. Powder Technology, 361, 424-434.

Koltermann, C.E., & Gorelick, S.M. (1995). Fractional packing model for hydraulic conductivity derived from sediment mixtures. Water Resources Research, 31(12), 3283-3297.

Liang, R., Schruff, T., Jia, X., Schüttrumpf, H., & Frings, R.M. (2015). Validation of a stochastic digital packing algorithm for porosity prediction in fluvial gravel deposits. Sedimentary Geology, 329, 18-27.

Mcgeary, R.K. (1961). Mechanical packing of spherical particles. Journal of the American Ceramic Society, 44(10), 513-522.

Mota, M., Teixeira, J., Bowen, W., & Yelshin, A. (2001). Binary spherical particle mixed beds: porosity and permeability relationship measurement. Transactions of the Filtration Society.

Mulatu, C.A., Crosato, A., Moges, M.M., Langendoen, E.J., & McClain, M. (2018). Morphodynamic Trends of the Ribb River, Ethiopia, Prior to Dam Construction. Geosciences, 2018, 8(7), 255.

Noack, M., Ortlepp, J., & Wieprecht, S. (2017). An Approach to Simulate Interstitial Habitat Conditions During the Incubation Phase of Gravel-Spawning Fish. River Research and Applications, 33(2), 192-201.

Novák-Szabó, T., Sipos, A.Á., Shaw, S., Bertoni, D., Pozzebon, A., Grottoli, E., Sarti, G., Ciavola, P., Domokos, G., & Jerolmack, D.J. (2018). Universal characteristics of particle shape evolution by bed-load chipping. Science Advances, 4(3), 4946.

Núñez-González, F., Martín-Vide, J.P., & Kleinhans, M.G. (2016). Porosity and size gradation of saturated gravel with percolated fines. Sedimentology, 63(5), 1209-1232.

Qian, Q., Wang, L., An, X., Wu, Y., Wang, J., Zhao, H., & Yang, X. (2018). DEM simulation on the vibrated packing densification of mono-sized equilateral cylindrical particles. Powder Technology, 325, 151-160.

Rettinger, C., Eibl, S., Rüde, U., & Vowinckel, B. (2022a). Rheology of mobile sediment beds in laminar shear flow: effects of creep and polydispersity. Journal of Fluid Mechanics, 932, A1.

Rettinger, C., Rüde, U., Vollmer, S., & Frings, R.M. (2022b). Effect of sediment form and form distribution on porosity: a simulation study based on the discrete element method. Granular Matter, 24(4), 1-23.

Rettinger, C., Tabesh, M., Rüde, U., Vollmer, S., & Frings, R.M. (2023). On the use of packing models for the prediction of fluvial sediment porosity. Earth Surface Dynamics, 11(6), 1097-1115.

Sawyer, A.H., & Cardenas, M.B. (2009). Hyporheic flow and residence time distributions in heterogeneous cross-bedded sediment. Water Resources Research, 45(8).

Schruff, T., Liang, R., Rüde, U., Schüttrumpf, H., & Frings, R.M. (2018). Generation of dense granular deposits for porosity analysis: assessment and application of large-scale non-smooth granular dynamics. Computational Particle Mechanics, 5(1), 59-70.

Tabesh, M., Hoffmann, T., Vollmer, S., Schüttrumpf, H., & Frings, R.M. (2019). In-situ measurement of river-bed sediment porosity using Structure-from-Motion image analysis. Geomorphology, 338, 61-67.

Tabesh, M., Vollmer, S., Schüttrumpf, H., & Frings, R.M. (2022). Spatial variability in river bed porosity determined by nuclear density gauging: A case study from a French gravel-bed river. Sedimentology, 69(2), 823-844.

Vollmer, S., & Kleinhans, M.G. (2007). Predicting incipient motion, including the effect of turbulent pressure fluctuations in the bed. Water Resources Research, 43(5), 5410.

Wadell, H. (1935). Volume, Shape, and Roundness of Quartz Particles. The Journal of Geology, 43(3), 250-280.

Westman, A.E.R. (1936). The packing of particles: empirical equations for intermediate diameter ratios. Journal of the American Ceramic Society, 19, 127-129.

Westman, A.E.R., & Hugill, H.R. (1930). The packing of particles. Journal of the American Ceramic Society, 13(10), 767-779.

Wooster, J.K., Dusterhoff, S.R., Cui, Y., Sklar, L.S., Dietrich, W.E., & Malko, M. (2008). Sediment supply and relative size distribution effects on fine sediment infiltration into immobile gravels. Water Resources Research, 44(3), 3424.

Wu, W., & Wang, S.S.Y. (2006). Formulas for sediment porosity and settling velocity. Journal of Hydraulic Engineering, 132(8), 858-862.

Xie, Z., An, X., Yang, X., Li, C., & Shen, Y. (2019). Numerical realization and structure characterization on random close packings of cuboid particles with different aspect ratios. Powder Technology, 344, 514-524.

Yerazunis, S., Cornell, S.W., & Wintner, B. (1965). Dense random packing of binary mixtures of spheres. Nature, 207, 835-837.

Yiming, Y., Zhang, L., & Luo, X. (2019). Calculating the primary porosity of unconsolidated sands based on packing texture: Application to braided river sands. Marine and Petroleum Geology, 107, 515-526.

Yu, A.B., & Standish, N. (1991). Estimation of the porosity of particle mixtures by a linear-mixture packing model. Industrial and Engineering Chemistry Research, 30(6), 1372-1385.

Yu, A.B., & Standish, N. (1993a). Characterisation of non-spherical particles from their packing behaviour. Powder Technology, 74(3), 205-213.

Yu, A.B, Standish, N., & McLean, A. (1993b). Porosity calculation of binary mixtures of nonspherical particles. Journal of the American Ceramic Society, 76(11), 2813-2816.

Yu, A.B, Zou, R.P, & Standish, N. (1992). Packing of ternary mixtures of nonspherical particles. Journal of the American Ceramic Society, 75(10), 2765-2772.

Zhang, G., An, X., Zhao, B., Qian, Q., & Zhao, H. (2019). Discrete element method dynamic simulation of icosahedral particle packing under three-dimensional mechanical vibration. Particuology, 44, 117-125.

Zhao, S., Zhang, N., Zhou, X., & Zhang, L. (2017). Particle shape effects on fabric of granular random packing. Powder Technology, 310, 175-186.

Zou, R.P., & Yu, A.B. (1996). Evaluation of the packing characteristics of mono-sized non-spherical particles. Powder Technology, 88, 71-79.

8

Conclusions

In this thesis, several achievements have been made, involving two major innovations and five minor discoveries. Two major innovations include developments of the Binary-Unit Conceptual (BUC) packing model and the Integrated Binary-Unit Conceptual (IBUC) packing model. Five minor discoveries comprise assessments of numerical methods, sediment shape approximation using ellipsoid, a new definition of sphericity, a general description of ellipsoids, and a general porosity-ellipsoid relation.

8.1 Two Major Innovations

The BUC packing model has been developed to predict the porosity of spherical packing systems. The key part of this model lies in the proposed binary-unit concept. It demonstrates that arbitrary spherical mixtures can be transformed into a binary unit spherical mixture that possesses the equivalent intraparticle interactions as the original mixture. Such transformation is achieved via the link of identical grain size statistics of mean, standard deviation and skewness, which are the basic elements describing the diverse intraparticle interactions from binary to large-component spherical packings. Using this concept, the porosity of arbitrary spherical packings can be easily estimated with models capable of predicting the porosity of spherical binary mixtures, such as the Westman equation. The BUC model offers highly accurate porosity predictions for spherical packings and also provides reasonably accurate results when applied to sub-spherical sediment packings.

The IBUC packing model has been established to enhance the functionality of the BUC model by integrating all other factors influencing porosity. Three theoretical transformations constitute the core architecture of the IBUC model, i.e., from sediment to ellipsoid packing, from ellipsoid to spherical packing, and from spherical to binary-unit spherical packing. As a result, a non-spherical sediment mixture can be treated as a spherical mixture with equivalent size interactions between particles, alongside an initial porosity capturing all other porosity-controlling effects, such as isolated grain shape and packing state. It shows that the grain size distribution (GSD) of the transformed spherical packing can be directly approximated with the measured GSD of the original sediment packing. Instead of measuring each of the sediment mixture's initial porosity, which is impractical, the use of a mean initial porosity is suggested for a general representation of a particular site being investigated. Despite this, the IBUC packing model is still able to achieve satisfied porosity predictions for complex fluvial sediment mixtures across various sedimentological environments. The IBUC packing model, due to its generality, simplicity, and accuracy, stands out as a state-of-the-art tool for examining spatial variability in riverbed porosity.

8.2 Five Minor Discoveries

Three numerical methods have been employed to generate digital riverbeds. The results indicate that both the physics-based non-smooth granular dynamics (NSGD) and the optimization-based non-linear programming (NLP) algorithms can produce random dense packings. In contrast, the stochastic digital packing algorithm tends to create random loose packings due to kinematic sorting effects and shape influences introduced by the random motion of particles.

The ellipsoidal shape has been identified as the best match to fluvial sediments in terms of solid volume, surface area, and sphericity. Additionally, the packing behavior of ellipsoids closely resembles that of fluvial sediments in both trend and accuracy.

A new definition of sphericity has been proposed, improving upon Wadell's definition. This new definition states that sphericity is the ratio of the surface area of a sphere with the same volume as the particle to the smoothed surface area of the particle itself.

Ellipsoids have been generally characterized using two well-defined parameters: Wadell's sphericity and Zingg's intercept ratio. Sphericity measures how closely an ellipsoid approximates a spherical shape, while the intercept ratio, an advanced version of the aspect ratio, captures the combined effects of flatness and elongation.

A general relationship between porosity and ellipsoids has been established. Three distinct trends are identified that show how porosity varies as a function of sphericity and intercept ratio. A piecewise formula describing these relationships has been derived and verified, showing good agreement in both trends and values.

8.3 Outlook

The binary-unit concept proposed in this thesis is anticipated to extend beyond just estimating porosity, as particle-particle interactions influence a wide range of other factors. This concept has the potential to address various challenges in particle packing systems, such as estimating permeability in sediment mixtures, determining the cut-off grain size for morphological changes, and even predicting the onset of sediment transport.

Permeability is another key property of fluvial sediment mixtures, reflecting their ability to allow fluids (gas or liquid) to flow through. It is influenced by both porosity and the connectivity of pores. Using the binary-unit concept, a transformed binary mixture could offer a clearer understanding of fluid flow through porous media and, consequently, permeability, by simplifying the complex pore size distributions found in heterogeneous sediment mixtures.

The cut-off size acts as a threshold that distinguishes between pore-filling load and bed-structure load. Particles smaller than this threshold typically fill the spaces between larger grains without altering the overall bed structure, as pore-filling load. In contrast, particles larger than the cut-off size interact with surrounding grains, leading to morphological changes as bed-structure load. By applying the binary-unit concept, the fine grain derived from the transformed binary mixture could provide direct insights into determining the value of this cut-off size.

Predicting the onset of sediment transport is a long-standing problem. Traditional methods often track transport rates for a single grain size, such as the median, which is straightforward but fails to capture the diversity of real sediment mixtures. Alternatively, estimating transport rates for each individual grain size fraction is theoretically accurate but impractical due to the complexity and labor involved. A more effective solution is the two-fraction approach, where transport rates for a binary bed composition are measured. This method simplifies the process while still accounting for the different transport behaviors of fine and coarse particles, which tend to move at varying rates. Using the binary-unit concept, the transformed binary mixture could serve as a representative model of the full grain size distribution, capturing the essential dynamics of both fine and coarse particles without needing to consider every grain size in the distribution.

List of Publications

Liang, R., Schruff, T., Jia, X., Schüttrumpf, H., Frings, R.M. (2015). Validation of a stochastic digital packing algorithm for porosity prediction in fluvial gravel deposits. Sedimentary Geology, 329, 18-27.

Frings, R.M., **Liang, R.**, Schruff, T., Schüttrumpf, H. (2015). Porosity prediction for fluvial gravel deposits. In: 9th River Coastal and Estuarine Morphodynamics, Iquitos, Peru.

Jin H., **Liang R.**, Wang Y., Tumula P. (2015). Flood-runoff in semi-arid and sub-humid regions, a case study: a simulation of Jianghe watershed in northern China. Water, 7(9), 5155-5172.

Schruff, T., **Liang, R.**, Rüde, U., Schüttrumpf, H., Frings, R.M. (2018). Generation of dense granular deposits for porosity analysis: assessment and application of large-scale non-smooth granular dynamics. Computational Particle Mechanics, 5(1), 59-70.

Liang R., Schüttrumpf H., Frings R.M. A binary-unit conceptual packing model for porosity prediction of spherical fluvial sediments. (to be submitted)

Liang R., Schüttrumpf H., Frings R.M. Grain shape approximation of fluvial sediments. (to be submitted)

Liang R., Lobato, R.D., Schüttrumpf H., Frings R.M. Characterization of ellipsoids and the porosity-shape relation. (to be submitted)

Liang R., Schüttrumpf H., Frings R.M. An integrated binary-unit conceptual packing model for porosity prediction of fluvial sediments. (to be submitted)